ATMIRE

Title	Near-real-time/real-time methane prediction and visualization in underground longwall coal mining
Item Type	Text
Authors	Demirkan, Doga Cagdas
Publisher	Colorado School of Mines. Arthur Lakes Library
Rights	Copyright of the original work is retained by the author.
Download date	2026-11-27 11:43:58
Link to Item	https://hdl.handle.net/11124/176714

NEAR-REAL-TIME/REAL-TIME METHANE PREDICTION AND VISUALIZATION IN UNDERGROUND LONGWALL COAL MINING

by

Doga Cagdas Demirkan

A thesis submitted to the Faculty and the Board of Trustees of the Colorado School of Mines in partial fulfillment of the requirements for the degree of Doctor of Philosophy (Mining and Earth Systems Engineering).

Golden, Colorado

Date: _____

Signed: _____

Doga Cagdas DEMIRKAN

Signed: _____

Dr. H. Sebnem Duzgun

Thesis Advisor

Golden, Colorado

Date: _____

Signed: _____

Dr. Stephen Enders

Professor and Department Head

Department of Mining Engineering

ABSTRACT

Preventing methane explosions remains a challenging task in underground longwall coal mines. Mine-wide real-time methane monitoring is a must to tackle this challenge. Real-time decision-making is critical to stop possible explosive methane accumulation and prevent accidents. To accomplish this, detecting and monitoring methane emissions and concentrations across the entire mine must be predicted.

Atmospheric monitoring systems are a critical part of monitoring mine ventilation systems in real-time, and the number and location of sensors are essential to detecting any possible hazard. However, sensors can not be installed in the most critical locations, such as the shearer cutting drum and along the longwall face, due to the nature of mining equipment's movement. Thus sensors provide information for a limited area, and their readings may have delays caused by the sensor response time, gas diffusion rate, and temperature.

Computational fluid dynamics modeling can provide relatively accurate predictions regarding the location of possible explosive gas concentrations; however, it requires significant computational resources and time, which is not conducive to real-time decision-making. Lastly, decision-makers (mining personnel) need to observe and assess predictions to take the required precautions. Although automated shutdown mechanisms can be used in the event of a sudden increase in methane emissions, these are not entirely reliable due to previous accidents. Such mechanisms might also interfere with productivity as a result of unnecessary stops, lost time, and decreased production. Therefore, the predictions need to be visualized in a way that offers the fastest and most accurate response time for personnel.

This dissertation explores, evaluates, and benchmarks suitable artificial intelligence (AI) algorithms for predicting 3D near-real-time explosion hazards. The prediction performance of 10 algorithms is compared using seven datasets and then assessed through classification accuracy. With the best performer chosen, an application-specific methodology is proposed with modified long short-term memory to detect the formation of explosive methane-air mixtures in the longwall face and identify possible explosive gas accumulations before they become hazards. Lastly, the visualization of the predictions is compared in three platforms, namely computer screen, virtual reality (VR), and augmented reality (AR), for accurate methane volume assessment and faster response time.

The best-performing algorithm, Long Short-Term Memory (LSTM), is modified, trained, tested, and validated based on CFD model outputs for six locations of the shearer for similar locations and operational conditions of the cutting machine. The results show that the algorithm can predict explosive gas zones in 3D with overall accuracies ranging from 87.9% to 92.4% for different settings. Depending on the prediction area, output predictions take between 30 seconds to two minutes after measurement data are fed into the algorithm.

Lastly, a user study is designed to investigate the effects of two visual variables, transparency/opacity and complex/simple, to compare different platforms. Four simulations are tested with 30 human subjects. Participants are asked to determine the explosive gas volume. The subjects` time of completion and eye-tracking data are also recorded. Along with the recordings, saliency maps of four simulations are created. Recorded data are evaluated with both quantitative and qualitative analysis. The quantitative analysis assesses the accuracy of explosive gas volume detection and completion time. In addition, the saliency maps of the designed simulations with the subject's eye-tracking data is analyzed to investigate the subjects' attention and reaction in AR, VR, and computer screen. The qualitative analysis assesses subjects` responses to questions about their feelings. The results of the quantitative analysis show a statistically significant difference between the computer screen and VR for the transparent and simple scenario. The subjects` accuracy of volume determination is better in VR. Moreover, the eye tracker data show that subjects spent more time in non-salience regions in VR than on the computer screen. In addition, the qualitative analysis reveals that 90% of the subjects preferred to use VR due to the immersive experience, and 67 % felt more confident in VR when investigating the explosive zones and flagging them as dangerous zones. Finally, the users' preference ranking of platforms for explosive zone estimation is VR, computer screens, and AR.

TABLE OF CONTENTS

ABSTRACT iii
TABLE OF CONTENTS v
LIST OF FIGURES viii
LIST OF TABLES ix
ACKNOWLEDGMENTS xi
CHAPTER 1 INTRODUCTION 1
1.1. Current Practices of Methane Monitoring in Longwall Mines 2
1.1.1. Methane Sensors 2
1.1.2. Computational Fluid Dynamics 2
1.2. Real-Time Predictions with Artificial Intelligence 3
1.3. Data Visualization: Principles, Variables and Importance in Decision Making 4
1.4. Virtual Reality and Augmented Reality in Data Visualization and Cognition 5
1.5. The Research Goal 6
1.6. Research Questions 7
1.7. The Original Contribution of the Dissertation 7
1.8. Structure of the Dissertation 8
CHAPTER 2 METHODOLOGY 9
CHAPTER 3 EXPLORATION AND EVALUATION OF REAL-TIME PREDICTION METHODS 11
3.1. Introduction 11
3.2. Overview of the AI Models for Time Series Data 11
3.3. Data Preparation 15
3.4. Benchmarking 17
3.4.1. Training, Testing, and Validation 18
3.5. Results 19
3.6. Conclusions 22
CHAPTER 4 DATA CURATION AND LONG SHORT TERM MEMORY (LSTM) ADAPTION 24

4.1. Introduction 24
4.2. Materials and Methods 26
4.2.1. Spatial and Temporal CFD Modeling 26
4.2.2. Data Curation 27
4.2.3. The Modified LSTM 28
4.3. Results 30
4.3.1. Training 31
4.3.2. Validation 32
4.3.3. Testing 32
4.4. Discussion 33
4.5. Conclusions 34
CHAPTER 5 VISUALIZATION OF PREDICTIONS AND USER STUDY 36
5.1. Introduction 37
5.2. Related Work 37
5.3. Experimental Design and Evaluation 39
5.3.1. Research Questions and Hypotheses 39
5.3.2. Simulation Model and Data 40
5.3.3. Participants 41
5.3.4. Procedure 42
5.4. Results 43
5.4.1. Volume Estimations 45
5.4.2. Task Completion Times 45
5.4.3. Comparison of Eye Tracker Data and Saliency Maps 46
5.4.4. Users' Feedback 47
5.5. Discussion 48
5.6. Conclusions 50
CHAPTER 6 IMPLEMENTATION OF AR ASSISTANCE 52
6.1. Introduction 52
6.2. Experimental Design and Evaluation 53

6.3. Results 55
6.4. Conclusions 55
CHAPTER 7 OVERALL CONCLUSIONS AND RECOMMENDATIONS FOR FUTURE WORK 57
REFERENCES 60
APPENDIX A COMMITTEE EXEMPTION NOTICE 69
APPENDIX B PRETEST SURVEY 70
APPENDIX C USER STUDY TRAINING SLIDES AND QUESTIONNAIRE 71
APPENDIX D POSTTEST SURVEY 72
APPENDIX E Q-Q PLOTS 74
APPENDIX F SIMULATION VISUALIZATIONS, EYE TRACKER HEAT MAPS AND SALIENCY MAPS 80
APPENDIX G PERMISSION TO USE COPYRIGHTED MATERIALS 82

LIST OF FIGURES

Figure 2.1 Overall research methodology 9

Figure 3.1 CFD Simulation Geometry of a Longwall Coal Mining Face. Colors represent the boundaries of regions with CH4 concentrations. Note that concentrations in orange are near-explosive, and those in red are explosive (Modified from [6]). 16

Figure 3.2 Visual representation of the extracted points 17

Figure 3.3 Train – Validation Loss of A-10 data with HIVE-COTE Algorithm 20

Figure 3.4 Train – Validation Loss of A-20 data with HIVE-COTE Algorithm 21

Figure 3.5 ROC Curves of the Algorithms 22

Figure 4.1 Research methodology 26

Figure 4.2 Six locations of the shearer and cutting directions during data collection. 27

Figure 4.3 A snapshot of the 120th second time step of shearer location 3. 28

Figure 4.4 Simplified LSTM architecture (modified from [97]). 30

Figure 4.5 Validation and training accuracy. 32

Figure 4.6 Side-by-side comparisons of CFD models and prediction visualizations 35

Figure 5.1 Visualization of simulation in (a) conventional methods and (b) this study's setup 41

Figure 5.2 Example snapshots of each simulation (a, e and I show the original viewpoints for VR, computer screen and AR, b, f and j show heat maps of the eye tracker, c, g, k show Itti Koch saliency maps, d, h and l show overlay of the eye tracker and saliency map) 47

Figure 5.3 Users' Word Cloud 48

Figure 6.1 Escape route 54

Figure 6.2 Illustration of the tested scenarios (a) fully illuminated scene, (b) illumination with the headlamp, (c) no illumination, (d) fully illuminated scene with rendered meshes, (e) illumination with the headlamp with rendered meshes (f) no illumination with rendered meshes 54

Figure A.1 IRB Committee Exemption Notice 69

Figure E.1 Q-Q Plots of Accuracy and Time Data from User Study 74

LIST OF TABLES

Table 3.1 TSC Algorithms by Data Characteristics: weighted DTW (WDTW); time warp edit (TWE; move–split–merge (MSM); complexity invariant distance (CID); derivative DTW (DD_{DTW}); derivative transform distance (DTD_C); elastic ensemble (EE); time series forest (TSF); time series bag of features (TSBF); learned pattern similarity (LPS); fast shapelets (FS); shapelet transform (ST); bag of patterns (BOP); SAX vector space model (SAXVSM); bag of SFA symbols (BOSS); DTW features(DTW_F); collective of transformation-based ensembles (COTE), adapted from [74] 12

Table 3.2 Best Performing Algorithms by Problem Type, adapted from [74] 13

Table 3.3 Longwall face Ventilation CFD Data Sets 16

Table 3.4 Accuracies for the Chlorine Data Set 18

Table 3.5 Number of methane data points for each dataset 19

Table 3.6 10-point and 20-point test with HIVE-COTE algorithm for 20-time instances 19

Table 3.7 Accuracies of Best Performing Algorithms with Different Datasets 21

Table 4.1 Training, validation, and testing datasets based on shearer locations. 31

Table 4.2 Overall accuracies of tests 33

Table 5.1 Visualization simulations with its visual variables and platform 42

Table 5.2 Statistically significant results of each platform with visual variables ($|\Delta V|$: mean error in volume estimation, $\bar{x}$: mean time spent in the tests) 44

Table 5.3 Platform comparison($|\Delta V|$: mean error in volume estimation, $\bar{x}$: mean time spent in the tests) 45

Table 6.1 Total time for of completing the route 55

Table C.1 User Study Training Slides and Questions 71

Table F.1 Original image, heatmap, saliency and overlay 80

To My Family

ACKNOWLEDGMENTS

I would like to express my sincere gratitude to my advisor, Dr. Sebnem Duzgun. I am forever indebted to the opportunity she provided to conduct this research. Working with her throughout this study made me able to be more innovative and consistent.

I would also like to extend my appreciation to my thesis committee members Dr. Jurgen Brune and Dr. Gregory Bogin, for their continuous support and weekly meetings. I feel very lucky to work with them closely. I would also like to thank my committee members Dr. William Z. Bernstein, for sharing his experience and valuable lessons while doing my internship and Dr. William Hoff for his discussion insights. I would also like to thank my committee member Dr. Jamal Rostami for his valuable suggestions.

This research was fully supported by the National Institute for Occupational Safety and Health (NIOSH) contract number 0000HCCR-2019-36403. My research has also been supported by scholarships and fellowships, including WAAIME and McQuiston fellowships. Thanks to their support, I was one step closer to my career goals.

I am deeply thankful to my friends for their support, encouragement, and hours of weekly phone calls. Without pouring out our grief to each other, I could not survive. I am forever grateful to my beloved mother and father for their unconditional love and support. I am also thankful to my mother- and father-in-law. Last but not least, I am forever thankful for my other half, best friend, and partner in crime, Cansu. I simply could not make it without your love, motivation, and encouragement. All journeys we took, all challenges we beat, and all joy we had is just the beginning. So buckle up!

CHAPTER 1

INTRODUCTION

Despite alternative energy sources, worldwide coal production is still increasing each year [1]. Depending on depth, coal extraction is performed by either underground or surface mining methods. While there are different types of underground methods, including longwall, room and pillar with the continuous miner, and conventional, longwall mining's high recovery and extraction rates make it the most productive and safest option for underground coal mining [2]. However, even in ordinary mining operations and conditions, coal mining still faces serious challenges [3]. Methane (CH_4) emission per volume of coal is generally higher in longwall mining due to the nature of this method [4]. Consequently, adequate ventilation is vital for the safety and health of workers [5]. Despite advancements in technology and safety management, longwall face explosions from accumulated methane gas are known to be the most common causes and types of methane explosions [6]. Existing industry practices depend on point-type methane sensors in critical areas to prevent explosive gas accumulations [7]. However, point sensors are not reliable at spotting and warning about explosion hazards, especially in crucial areas, such as near the cutting drum, tailgate, and headgate areas of the longwall face [8]. One catastrophic example of a methane explosion accident was the 2010 Upper Big Branch Mine in West Virginia. [8]. Although atmospheric monitoring systems can report real-time methane concentrations, they fall behind due to their limited number of sensors and locations [9], which lack full coverage of the whole longwall face.

As it is not possible to equip the entire mine with sensors, the numerical modeling method, namely, computational fluid dynamics (CFD) modeling, is employed to simulate ventilation conditions in longwall faces to reproduce airflow dynamics and the formation of hazardous gas mixtures which are not detectable using conventional monitoring and ventilation inspection practices [7]. Although CFD modeling can accurately predict explosive gas zones [6], high computational power and time requirements render its use for real-time ventilation monitoring purposes impossible [9].

As AMS or CFD data reaches mining personnel, it requires human perception to determine risks and precautions to stop any hazard. The data itself either comes as lines and numbers or shows up on the mine layout simulation. Therefore, human interaction is still necessary for hazard mitigation. Data visualization is a crucial part of knowledge extraction and decision-making, and effective visualization will affect users' cognition, reaction, and understanding of the data[10]. Over several decades, researchers such as Bertin [11], MacEachren [12], Morrison [13] , and others have proposed effective data visualization guidelines consisting of visual variables including but not limited to shape, color lightness, and transparency.

Recent technological developments yield novel methods and platforms that provide innovative visualization opportunities for engineers, data scientists, and others [14]. Among the possible platforms,

virtual reality (VR) and augmented reality (AR) options are increasingly preferred as they are not only capable of representing real-world simulations but also delivering insights into the phenomena via an immersive experience.

In the following subsections, the background of the current applications of methane monitoring and AMS systems, CFD modeling and simulation, real-time prediction algorithms of AI, the importance of visualization in decision-making and human perception, and current approaches of mixed reality devices in data visualization are given to set the motivation, goal, and contribution of this dissertation.

1.1. Current Practices of Methane Monitoring in Longwall Mines

The Mine Safety and Health Administration (MSHA) is an agency of the United States Department of Labor (DOL) with oversight of the nation's mining operations. Under MSHA regulations, 30 CFR §27.24 and §75.342, methane monitoring systems and warning devices are to be installed on all face-cutting machines, continuous miners, equipment, and machines that are utilized to extract, load, and transport coal. These warning devices trigger and can shut down equipment when CH_4 concentrations exceed 1.0% and 2.0%, respectively. Moreover, sensors might be installed at critical locations such as the return air end of the longwall face, on shearers, supports, and as close to the cutting heads[15].

1.1.1. Methane Sensors

According to MSHA, methane detector and monitor names are changed based on placement. Current practices of AMS rely on placements of detectors and monitors which has methane sensors in them. Two sensor types are currently utilized in longwall mining faces, i) catalytic bead sensor and ii) infrared sensor.

The vast majority of sensors are catalytic bead sensors. However, these sensors are not reliable when methane concentrations are above 8%. Conversely, infrared sensors are reliable in any concentration range, but they are susceptible to the filter conditions at the entrance of the devices [16]–[19].

Sensor response times of the sensors are another critical part of methane monitoring. While catalytic-type sensors have a response time between 30 - 40 seconds, infrared sensors have a response time between 10 - 30 seconds [16]–[19]. Sensor measurements in the mining literature are considered "real-time" measurements. However, the delay in the measurement is indicated as "near-real-time" for some other topic areas. It should be noted that in Chapter 3, the terms "near-real-time and real-time" are used together, but in Chapter 4, only the term " real-time " is used. Regardless of how it is used, all measurements have unavoidable delays.

1.1.2. Computational Fluid Dynamics

Computational fluid dynamics (CFD) is employed to simulate ventilation conditions in longwall faces to reproduce airflow dynamics and the formation of hazardous gas mixtures which are not detectable using conventional monitoring and ventilation inspection practices [7].

It should be noted that although each mine ventilation condition is unique, previously conducted studies [20][21][22][23][24] validate that simulated data are consistent with the actual situation that includes but is not limited to "(*i*) *continuous leakage of fresh air from the face to the gob, and the higher accumulation of methane as the supplied air travels from the headgate to tailgate side of the face; (ii) higher leakage around the headgate and tailgate corners of the face due to the high porosity and permeability around the edge of the gob; (iii) Methane accumulation seems to follow linear regression based on ventilation surveys done in several longwall operations."* [6]. Although CFD modeling can accurately predict explosive gas zones, high computational power and time requirements render its use for real-time ventilation monitoring purposes impossible [9]

1.2. Real-Time Predictions with Artificial Intelligence

AI is an umbrella term that covers machine learning, natural language processing, expert systems, vision, speech, planning, and robotics. Although significant artificial intelligence (AI) researchers can not agree on its definition, it is a term that, in its broadest sense, would indicate a machine's ability to learn, mimic reason and predict its environment as the human mind [25].

AI proved its value for reliable time-critical, near-real-time/real-time predictions in various areas, such as healthcare, the production industry, autonomous vehicles, aviation, and many other applications. Wang et al. (2010) designed a real-time driving danger-level prediction prototype in which the vehicle's dynamic parameters communicated an audiovisual warning system to the drivers [26]. Kaur and Mann (2018) proposed a proactive framework for the healthcare sector. The algorithm uses patients' data to help the decision-making process of doctors [27]. Lykou et al. (2020) created a tool to detect and predict the most critical airports and flights for the aviation network [28]. Finkeldey et al. (2020) worked with the production industry to optimize the milling process by predicting cutting tools' wear times [29].

There are different methods in the literature that can predict time and value of the parameter. Mainly statistical methods are employed as prediction models like Naïve 2, simple exponential smoothing, HOLT, ARIMA and ETS. The main outcomes for the Naïve 2, simple exponential smoothing and HOLT is that, these algorithms can only predict, within a confidence interval, one step ahead of time. From this project's point of view, it is impossible to implement these algorithms for real-time prediction because each location has approximately 31 million cells. Since every cell is connected to each other and has an effect on methane concentration, these methods fail to deliver accurate predictions. On the other hand, ARIMA and ETS can predict long-term methane concentrations for a specific cell. However, the longwall's geometry is 3D and these statistical methods are not successful in predicting in a 3D environment.

Conversely, ARIMA and ETS can predict long-term methane concentrations for a specific cell. However, the longwall's geometry is 3D, and these statistical methods are not successful in predicting a 3D environment.

AI algorithms were recently introduced for predicting the time and the location of a parameter. It is still a newly studied area as of 2022; however, preliminary results for a range of studies are promising. The

most promising algorithms at the time of this research were Multi-Layer Perceptron (MLP), Bayesian Neural Network (BNN), Radial Basis Functions (RBF), Generalized Regression Neural Networks (GRNN), K-Nearest Neighbor regression (KNN), CART regression trees (CART), Recurrent Neural Network (RNN), and Long Short-Term Memory (LSTM). The MLP, BNN, RBF, and GRNN are statistical-based models and their capabilities are similar to the ARIMA and ETS. KNN and CART algorithms' application areas are so broad they are not considered as viable as their competitors for the time series predictions. Lastly, two new algorithms have been introduced to the literature, namely, RNN and LSTM.

The RNN algorithm uses data to predict the location and variable of the data. On the other hand, the LSTM algorithm uses previously recorded data and readings to predict the location and the parameter content. The main advantages of RNNs and LSTMs are;

i) the algorithm can store information for a specified time duration,

ii) the algorithm is resistant to noise,

iii) the parameters are trainable [30]

RNNs contain cycles from a previous time step as inputs to the network to influence predictions at the current time step. These timestamps are stored in the internal states of the network, which allows RNN to exploit a dynamically changing contextual window over the input sequence history [31] [32].

Unfortunately, the range of contextual information that standard RNNs can access is, in practice, quite limited. The problem is the influence of a given input on the hidden layer, and therefore on the network output, either decay or raise exponentially as it cycles around the network's recurrent connections. This shortcoming is referred to in the literature as the vanishing gradient problem. Long Short-Term Memory (LSTM) is an RNN architecture specifically designed to address the vanishing gradient problem [33].

LSTM architecture performs reasonably well on various datasets and the learning rate and network size are the most crucial tunable LSTM hyperparameters. This implies that the hyperparameters can be tuned independently. In particular, the learning rate can be calibrated first using a fairly small network, thus saving a lot of experimentation time [34]. Related literature (see Section 3.2) supports the long time stamps' effect on the upcoming predictions. Therefore the methane prediction data can be reasonably fitted into that type of architecture.

1.3. Data Visualization: Principles, Variables and Importance in Decision Making

Data visualization has roots dating back more than 7000 years, utilizing visual representation of the data with charts, tables, and graphs [35]. Principles of data visualization are discussed more formally by Cairo [36], Knaflic [37], Ware [38], Tufte [39], and many other talented experts of the 19th Century [40]. The straightforward way to represent data is by visualizing it in two-dimensional x-y space, such as on paper. According to Bertin and Morrison, 2D visual variables have five characteristics: associative, selective, quantitative, ordered, and the length of the variable. These characteristics are defined by variables such as size, color value, color hue, orientation, shape, position, and texture [41]. With the

advancement of technology, data can be represented in three-dimensional space, such as on a computer screen.

While converting 2D visuals into 3D, some additional variables can be applied to increase data understandability. In addition to 2D variables, focus, resolution, spacing, transparency, and perspective height can be added while creating 3D environments [42]. Although numerous studies investigated how to deliver data effectively in a 2D environment, few studies focus on their extended structure with design mechanisms in 3D environments.

The experience of visual variables in a 2D environment differs in many aspects compared to their perception in a 3D environment. In a 3D environment, global mechanisms such as lighting, shading, shadowing, exposure, background and environmental properties can be defined. In data visualization, scene complexity can also be defined by these global mechanisms are affecting factors of the perception. Additionally, change in viewport can impact the recognition and perspective views affects depth of field. [14]. Therefore, expressions of visual variables are tightly linked with global and viewing design mechanisms that define scene complexity hence cognitive load. Like visual variables, cognitive load also affects the perspective and reasoning of the data in a timely manner [43]. Many studies showed that when the cognitive load is low, the learning time and mistakes made are decreased, and data understanding is more rapid [44][45][46][47].

1.4. Virtual Reality and Augmented Reality in Data Visualization and Cognition

Immersive analytics is an emerging field combining data, visualization, immersive environments, and human-computer interaction [48]. With recent developments in technology, the most commonly known immersive environments, VR and AR, equipment also advanced rapidly. Thus, researchers leveraged its newly enhanced benefits, such as sensory advancements and diversified interactions and connections, to support human data understanding and cognitive load[49].

Prouzeau et al. (2020) developed an AR author tool in a VR environment and tested the awareness and decision-making of the users for three use cases, i) equipment debugging, ii) incident playback, and iii) operations simulation. They conclude the toolkit improves efficiency and decreases task errors. However, using a VR device overwhelmed users throughout the experiment [50]. Lee et al. (2021) tested the effect of 3D objects and surfaces in VR on visualization tasks and found that the VR environment helped share findings and increased user awareness [51]. However, the researchers only used specific objects and surfaces and did not investigate in depth for visualization variables. Liu et al. (2020) conducted a study on the effects of the layout with a different number of objects in VR settings for executing the tasks. They suggested that, with low-intensity (simple) data, 2D or flat layouts perform better in visualizing the data. On the other hand, with increasing the dimensions and complexity of the data, users became disoriented while executing the tasks [52]. However, they did not investigate different types of 3D visualization parameters. Satriadi et al. (2019). investigated a hybrid approach for input management in AR for task completion. They implemented hand gestures for data examination. Users

successfully examined the data, but the task completion time did not improve [53]. Researchers did not take into account the cognitive aspects of the inversive environment. Ivanov et al. (2018) examined the potential unit visualization in VR to see how these visuals aided users in data exploration. They successfully imported and tested the data but reported a few problems, including disorientation and unpleasant user experiences [54], since they did not consider the visualization parameters while building the models.

Whitlock et al. (2020) compared data understandability using a computer screen and VR. They used synthetic data with different visual parameters such as color, size, and orientation to test the understandability, finding users perform and feel better while working with the low-intensity data. However, with the high-intensity data, users got disoriented and failed to examine the data [55]. Researchers tried to test the different visual parameters; however, they only considered the 2D visual variables for the immersive environment. Yang et al. investigated the presentation of data as 2D and/or 3D in an AR display. They did not encounter any downsides while working with 2D data in simple surfaces and textures. However, they noted that if the data is not homogeneously distributed, the scale of the visuals obstructs users' perception and understandability [56].

The studies [50], [53], [54], [56], and [57] did not take into account the principles of visualization in any dimensional space. On the other hand, studies [51] and [52] used the 2D visualization principles but did not test its effects on perception, attention, and cognitive load to users in the immersive environment. Lastly, [55] compared color, size, orientation, height, and depth as visual parameters, though they did not consider scene complexity effects on perception like background visual parameters testing in the immersive environment.

The Association for Computing Machinery (ACM) Conference on Human Factors in Computing Systems (CHI) is one of the most prestigious [58] conferences in human-computer interaction. CHI published a workshop paper at the CHI2021 conference entitled "Grand Challenges in Immersive Analytics" in which the gaps are discussed by 24 different groups of experts in their respective fields of expertise. The researchers point out 17 current key challenges and gaps for the future of the research field. These challenges can be categorized into four different headings: spatially situated data visualization, interacting with immersive analytics systems, collaborative analytics, and *user scenarios and evaluation* [59]. All these categories have a common area which is adopting visualization principles into immersive environments.

1.5. The Research Goal

Detecting the formation of explosive methane-air mixtures at a longwall face is still a challenging task. Even though atmospheric monitoring systems are utilized for real-time methane measurements, they are not sufficient as a warning system in critical regions such as near-cutting drums. Moreover, computational fluid dynamics modeling is used to inspect methane concentrations in critical regions but is behind in real-

time capabilities. Furthermore, the methane measurements and predictions are hard to understand for fast response and hazard mitigation purposes.

This dissertation aims to combine the strong sides of the AMS and CFD to have accurate 3D methane predictions in real-time to prevent explosive methane accidents. Moreover, by providing easy-to-understand visuals, this dissertation aims to help mining personnel to investigate the 3D real-time methane data faster and more accurately.

1.6. Research Questions

There are several research questions in this dissertation and the associated reasons to explore the answers to these questions:

1. What is the appropriate AI method to utilize for 3D methane concentration predictions in real-time?

This question hypothesizes that deep learning-based algorithms can be promising for 3D methane predictions in real-time. AI's real-time prediction capabilities are promising in various fields but have not been implemented for ventilation monitoring purposes. Therefore the capabilities and applicabilities need to be investigated among the advantages and disadvantages of different approaches.

2. How can the best AI algorithm be adapted for methane monitoring for accurate, 3D, and real-time methane predictions?

This question hypothesizes that with modifications to the long-short term memory algorithm, CFD and methane sensor data can be used to predict methane concentrations in 3D and real-time. The algorithms in the literature are optimized for generalized uses, including but not limited to image prediction and sensor data. CFD data and methane monitors are unique datasets with underground mining environments. Although there are minor similarities, in general, extensive modifications are needed for 3D methane predictions in real-time.

3. What are the best ways to visualize prediction data for accurate and fast assessment for users in the field?

This question hypothesizes that instead of conventional visualization methods, emerging technologies such as VR and AR might help increase volume estimation accuracy and decrease assessment time hence cognitive load. AI predictions consist of lines and numbers. They need to be converted into visuals to be understood by humans. In the literature, there are guidelines on how to visualize data, but with emerging technology, new visualization platforms are utilized for data visualization. There might be better options for accurate and faster assessment of methane concentrations.

1.7. The Original Contribution of the Dissertation

AI predictions of 3D real time methane monitoring have not been achieved yet despite AI’s promising results in other fields. In this dissertation, the possible AI algorithms’ success is presented for this

application. This research provides the first exploration of different AI architectures for 3D real-time methane prediction in longwall coal mines.

It is known that any AI architecture is developed and aimed at general purposes. This dissertation presents how to modify an architecture that can be trained with CFD simulations and predict the methane concentrations for 3D longwall faces.

Lastly, data visualizations and visual variables are well-defined for conventional methods (white paper and computer screen) but not studied in AR and VR. This dissertation presents the effects of visual variables on data understandability by comparing computer screens, AR, and VR via a user study.

1.8. Structure of the Dissertation

This dissertation has seven chapters. Chapter 2 introduces the overall research methodology followed in this dissertation. Chapter 3 presents the exploration of different AI architectures. Chapter 4 presents the adaption of the best performing AI algorithm and its modifications for 3D and real-time methane predictions. Chapter 5 compares the conventional visualization methodology with the AR and VR platforms. Chapter 6 presents real-life implementation in an underground mine. Finally, Chapter 7 presents the overall conclusions of this dissertation and recommendations for future work.

CHAPTER 2

METHODOLOGY

Methane emissions and monitoring have a critical role in the longwall coal mines. Mine personnel uses point sensor reading and CFD simulation outputs to determine the explosive methane occurrences. Since sensors can not cover all mining areas and CFD models lack real-time data stream, this dissertation seeks to combine the strengths of point sensors and CFD models by following four main steps that constitute the overall research methodology (Figure 2.1).

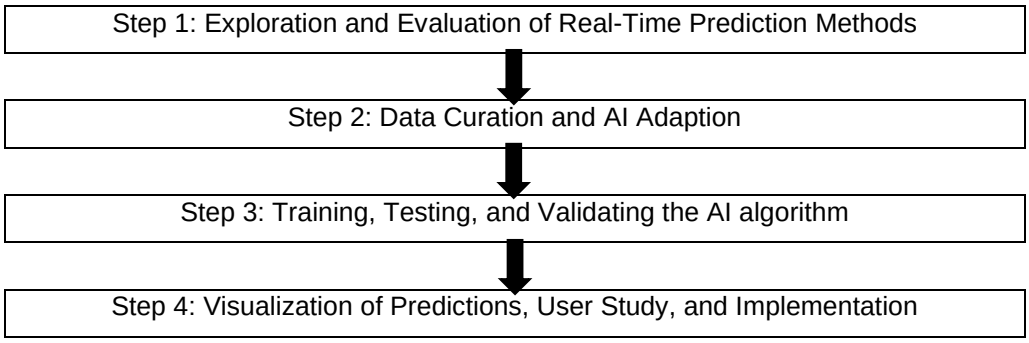

Figure 2.1 Overall research methodology

In the first step, we explore possible real-time prediction methods and evaluate appropriate approaches. We select ten out of 30 possible architectures based on their success with similar data sets. We then test these algorithms with sample CFD simulation data sets to see which AI architectures are suitable for the objectives of this research. This step seeks to answer Research Question 1: “What is the appropriate AI method to utilize for 3D methane concentration predictions in real-time?”, and is discussed in Chapter 3.

In the second step, we utilize Ansys Fluent software version 18.2 to model and simulate a longwall face with a 300-meter width, a mining height of 3 m and a depth of 6 m. We also model two primary pieces of equipment: (i) support equipment (shields) and (ii) cutting equipment (shearers). We exemplify the simulation by a transient CFD model of methane gas emission from the coal face based on a bleeder ventilation system with a tailgate (TG) back return setup. We simulate each transient model for 180 seconds and record at one-second intervals. The data contains methane concentration, measurement time, air velocity, and cell volume. The implementation of this step is further explained in Chapter 4.

In the third step, we modify the long-short term memory (LSTM) architecture based on the needs of this dissertation’s data and objective, including; input type modification, parameter optimization, solver type modification, layer architecture, and function alteration. Finally, we train, test, and validate AI with the data curated in the second step. This step seeks to answer *Research Question 2: “How can the best AI*

algorithm be adapted for methane monitoring for accurate, 3D, and real-time methane predictions?", which is presented in Chapter 4.

In the fourth and final step, we convert predictions into visualizations, and conduct a user study. We test visual variables to investigate the effects on reaction time and assessment accuracy. Moreover, we compare the saliency maps of the simulations with eye-tracking data. Finally, we test the applicability of the AR platform in an underground mine. This step seeks to answer *Research Question 3*: *"What are the best ways to visualize prediction data for accurate and fast assessment for users in the field?",* and is discussed in Chapters 5 and 6.

CHAPTER 3

EXPLORATION AND EVALUATION OF REAL-TIME PREDICTION METHODS

An article published in the CIM Journal

Doga Cagdas Demirkan[1,2], H. Sebnem Duzgun[2], A. Juganda[2], J. Brune[2], G. Bogin[3]

This chapter addresses Research Question 1: “What is the appropriate AI method to utilize for 3D methane concentration predictions in real-time?” by exploring and evaluating the real-time prediction methods as stated in Step 1 of the overall methodology in this dissertation (see Figure 2.1).

3.1. Introduction

Atmospheric Monitoring Systems (AMS) are critical in underground coal mine ventilation designs where methane explosion hazards can develop. The number and location of sensors are important for ventilation monitoring. AMS sensors should be installed near the most critical locations including the shearer cutting drum and along the longwall face. Sensors can provide information for a limited area, and their readings may have delays caused by sensor response time, gas diffusion rate, and temperature. Computational Fluid Dynamics (CFD) modeling can provide relatively accurate predictions, however, it requires significant computational resources and time, which is not conducive to real-time decision-making. This paper evaluates artificial intelligence (AI) systems in predicting near-real-time explosion hazards. The prediction performance of ten-time series algorithms are compared by using seven different data sets., and assessed by classification accuracy. It is found that accurate, real-time/near-real-time methane predictions are possible with the HIVE-COTE, ROCKET and RISE algorithms. Initial results demonstrate that near-real-time decision-making for explosive hazard warning systems is accurate and robust and AI modeling of explosion hazards enhances mine safety.

3.2. Overview of the AI Models for Time Series Data

Time series forecasting (TSF), time series classification (TSC), or time series analysis (TSA) are subsets of machine learning (ML) methods used to predict future values based on previously observed measurements [60]. Evaluation of these data can be used to predict near-real-time/real-time future values [61][62]. In 2002, researchers from the University of California Riverside (UCR) released the first univariate archive containing 128 different time series data sets [63]. After a short period of time,

[1] Corresponding author. Direct correspondence to demirkan@mines.edu
[2] Mining Engineering Department, Colorado School of Mines, 1500 Illinois St., Golden, CO 80401, USA
[3] Mechanical Engineering Department, Colorado School of Mines, Golden, CO 80401, USA

researchers from the University of East Anglia (UEA) released 30 different multivariate time series data sets [64]. Later on, the Alan Turing Institute in the United Kingdom contributed to the research with TSC algorithms. Even if there is still limited literature on TSC, this research demonstrates the potential of implementing AI models for time series prediction. Fawaz et al. [65] suggested that TSC could potentially be improved if the model is fine-tuned from pre-trained models. Meanwhile, Ye and Dai [66] tested nine different algorithms on nine different data sets, and Gupta et al. [67] adopted a universal time-series feature extractor, called TimeNet [68], to health care tasks. Research shows that it is possible to achieve accurate real-time/near-real-time predictions with a limited data set.

Based on previous research, the most commonly used and successful AI models are, Word ExtrAction for time SEries cLassification (WEASEL) [69], Bag of SFA Symbols (BOSS) and Bag of SFA Symbols in Vector Space (BOSS-VS) [70], Time Series Forest (TSF) [71], Hierarchical Vote Collective of Transformation-based Ensembles (HIVE-COTE) [72] and Time Warp Edit Distance (TWED) [73]. Table 3.1 represents a summary of algorithm taxonomy by data characteristics, and Table 3.2 lists the problem types and best-performing algorithms for each problem type.

Bagnall et al. (2017) suggested that there were several ways to group the algorithms; however, classifying algorithms based on their outputs was the most convenient way to apply them for the purpose of this research. The algorithm categories mentioned in Table 3.1, namely "Whole Series," "Intervals," "Shapelets," and "Dictionary," are the main types of outputs. Whole Series compares two series either in a vector form or by distance measure. Intervals use one or more intervals of the time data and extract features. Shapelets focuses on finding short patterns and defines classes. Dictionary searches for frequency and/or repetition of data.

In Table 3.2, the problem types and best-performing algorithms are also categorized by the authors. The problem types, namely, "Image," "Sensor," "Motion," "Spectrographs," Electric Devices," "ECG," and "Simulated," combine all 158 data sets in generalized fields. The *image* problem contains measurements of digital images in red, green, and blue (RGB) bands. The s*ensor* problem contains a range of sensor data, including but not limited to chemical composition sensors and electrical current sensors. *Motion* includes motion capture camera data. *Spectrographs* contains digital images like the *Image* problem but have more bands besides RGB. *Electric Devices* covers the measurement of various household equipment's (e.g., coffee machine, refrigerator, etc.) power usage. The *ECG* problem contains measurements of the electrical activity of the heart. Lastly, the *Simulated* problem contains all the simulated data sets.

In Table 3.2, the best-performing algorithms by each problem type are given. All Dictionary, Interval, and Shapelet algorithms yield similar results. Therefore, the names of the algorithms are not explicitly given. On the other hand, COTE, EE, and SAXVSM results significantly differ from their main group algorithms; thus, the results of these algorithms are given explicitly.

Table 3.1 TSC Algorithms by Data Characteristics: weighted DTW (WDTW); time warp edit (TWE; move–split–merge (MSM); complexity invariant distance (CID); derivative DTW (DD_{DTW}); derivative transform

distance (DTD_C); elastic ensemble (EE); time series forest (TSF); time series bag of features (TSBF); learned pattern similarity (LPS); fast shapelets (FS); shapelet transform (ST); bag of patterns (BOP); SAX vector space model (SAXVSM); bag of SFA symbols (BOSS); DTW features(DTW_F); collective of transformation-based ensembles (COTE), adapted from [74]

Whole Series	Intervals	Shapelets	Dictionary
WDTW	TSF	FS	BOP
TWE	TSBF	ST	SAXVSM
MSM	LPS	LS	BOSS
CID		COTE	DTW_F
DD_{DTW}			
DTD_C			
EE			
COTE			

Table 3.2 Best Performing Algorithms by Problem Type, adapted from [74]

Problems/ Algorithms	COTE (%)	Dictionary (%)	Elastic (EE)(%)	Interval (%)	Shapelet (%)	Vector (SAXVSM) (%)	Number of the data sets
Image	20.7	17.2	**24.1**	0.00	17.2	20.7	29
Sensor	**38.9**	0.00	16.7	5.56	22.2	16.7	18
Motion	**35.7**	21.5	14.3	14.3	14.3	0.00	14
Spectrographs	0.00	0.00	0.00	0.00	0.00	**100**	7
Electric Devices	0.00	33.3	0.00	16.7	**50.0**	0.00	6
ECG	33.3	16.7	0.00	0.00	**50.0**	0.00	6
Simulated	**40.0**	20.0	20.0	0.00	20.0	0.00	5

In TSC, there are two different methods for forecasting near-real-time/real-time values, namely "point-based" or "whole dataset" forecasting. The point-based is a more straightforward approach, and the idea behind it is that the predictions are based on individual points inside the data set. On the other hand, in the whole data set prediction approach, all data points have an influence on each other depending on their location, size, and measurement content. Testing and validation of the "whole dataset" approach is given in more detail in Section 4. The models that are used in this research are HIVE-COTE, ROKET, TS-CHIEF, Inception Time, Res-Net, ST, WEASEL, Proximity Forest, TSF, and RISE. The main reason that we chose these algorithms is that they are either the best-performing or the most promising options with data sets similar to those used in this study.

HIVE-COTE uses a modular hierarchical meta-ensemble structure. It is proposed mainly to overcome the design bias by modularizing the elements of each group of classifiers. It allows only a single probabilistic prediction from each domain. The algorithm acts as combining module predictions into one overall estimate [72]. HIVE-COTE was chosen since this algorithm performs best in three problem types, and hence it was worthwhile to be tested further in the underground longwall mine dataset.

ROCKET transforms time series using a large number of random convolutional kernels, i.e., kernels with random length, weights, bias, dilation, and padding. The transformed features are used to train a linear classifier. The combination of ROCKET and logistic regression forms a single-layer convolutional neural network with random kernel weights, where the transformed features form the input for a trained layer [75]. The high-level objective of this study is to create a real-time/near-real-time explosive hazard warning system. ROCKET algorithm proposes a faster training and prediction methodology. Therefore, we think that this algorithm also needs to be tested.

TS-CHIEF is an ensemble algorithm that couples the tree classifiers with the accuracy for time series classification. Traditional attribute-value decision trees form a tree by recursively splitting the data in regard to the significance of a selected attribute [76]. TS-CHIEF algorithm is proposed as a rival to the HIVE-COTE algorithm. The authors suggested that HIVE-COTE outperforms TS-CHIEF both in accuracy and prediction time.

Res-Net is a residual learning framework for more straightforward training of networks that are substantially deeper than before. Instead of learning unreferenced data, Res-Net simplifies and reformulates the layers as learning residual functions with reference to the layer inputs. It proves that these residual networks are easier to optimize and gain accuracy from considerably increased depth [77]. Res-Net suggests a more straightforward training and an easier-to-optimize algorithm. Therefore, the algorithm proposes a fast implementation to new data sets.

Inception Time consists of an ensemble of five different Inception networks initialized randomly. The composition of an Inception network classifier contains two different residual blocks, as opposed to ResNet, which is comprised of three. For the Inception network, each block consists of three Inception modules rather than traditional fully convolutional layers. Each residual block's input is transferred via a shortcut linear connection to be added to the next block's input, thus mitigating the vanishing gradient problem by allowing a direct flow of the gradient [78]. Inception Time is the most recent rival of the Res-Net. To compare both with our data set, we add the Inception Time algorithm.

STC extracts the k best shapelets from a data set in a single pass and then uses these shapelets to transform data by calculating distances from a series to each shapelet [79]. This algorithm proposed a self-clustering algorithm. Since the data labeling is time-consuming, and the end goal is to create a real-time prediction model, unsupervised learning also needs to be tested.

WEASEL transforms time series into feature vectors using a sliding-window approach, which is then analyzed through a classifier. Method for deriving features, resulting in a much smaller yet much more discriminative feature set. It is more accurate than the best current non-ensemble algorithms at orders-of-magnitude lower classification and training times, and it is almost as accurate as ensemble classifiers, whose computational complexity makes them inapplicable even for midsize datasets [69]. WEASEL algorithm is the best performing algorithm under the Vector type models. Among all algorithms, this algorithm is the most suitable to test with this study's data set.

Proximity Forest models are ensembles of highly randomized Proximity Trees. In contrast, conventional decision trees branch on attribute values and usually perform poorly on time series. Proximity Forest gains both efficiency and accuracy by the stochastic selection of both exemplars and similarity measures [80]. This algorithm is based on one of the major AI models, namely the decision tree. Therefore, this type of model needs to be considered.

TSF overcomes the considerable interval feature space problem by employing a random forest approach, using summary statistics of each interval as features. Training a single tree involves selecting random intervals, generating the mean, standard deviation, and slope of the random intervals for every series then creating and training a tree on the resulting features. Classification is a majority vote of all the trees in the ensemble [71]. This algorithm is the best-performing algorithm in the Interval algorithm class.

RISE is a recently introduced tree-based time series classification algorithm in which each tree is built on a distinct set of Fourier, autocorrelation and partial autocorrelation features. This is prohibitively slow when considering long series, which are common in audio classification problems, where spectral approaches are likely to perform better than classifiers built in the time domain [78]. RISE is the recent tree-based algorithm that shows accurate and robust results.

3.3. Data Preparation

In this paper, we collected previous AMS readings and CFD inputs and outputs, and process them as data sets for training and testing the AI models. In Table 3.3, the AMS data set named "C" contains five fixed methane sensor readings inside a mine face. The measurements are taken every minute throughout the 24-hour time period. Since this data set comes from an actual working mine, the geometry and other parameters' details cannot be disclosed.

CFD modeling simulates the real environment by creating the geometry, applying the volume of fluids, and defining the physical parameters and boundary conditions. Along with the pre-processing steps, CFD modeling identifies critical areas where ventilation needs to be monitored and helps with mining ventilation and methane monitoring. [7].

Table 3.3 shows the data sets exported from the previously conducted CFD simulation with their data size and timestamps. The geometry in that simulation is shown in Figure 3.1, which has dimensions of 300, 30, and 3 m in x, y, and z coordinates, respectively. In addition to that, there are 31 million cells that create the internal geometry and simulate flow. The cells contain, including but are not limited to local coordinates of x,y, and z, methane concentration by volume, pressure, turbulent parameters, and flow velocity. However, for AI training purposes, we obtained only the coordinates and methane concentration by volume as data sets for this research and each data set is shown in Table 3.3.

Table 3.3 represents the data sets extracted from the initial simulation, literature, and experimental data. These data sets are named A-10, A-20, A-29, A-M, A-L, and A-V. The Chlorine data set was taken from the literature and used for benchmarking, as explained in Section 3.4. Lastly, data set C was taken from an operating mine. The A-10 dataset contained 10 random points extracted from the CFD simulation

with 20 timestamps each. The recording time stamps were one second apart from each other. Similarly, data sets A-20 and A-29 had 20 and 29 points with 20 timestamps each. The data set *A-M* was taken next to the TG drum, where the methane fluctuation is the highest. The data set *A-L* was taken horizontally to the ground plane with five equally distanced parallel planes (1 m each) and contained 53,500 points. The planes expanded the entire width of the face. Lastly, the data set *A-V* was extracted in vertical planes equally distanced (20 meters) from each other and contains 1000 points.

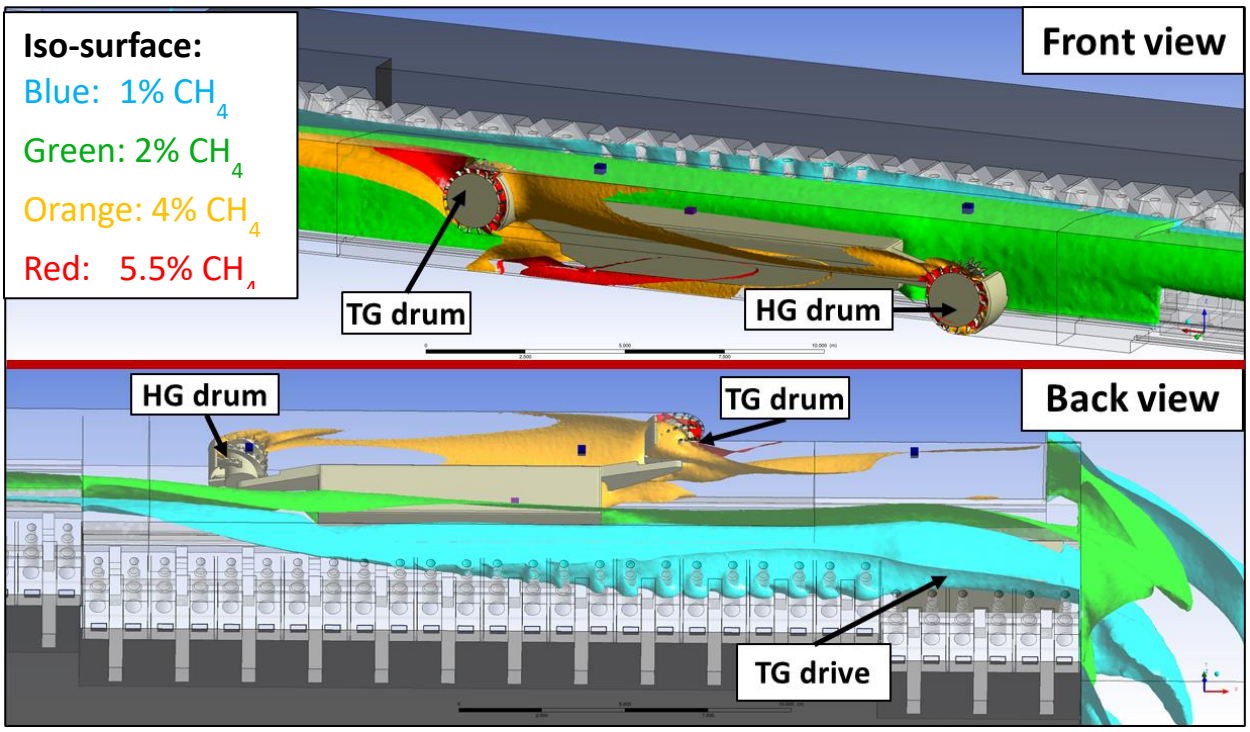

Figure 3.1 CFD Simulation Geometry of a Longwall Coal Mining Face. Colors represent the boundaries of regions with CH4 concentrations. Note that concentrations in orange are near-explosive, and those in red are explosive (Modified from [6]).

Table 3.3 Longwall face Ventilation CFD Data Sets

Dataset Name	Explanations
Chlorine	Data size: 166 points Timestamp: 4310 Source: [74]
A-10	Data size: 10 points Timestamp: 20 Source: CFD model result Horizontal line sampling
A-20	Data size: 20 points Timestamp: 20 Source: CFD model result Horizontal line sampling
A-29	Data size: 29 points Timestamp: 20 Source: CFD model result Horizontal line sampling
A-M	Data size: 20 points Timestamp: 20 Source: CFD model result Horizontal line sampling
A-V	Data size: 1000 points Timestamp: 20 Source: CFD model result Horizontal line sampling
C	Data size: 5 points Timestamp: 1440 Source: CH4 sensor
A-L	Data size: 53500 points Timestamp: 20 Source: CFD model result Vertical line sampling

While Table 3.3 shows the available data sets and their explanations, Figure 3.2 (a-b) shows A-V and A-L data set sampling, respectively.

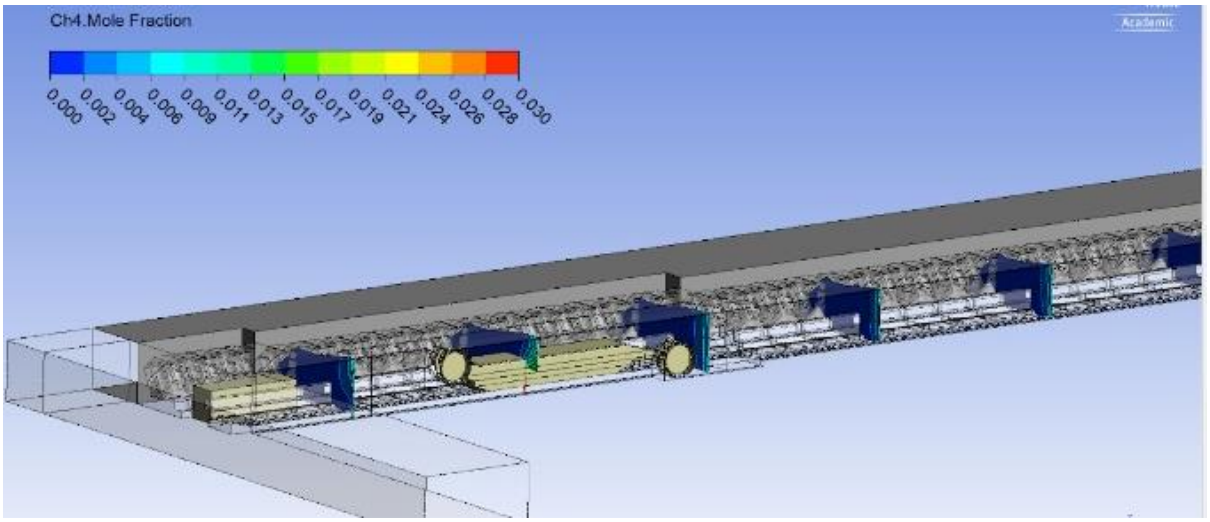

(a) A-V data set

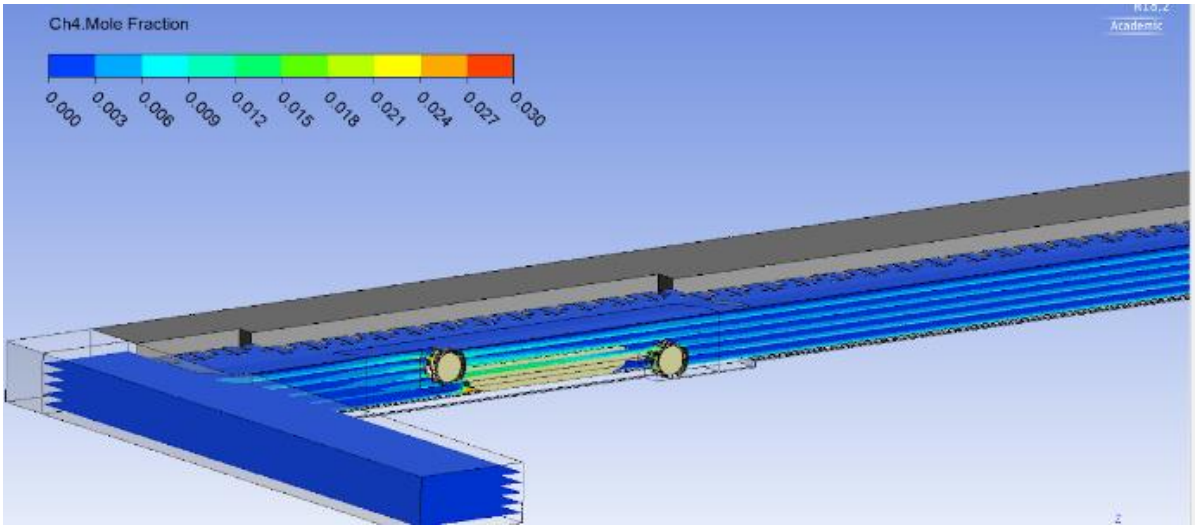

(b) A-L data set

Figure 3.2 Visual representation of the extracted points

Although data extraction was done in verticle and horizontal sampling with varying distances, it should be noted that verticle data collection is more challenging in mining environments. The reason behind that is the constant movement of the cutting (shearer) and support (shields) equipment.

3.4. Benchmarking

The algorithms discussed in Section 3.2 were tested with 158 different data sets. The "*Chlorine*" data set was tested with the algorithms used in this research. It was chosen because of its similarity to CFD methane and the EGZ data set, such as time, location, and measurement constraints. This data set was

used for benchmarking the algorithms. The data set contained x and y coordinates and the chlorine content of the measurement location. There were some differences between the CFD methane dataset and the Chlorine data set geometrically, the CFD methane data set was 3D, whereas the Chlorine data set was 2D in terms of geometry. The second difference was that the CFD methane data set contained the flow velocity of the flow, while Chlorine did not. However, the Chlorine data set was the closest to the methane readings among other data sets.

Table 3.4 shows the results of the Chlorine data set. It should be noted that the overall accuracies of the algorithms were the same as the original papers [74]. Therefore, we can say the algorithms were built and fine-tuned as suggested.

Table 3.4 Accuracies for the Chlorine Data Set

HIVE-COTE	ROCKET	TS-CHIEF	Inception Time	Res Net	STC	WEASEL	Proximity Forest	TSF	RISE
0.75	0.83	0.65	0.84	0.84	0.73	0.72	0.62	0.72	0.77

3.4.1. Training, Testing, and Validation

After data acquisition and benchmarking, the data sets were pre-processed by deleting unnecessary information, followed by conversion into a readable format by the algorithms. It should be noted that the algorithms were trained, optimized, and tested with 158 different data sets without any modification. This method helped researchers to generalize and benchmark the performance of the algorithms on time series data sets. Although optimizing the algorithms for the specific data sets might yield higher accuracy and performance, it could disturb the nature of the benchmarking.

The high-level objective of this study was to create a near-real-time prediction of Explosive Gas Zones (EGZs), as discussed earlier. According to the National Institute for Occupational Safety and Health (NIOSH) (2013), if the CH4 concentration in the air exceeds 5% by volume, there can be an explosive hazard [81]. Based on the explosive zone definition in the literature, every point in the data set was labeled by the thresholding method, where, if the CH4 readings exceed the lower explosive level (5%) at any given time, it is classified as "1" - indicating "EGZ warning." On the contrary, if the methane value was smaller than the lower explosive level (5%), it was classified as "0", which means no EGZ warning.

After labeling, we split the data sets into training, validation, and test sets. The training, test, and validation split was done by the recommendations for the original algorithms, which were roughly 60%, 20%, and 20%, respectively. It should be noted that each data set had a different number of data points and each data point had a different number of time intervals. The breakdown of the data points and time steps are given in Table 3.5. The total number of data points is obtained by multiplying points and time

steps. For example, the data set A-10 had ten different x,y,z coordinates as points, each point with 20 different time steps, equaling a total of 200 data points (Table 3.5). The algorithms take into account all the points and times while learning and predicting. The exact split numbers for each data set are given in Table 3.5.

Table 3.5 Number of methane data points for each dataset

Dataset Name	# of Total Data Points	# of points in Training Set	# of points in Validation Set	# of points in Test Set
A-10	200	120	40	40
A-20	400	240	80	80
A-29	580	350	115	115
C	7200	4320	1440	1440
A-M	400	240	80	80
A-L	20000	12000	4000	4000
A-V	1070000	642000	214000	214000

3.5. Results

One of the most critical factors for getting a robust real-time/near-real-time prediction is the number of data points. Bagnall et al. (2017) suggested at least 30 points are needed for meaningful results in time-series predictions. To test our datasets as well as the suggestion, we did the testing with seven different datasets using the models of HIVE-COTE, ROKET, TS-CHIEF, Inception Time, Res-Net, STC, WEASEL, Proximity Forest, TSF, and RISE.

The results showed that the algorithm cannot be trained with six points, more specifically the A-10 data set, to classify the unknown points. On the other hand, increasing the number of points increased the algorithm's training performance, which yielded a higher classification accuracy. In Table 3.6, the confusion matrix for the *A-10* and *A-20* tests with the HIVE-COTE algorithm is given to show the drastic change in increasing the number of points and the effect on accuracy.

Table 3.6 10-point and 20-point test with HIVE-COTE algorithm for 20-time instances

10 Point Test with 20 Time Stamp – HIVE-COTE

	Explosive Zone	Safe Zone		
Explosive Zone	7	4	Sensitivity	63.6%
Safe Zone	12	17	Specificity	58.6%
	Precision	Recall		
	36.8%	81.0%		Overall Accuracy: 60.0%

20 Point Test with 20 Time Stamp – HIVE-COTE

	Explosive Zone	Safe Zone		
Explosive Zone	16	3	Sensitivity	84.2%
Safe Zone	9	52	Specificity	85.3%
	Precision	Recall		
	64.0%	94.6%		Overall Accuracy: 85.0%

Figure 3.3 shows the train-validation losses for data set A-10 for the HIVE-COTE algorithms. As it is expected and can be seen in Table 3.6, training of the models was not sufficient for the A-10 data set with 40 training points and yielded low accuracy with all the algorithms as compared to the literature.

Figure 3.4 demonstrates the train-validation losses for data set A-20 for the HIVE-COTE algorithms. According to the A-20 dataset train-validation curve, the learning was improved; hence the accuracies were also improved. In general, as the amount of data acquisition points and temporal information increase, the 'algorithms' performances improve. Besides the number of data points, we saw that a minimum timestamp was needed to fully train the model while testing these algorithms. In our case, training and testing with 800 data points yielded consistent results.

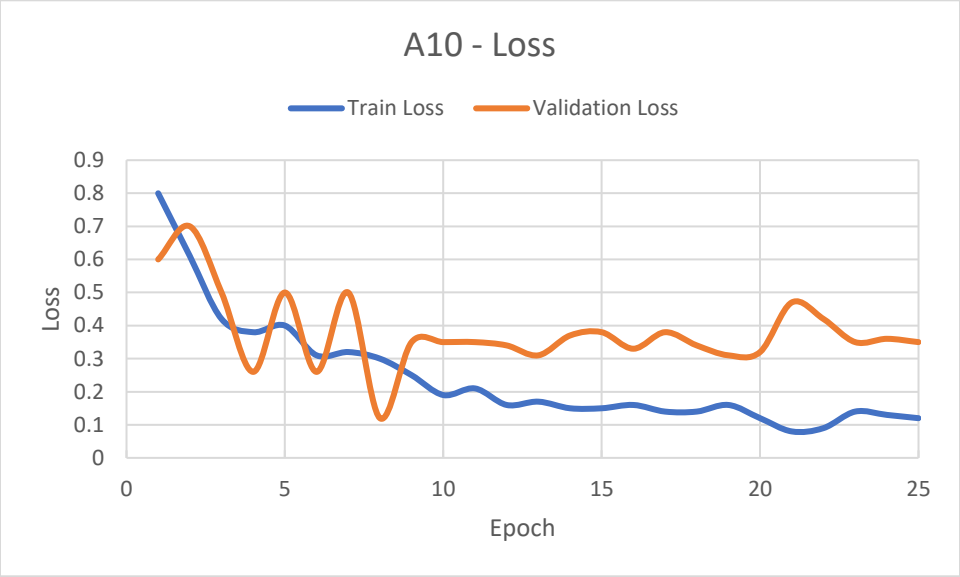

Figure 3.3 Train – Validation Loss of A-10 data with HIVE-COTE Algorithm

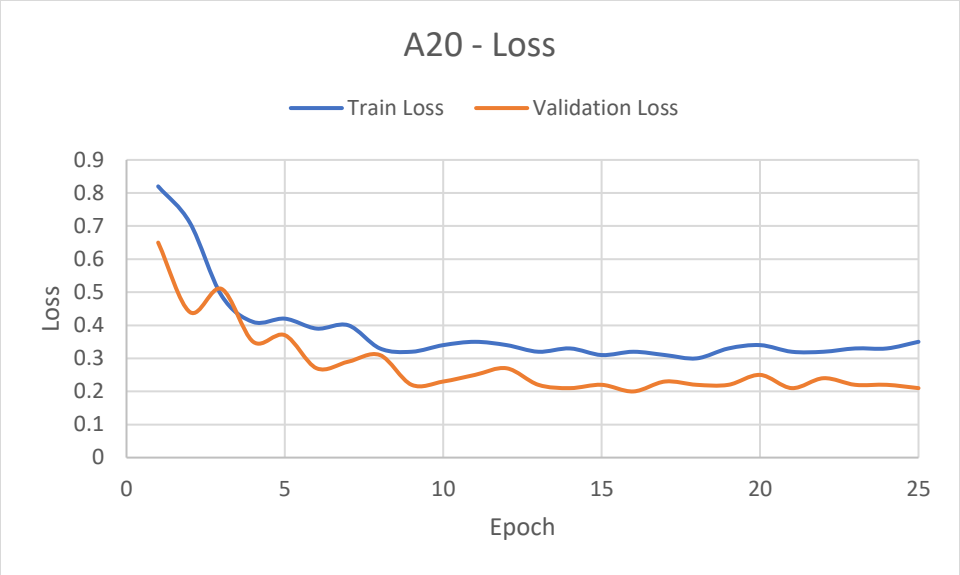

Figure 3.4 Train – Validation Loss of A-20 data with HIVE-COTE Algorithm

The hardware used for this study included a high-end gaming PC with the following specs; CPU: 10th Generation Intel Core i7-10875H (8-Core, 16MB Cache, up to 5.1GHz w/ Turbo Boost 2.0), GPU: NVIDIA(R) GeForce RTX(TM)2070 8GB GDDR6, Memory:32GB DDR4 2666MHz, Storage: 2TB PCIe M.2 SSD. The training of each algorithm took around six hours, and the prediction time was 30 seconds. As the near-real-time/real-time awareness is of utmost importance in hazard prevention, the 30 seconds of each prediction is suitable for use in real-life in terms of efficiency.

Table 3.7 shows the accuracies of the best-performing algorithms with different datasets. The given accuracies were calculated by dividing the total correctly predicted data by the total number of points for each data set. An example calculation is shown in detail in Table 3.6.

The ROC curves for these algorithms are presented in Figure 3.5. As seen in ROC curves, HIVE-COTE and RISE algorithms performed the best in predicting the methane concentration in a given data set.

Table 3.7 Accuracies of Best Performing Algorithms with Different Datasets

Data/ Model	HIVE-COTE	ROCKET	TS-CHIEF	Inception Time	Res Net	STC	WEASEL	Proximity Forest	TSF	RISE
A-10	0.60	0.70	0.65	0.70	0.55	0.80	0.70	0.55	0.75	0.80
A-20	0.95	0.75	0.80	0.70	0.85	0.90	0.80	0.90	0.8	0.85
A-29	0.95	0.75	0.85	0.75	0.75	0.85	0.85	0.90	0.8	0.85
C	0.93	0.92	0.90	0.92	0.90	0.95	0.93	0.75	0.92	0.97
A-M	0.80	0.90	0.80	0.15	0.8	0.15	0.45	0.35	0.35	0.85
A-L	0.98	0.99	0.98	0.92	0.99	0.94	0.51	0.48	0.84	0.99
A-V	0.92	0.88	0.89	0.87	0.89	0.91	0.85	0.69	0.87	0.93

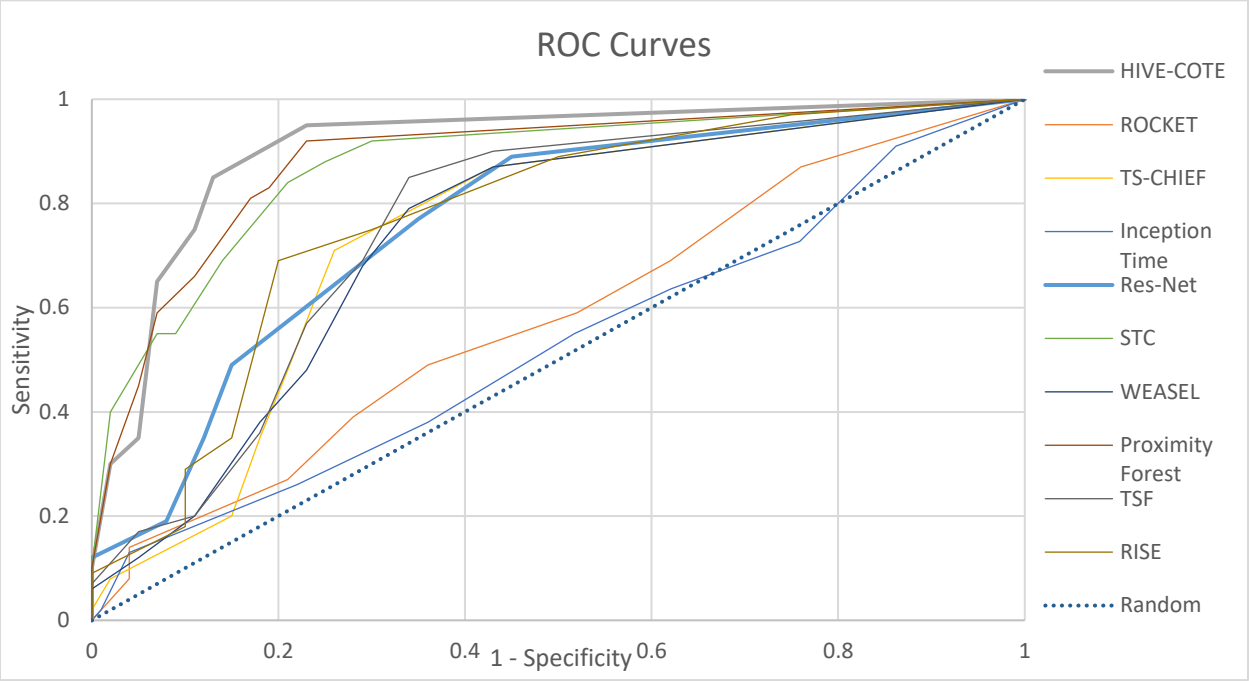

Figure 3.5 ROC Curves of the Algorithms

3.6. Conclusions

Monitoring CH4 is one of the most critical tasks in underground coal mining, requiring constant attention. This paper provided a new perspective on real-time and near-real-time explosion hazard predictions using artificial intelligence (AI) through traininig and testing time series classification and prediction models and comparing their performance to Computational Fluid Dynamics (CFD) models.

The test results indicate that RISE and HIVE-COTE algorithms match the CFD data well. AI computational times are close to real-time and much faster than CFD modeling. A key finding is that the CH4 concentrations obtained from either AMS sensor data or CFD modeling can be treated as time-series data for real-time or near-real-time prediction of explosion hazards. This is essential, as the AI model can be used to shut down mining equipment if explosive atmospheres are detected. A suitable model for time and location is critical for the prediction of explosive gas zones. We also tested the other algorithms for the prediction, but the accuracies were not robust and required further research. The data collection locations and intensities had an influence over the performance of the algorithms, ROCKET, TS-CHIEF, InceptionTime, ResNet, STC, WEASEL, Proximity Forest, and TSF. On the other hand, HIVE-COTE and RISE algorithms were more resilient to the data collection location and number of samples.

Given only the location, time, and methane content, AI models provided good flexibility and can provide essential support for explosion hazard detection. Exporting additional data sets with more

information might help to increase accuracy. Moreover, adapting the best-performing algorithm for the specific purpose of methane prediction might yield more robust and reliable results. In the next chapter, these modifications are discussed and tested.

CHAPTER 4

DATA CURATION AND LONG SHORT TERM MEMORY (LSTM) ADAPTION

An article published in Energies Journal Special Issue Volume II: Mining Innovation

Doga Cagdas DEMIRKAN[4,5], H. Sebnem Duzgun[5], A. Juganda[5], J. Brune[5], G. Bogin[6]

This chapter addresses Research Question 2: “How can the best AI algorithm be adapted for methane monitoring for accurate, 3D, and real-time methane predictions?” by focusing on data curation and the adaption of the Long Short Term Memory (LSTM) algorithm. Steps 2 and 3 of the overall methodology of this dissertation (see Figure 2.1) are explained in the following sections.

4.1. Introduction

Detecting the formation of explosive methane–air mixtures in a longwall face is still a challenging task. Even though atmospheric monitoring systems and computational fluid dynamics modeling are utilized to inspect methane concentrations, they are not sufficient as a warning system in critical regions, such as near cutting drums, in real-time. The long short-term memory algorithm has been established to predict and manage explosive gas zones in longwall mining operations before explosions happen. This paper introduces a novel methodology with an artificial intelligence algorithm, namely, modified long short-term memory, to detect the formation of explosive methane–air mixtures in the longwall face and identify possible explosive gas accumulations prior to them becoming hazards. The algorithm was trained and tested based on CFD model outputs for six locations of the shearer for similar locations and operational conditions of the cutting machine. Results show that the algorithm can predict explosive gas zones in 3D with overall accuracies ranging from 87.9% to 92.4% for different settings; output predictions took two minutes after measurement data were fed into the algorithm. It was found that faster and more prominent coverage of accurate real-time explosive gas accumulation predictions are possible using the proposed algorithm compared to computational fluid dynamics and atmospheric monitoring systems.

Karacan (2008) proposed principal component analysis and an artificial neural network-based approach to predict methane emission rate throughout 63 longwall mines. The study shows that the extraction rate is the most important parameter and the volume of daily methane emission from each mine can be accurately predicted [82]. Dougherty and Karacan (2011) utilized the prediction model [82]

[4] Corresponding author. Direct correspondence to demirkan@mines.edu
[5] Mining Engineering Department, Colorado School of Mines, 1500 Illinois St., Golden, CO 80401, USA
[6] Mechanical Engineering Department, Colorado School of Mines, Golden, CO 80401, USA

and developed software to predict ventilation emissions with elastic properties [83]. Duda and Krzemień (2018) proposed a framework for forecasting methane emissions from seams to gobs/goafs; they predicted the average volume of methane per minute in each year of mine life [84]. Sidorenko et al. (2021) provided the necessary parameters to predict methane emissions from seams to gobs/goafs [85]. Although these studies discuss prediction, these predictions are neither real-time nor spatial outputs.

Previous studies demonstrate the successful implementation of artificial intelligence (AI) in various fields with real-time predictions. For example, Chen et al. (2019) proposed a real-time AI integration for cancer diagnosis by implementing image processing algorithms for body scans [86]. Nyanteh et al. (2013) implemented an AI for real-time fault detection [87]. To improve weather forecasting for high-impact weather, McGovern et al. (2017) integrated an AI with expert opinions [88]. Imran et al. (2014) classified real-time messages in social media using AI to help the public access important disaster response information [89]. Dong et al. (2021) used the AI model for real-time monitoring and predicting of slope failures [90]. Rodríguez-Rangel et al. (2022) incorporated big data analytics for autonomous vehicles' speed estimation [91]. Wahyono et al. (2022) proposed combining AI with data mining for real-time forest fire detection [92]. However, there is still a gap in the implementation of AI for methane prediction in longwall coal mines.

Real-time prediction of methane in a longwall face requires predicting explosive gas zone formation in time, and its location in 3D (x, y, and z coordinates). Predictions in time are mainly conducted using time series classification/analysis [74]. Spatiotemporal AI models and time series classification are relatively new to the field. Moreover, the vast majority of successful models only take into account one or two spatial dimensions, such as x and/or y coordinates, and the data of interest [61], [69], [71], [72], [75]–[78], [80]. For example, whereas climate change studies that track carbon emissions use latitude, longitude, and carbon content [93], water quality studies use one-dimensional distance of the intersections and water content [74]. This study proposes a 3D spatiotemporal prediction model for the real-time prediction of methane in the coal face.

Current explosive gas accumulation monitoring practices in longwall coal mines rely on two methods, namely, point sensors and CFD modeling. Point sensors take real-time measurements along the face and provide methane concentration values at the installed locations. CFD modeling provides methane prediction for the whole longwall face. However, due to computational cost, predictions take days or weeks, depending on the resolution of the study area. In this study, a continuation of our previous work [9] benchmarking and analyzing the suitability of the dataset and off-the-shelf algorithms, we developed an AI algorithm and methodology for use as a real-time explosion hazard warning system. We used six CFD analyses with varying shearer locations to train, test, and validate our model. This approach lays the foundation for more accurate methane predictions in real-time for underground mines by combining the most potent advantages of point sensors and CFD models, decreasing the computational cost of CFD modeling, and increasing the coverage of point sensors.

Previously conducted methane prediction studies mainly focused on total methane emissions from the seam or the entire mine. To the best of our knowledge, a 3D real-time methane prediction approach in longwall mining that integrates CFD data with an AI model has not been developed yet. Previous studies of methane prediction in longwall coal mines primarily focused on total methane emissions of the whole mine or the whole face with varying time intervals of years to minutes. Moreover, the predictions in these studies do not consider critical methane emission zones, such as near the drums or shearer. In this paper, we seek to fill these gaps. The approach presented herein can provide methane emission data not only in the 3D spatial domain but also in real-time at the mining face, including, but not limited to, areas near cutting drums, the shearer, the tailgate, and the headgate.

4.2. Materials and Methods

The developed research methodology exploits the advantages of CFD modeling and point sensors. Figure 4.1 illustrates how AI was integrated into real-time methane concentration prediction.

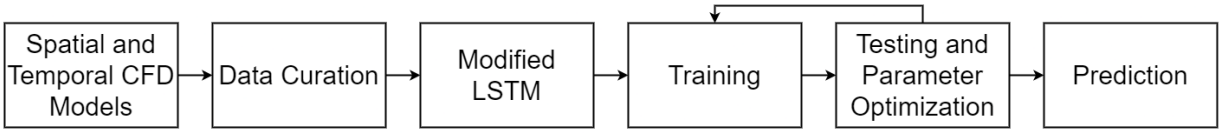

Figure 4.1 Research methodology

After finding the best-performing algorithm (LSTM) with small data sets (see Section 3.4), spatially larger and temporally longer data sets were created with additional details as CFD simulations. In the second step, these data sets were cleaned, organized, and integrated for the LSTM's needs. The third step shows the input modification from 2D to 3D, pointwise operations from 2D matrix to 3D array, and 2D outputs to 3D. Then the algorithm was trained with six locations and tested the corresponding shearer location, and parameters were optimized with 256 cells and two layers of recurring data feed. In the last step, predictions for spatial and temporal results were discussed with overall prediction accuracy.

4.2.1. Spatial and Temporal CFD Modeling

In this paper, we utilized the Ansys Fluent software version 18.2 to model and simulate a longwall face. The modeled longwall face was 300 m long with a mining height of 3 m and a depth of 6 m. Two primary pieces of equipment were also modeled: (i) support equipment (shields) and (ii) cutting equipment (shearers). There were 150 shields, each 2 m long, fixed within the model. One 10 m long shearer was placed along the longwall face in six locations. Location details are provided in Section 2.2. Finally, the modeled area was covered with approximately 31 million hexagonal and octagonal meshes. Mesh sizes ranged from 3 cm to 30 cm, which increased prediction resolution.

The simulation used a transient CFD model of methane (CH_4) gas emission from the coal face based on a bleeder ventilation system with a tailgate (TG) back return setup. We simulated each transient model for 180 s and recorded at 1 s intervals.

4.2.2. Data Curation

We collected data after modeling the longwall and simulating methane emissions. It should be noted that although each mine ventilation condition is unique, previously conducted studies [30–34] validate that simulated data are consistent with the actual situation that includes but is not limited to "(*i*) *continuous leakage of fresh air from the face to the gob, and the higher accumulation of methane as the supplied air travels from the headgate to tailgate side of the face; (ii) higher leakage around the headgate and tailgate corners of the face due to the high porosity and permeability around the edge of the gob; (iii) Methane accumulation seems to follow linear regression based on ventilation surveys done in several longwall operations."* [6].

Each simulation had approximately 31 million cells; data for each cell for each second of recording included pressure, airflow velocity (*Vx, Vy*, and *Vz*), CH_4 concentration, cell volume, and x, y, and z coordinates. We repeated data collection for each of the six locations of the shearer, which required ten days for each location. Details of specific shearer locations and the cutting direction during data collection are provided in Figure 4.2.

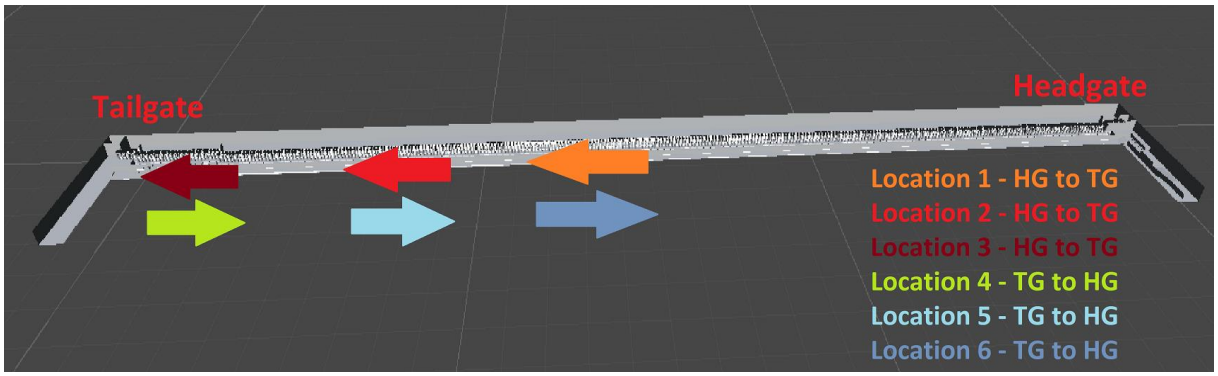

Figure 4.2 Six locations of the shearer and cutting directions during data collection.

Figure 4.3 represents a snapshot of the 120th second of location 3 as an example. Other locations and timestamps acted similarly; thus, only one example is provided to avoid redundancy.

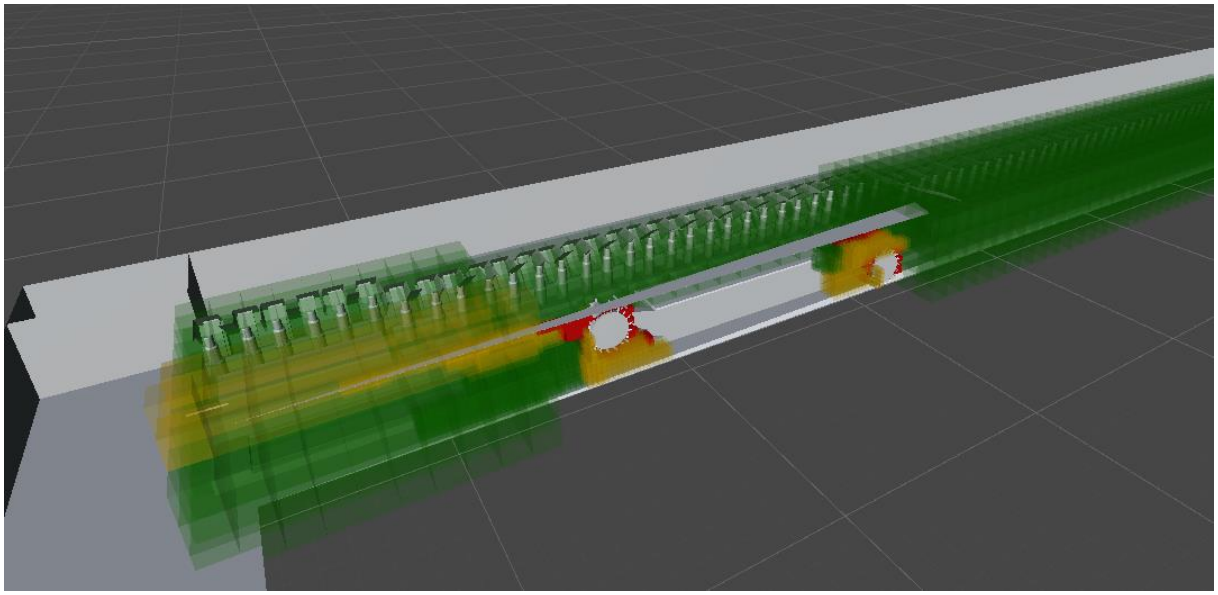

Figure 4.3 A snapshot of the 120th second time step of shearer location 3.

We preprocessed raw data from the Fluent software. This included data conversion into CSV files, removing empty fields, adding cutting directions, and fixing the two significant figures for all fields. There were two terabytes (TBs) of end data for each location; 12 TBs of data were input into the AI.

4.2.3. The Modified LSTM

The literature discusses different methods for the spatiotemporal prediction of a parameter, namely, the Naïve 2 method, simple exponential smoothing, the Holt method, the ARIMA method, and the ETS method [94]. The primary disadvantage of using the Naïve 2, simple exponential smoothing, and HOLT methods is that these algorithms can only predict one step ahead of time within a confidence interval. In a dynamic environment such as longwall mining, continuous monitoring is the key to preventing explosive hazards; hence, one-step-ahead predictions were not sufficient for the aim of this study.

Also, it was not feasible to implement these methods for real-time prediction considering the required computational power and data size. For example, each location had approximately 32 million cells, each connected to the other and affected methane concentration. In contrast, the ARIMA and ETS methods can predict long-term methane concentrations for a specific cell. However, the longwall's geometry was 3D, and these statistical methods are not effective at predicting in a 3D environment. Unlike AI models, statistical methods utilize interpolation that cannot learn the extreme fluctuations of data.

AI and machine learning (ML) algorithms were recently introduced to predict the time and location of a parameter of interest. Although applications are still limited, preliminary results of a range of studies (discussed briefly in Section 4.1) are promising. Moreover, in-depth analysis and benchmarking of the most promising algorithms for real-time methane prediction were examined in a previous study [9].

In light of the literature and previous tests, a recurrent neural network (RNN) was determined to be the best candidate for real-time methane prediction in longwall coal mines. An RNN contains cycles from previous time steps as network inputs to influence predictions at the current time step. These timestamps are stored in the RNN's internal states, allowing it to exploit a dynamically changing contextual window over the input sequence history [37–39].

Unfortunately, the range of contextual information that a standard RNN can access is, in practice, quite limited. The challenge is that the influence of a given input on the hidden layer, and therefore on the network output, either decays or raises exponentially as it cycles around the network's recurrent connections. This shortcoming is referred to in the literature as the vanishing gradient problem [33].

Long short-term memory (LSTM) is an RNN architecture specifically designed to address the vanishing gradient problem [40–42]. LSTMs were introduced in about 1997; their main advantages include that they are (i) algorithms that can store information for a specified time duration, (ii) resistant to noise, and (iii) trainable parameters [43,44]. According to our previous study [9], any future prediction using AI can be categorized into seven problem types (image, sensor, motion, spectrographs, electronic devices, electrocardiograms, and simulations). As methane prediction is similar to the sensor-type problem, we adapted one of the best performing algorithms, an LSTM network (a special type of RNN) for this study.

Figure 4.4 shows the simplified architecture of the LSTM model, modified from the blog post by Olah [97]. In the forget gate, the cell takes the previous time step and determines which information should be kept and which should be omitted. In the input gate, the cell takes information and keeps only what is relevant for prediction. In the update gate, the cell takes previous neural network information and updates prediction weights. Lastly, the output gate determines which parameters and data to output and feed to the next cell.

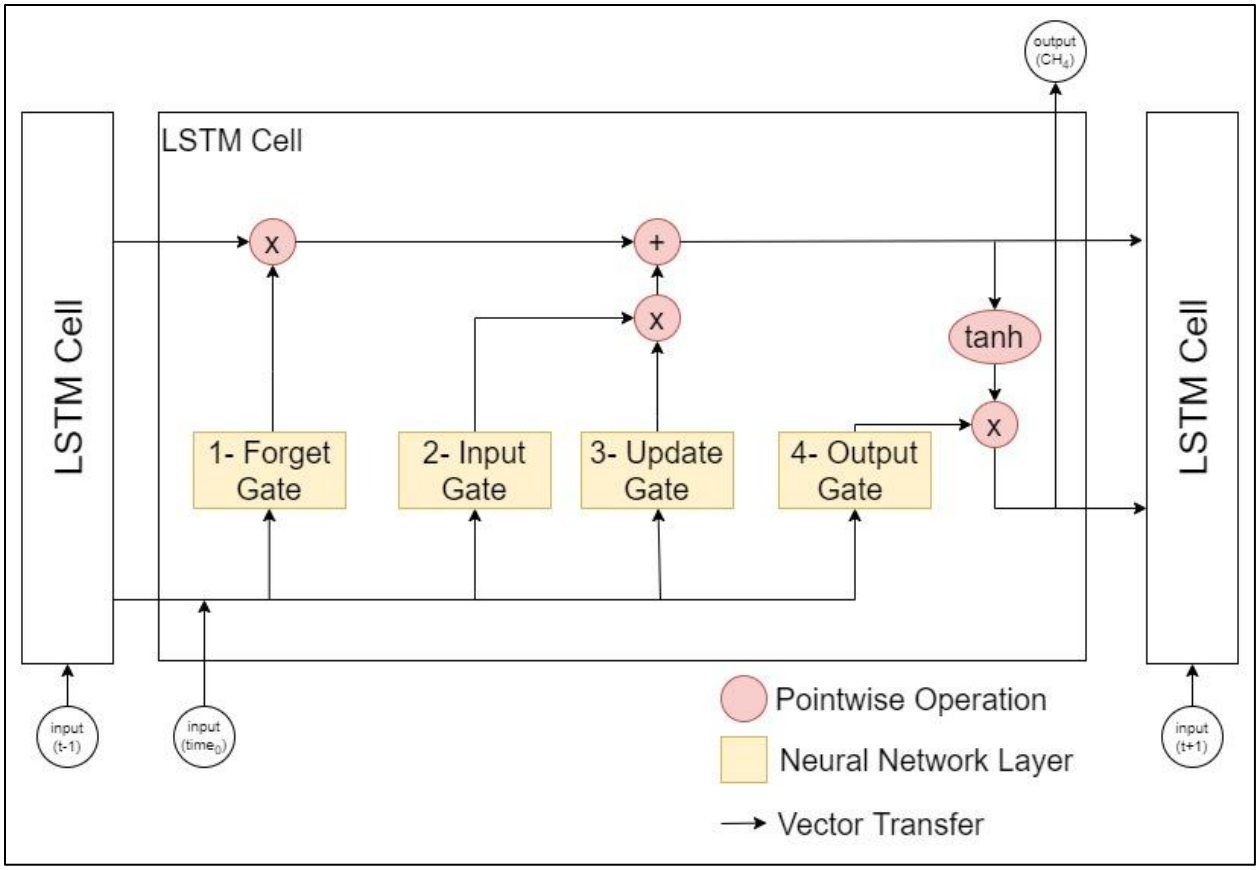

Figure 4.4 Simplified LSTM architecture (modified from [97]).

As LSTMs are viewed as feed-forward neural networks where each cell shares the same model parameters, they are considered deep architectures or deep neural networks [31]. In this study, the LSTM network was modified, trained, and tested with CFD outputs.

A conventional LSTM network accepts 2D data. LSTM model modifications implemented in this study include (i) changing the input shape for the 3D space and (ii) adding 3D operations and vector calculations. The inputs to the modified LSTM model were; x, y, and z coordinates, the smallest distance to the shearer, airflow velocity, methane concentration, and the volume of each cell for 180 seconds, which were recorded at 1 second intervals.

4.3. Results

Even the best-performing algorithms might fail to predict results without high-quality data. Therefore, training, validation, and testing of the algorithm are critical for reliable predictions; if these steps are not performed correctly results might be biased. Table 4.1 provides a data breakdown, and is followed by an explanation of each topic in respective subsections. Note that similar shearer locations were selected for training and predicting methane content. For example, Figure 4.2 illustrates that shearer locations 1 and 6

had a similar location in the middle of the longwall face, and locations 3 and 4 had a similar location on the tailgate side. In addition to slight changes in the exact positions of cutting equipment, cutting directions were also changed. Datasets for similar locations were divided 50–50 for training and testing. The first 50% was divided into 80% to 20% for training and validation; the detailed distribution is provided in Table 4.1.

Table 4.1 Training, validation, and testing datasets based on shearer locations.

Training DataSet	Validation DataSet	Cutting Direction	Testing DataSet	Cutting Direction
80% of Location 1	20% of Location 1	Headgate to Tailgate	Location 6	Tailgate to Headgate
80% of Location 2	20% of Location 2	Headgate to Tailgate	Location 5	Tailgate to Headgate
80% of Location 3	20% of Location 3	Headgate to Tailgate	Location 4	Tailgate to Headgate
80% of Location 4	20% of Location 4	Tailgate to Headgate	Location 3	Headgate to Tailgate
80% of Location 5	20% of Location 5	Tailgate to Headgate	Location 2	Headgate to Tailgate
80% of Location 6	20% of Location 6	Tailgate to Headgate	Location 1	Headgate to Tailgate

The common practice of splitting data into training, validation, and test sets depends on the dataset and might range from 50–50% to 80–20%. With smaller number of data points ($n < 10{,}000$), 70–30% splitting is used. However, if the number of recordings is high ($n > 1{,}000{,}000$), the importance of split ratios decays. Overall, the most important element in splitting a dataset is having good data representation in the train and test sets. In this study, the number of recordings was close to 64,300,000; hence, we conducted training by using a specific shearer direction and tested using the opposite direction but the same position [45–49].

The training and validation of each instance took approximately seven days; testing time was 15 minutes with a high-performance computing system using the following specifications:

- CPU: Intel Xeon COU E704830 v3@2.10GHz (4 CPUs/node, 48 cores/node)
- GPU: five Tesla K80
- Memory: 2133 MT/s, Dual Rank, x4 Data Width RDIMM (42.7 GB/Core)
- Storage: 20 TBs

Input data were approximately 5 TBs for each instance, with 2 TBs of output.

4.3.1. Training

We used training data to teach patterns and features to the AI model. We repeatedly gave the same training data to the model until a threshold level was reached. Feeding the same data repeatedly is called

an epoch. The simple explanation of an epoch is one complete pass of the dataset through the designed network. The algorithm updated its parameters with each epoch while learning the input dataset. We divided training data into 80% and 20% for each instance using the stratified K-folds cross-validation method. This yielded a balanced data division, which preserved the percentage of samples for each methane content. We used the divided 80% of data to train the model.

4.3.2. Validation

Validation data were separated from training data, which validated the AI's performance. Training and validation accuracy helps users evaluate their mode. Figure 4.5 illustrates a commonly used metric for assessing algorithm performance, validation, and training accuracy versus an epoch.

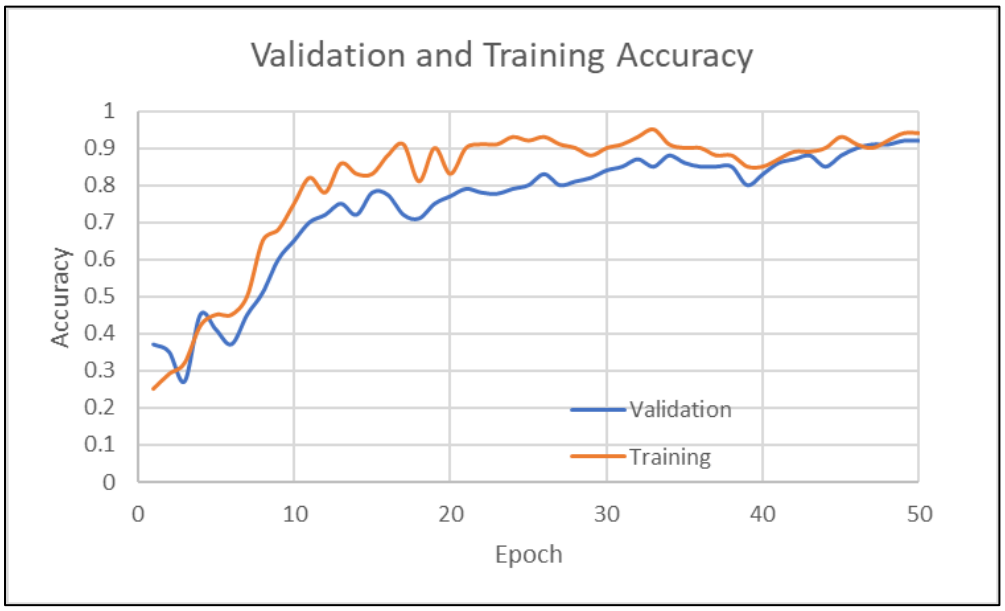

Figure 4.5 Validation and training accuracy.

In the above graph, the curves' slopes approach horizontal after the 12th epoch, which indicates that data did not make a significant learning process over the algorithm. At approximately the 20th epoch, the learning curve became almost horizontal. This indicates that no further training was necessary after the 20th epoch, as the accuracies did not change considerably and ranged from 89.1% to 93.8%. Finally, the validation curve standing below the training curve indicates that the model was fed a good representation of data, was ready for testing and was able to provide reliable predictions.

4.3.3. Testing

After training and validation, we used the test data to evaluate the AI model's performance for predicting methane. We analyzed the model's performance using the actual and predicted methane

content of the testing data for each training and testing coupled set, as provided in Table 4.2. These results show the modified LSTM [7]algorithm predicted methane concentration with an accuracy ranging from 87.9% to 92.4% .

Table 4.2 Overall accuracies of tests

Couple Name	Training DataSet	Testing DataSet	Overall Accuracy
L1L6	Location 1	Location 6	92.4%
L2L5	Location 2	Location 5	89.1%
L3L4	Location 3	Location 4	87.9%
L4L3	Location 4	Location 3	88.3%
L5L2	Location 5	Location 2	91.0%
L6L1	Location 6	Location 1	91.6%

4.4. Discussion

Our analysis revealed that the modified LSTM algorithm can possibly combine effective aspects of CFD modeling and point sensor measurements. AI algorithms can achieve 3D coverage of CFD modeling and real-time point sensor data measurements. The overall accuracies of different locations ranged from 87.9% to 92.4%. Although accuracies were relatively high, some locations (such as locations 3 and 4) had less accurate results than others, possibly because the closer the shearer was to the headgate and tailgate (locations 1 and 6), the more the methane emissions fluctuated.

The algorithm was more agile when spotting fluctuations; thus, relatively constant methane emissions may be a reason for lower test accuracies in locations 3 and 4. Although the accuracies showed promising results, with additional datasets they might increase. Even if a single location had approximately 32 million points, the entire measurement only contained 180 s of data. If these measurements could be increased, accuracies might also increase. Given the current data storage and computational power advancements in supercomputers, the required time for training was 45 days. Moreover, an increase in data size will increase the required computational power and time required for training; however, time requirements will change more exponentially than linearly. Training times will not affect prediction times; once the algorithm is trained, the required prediction time will not change drastically.

[7] The source code is available on GitHub at: https://github.com/DogaCagdasD/demirkan_phd_codes

Whereas explosive gas zone monitoring relies on point sensors, critical regions of a longwall face cannot be tracked in real-time. CFD modeling can overcome the sensors' coverage, but the required prediction time could be days to weeks, depending on the resolution of the simulation. This study's methodology eliminates these shortfalls. The system proposed herein yields highly accurate real-time predictions with detailed coverage of the longwall face. Therefore, modified LSTM-based methane prediction might help early warning systems for miners and engineers reduce safety risks and prevent accidents such as the Upper Big Branch in April 2010. Lastly, the system can increase production by reducing unnecessary stops of the shearer.

However, AI's prediction capabilities depend on simulated CFD model results and, predictions can only be as accurate as similar longwall face models. Training the AI model using different longwall face models can increase the AI model's capacity. If the AI model can be trained with more data, it might be used for all longwall mines in the world.

4.5. Conclusions

As was the case with the Upper Big Branch accident, longwall mine methane explosions can be fatal. Current explosive gas zone management practices are carried out either with point sensors or CFD modeling. Leveraging the power of AI might be crucial for monitoring explosive methane concentration. The primary objective of this study was to combine the advantages of current methane monitoring practices and eliminate their disadvantages. For this purpose, we utilized modified LSTM architecture for real-time methane prediction.

This study is unique as it provided real-time methane prediction in 3D space. Our study successfully leveraged a significant amount (12TB) of CFD data for location and time prediction of a possible explosive methane accumulation. Unnecessary stops, high fan speeds, and other unnecessary operating costs can be reduced using the proposed method, which can help increase safety and productivity for all longwall coal mines by monitoring the methane gas along the face.

While the proposed methodology successfully predicted methane concentrations throughout the longwall face, the results only contained numbers representing location, time, and methane content. Results consisted of lines of numbers that could not be interpreted or used by engineers and/or miners to determine if the explosive gas accumulation was hazardous.

Future research associated with this study will consist of two parts. First, the algorithm will be trained using other mines' layouts and methane emission models. This will increase the algorithm's prediction capabilities and enable its usage and implementation on different mine layouts. Second, the predictions of the AI model will be imported into Unity software for visualization purposes. This will help facilitate the integration of real-time predictions with augmented and virtual reality environments, which are already implemented in other industries, such as construction, production, health, and many more. The final product might ease the judgment burden placed on engineers and workers in times of critical methane

emission levels. We will convert results into more robust, understandable visualizations that resemble CFD output; providing a familiar output will help engineers and workers by decreasing their cognitive load.

We have started the second development phase; a side-by-side comparison of the CFD model and our visualizations for different time stamps are shown below in Figure 4.6.

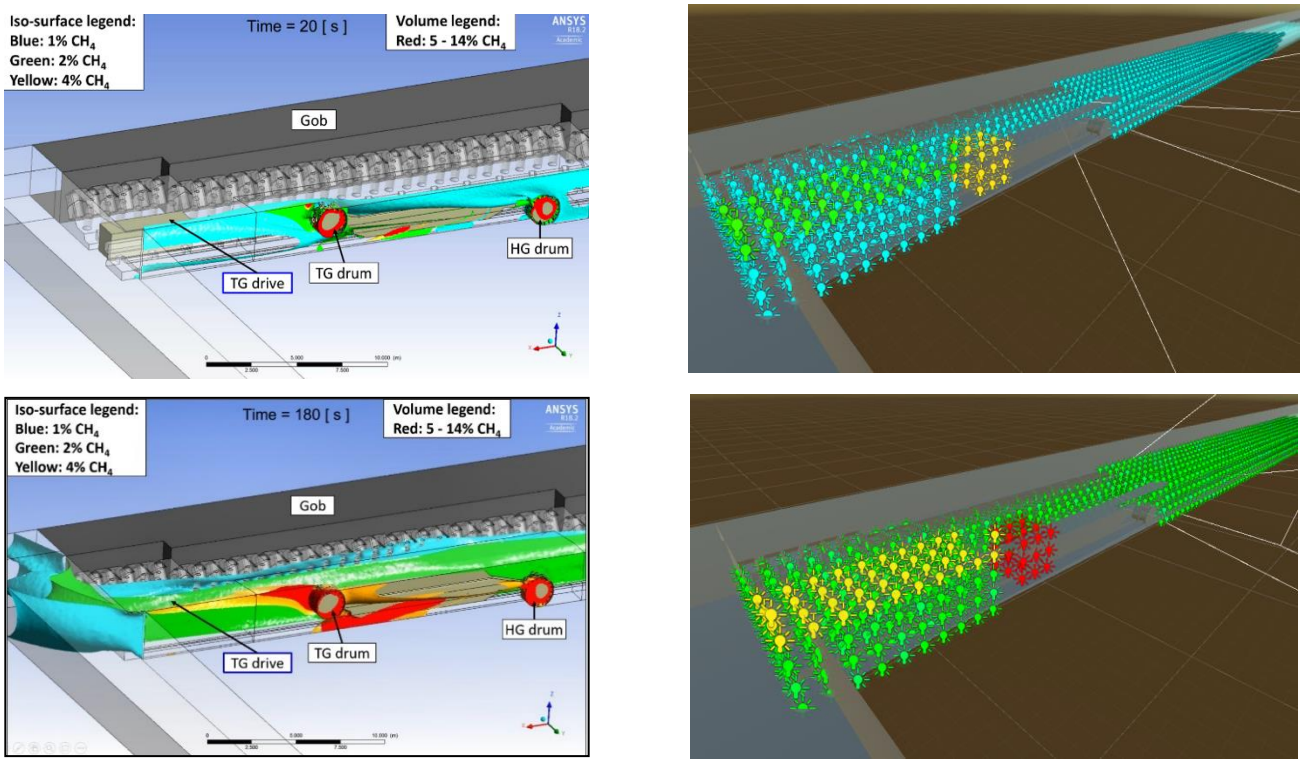

Figure 4.6 Side-by-side comparisons of CFD models and prediction visualizations

These visualizations will help us conduct a user study with the aim of discovering a better way to visualize AI outcomes. The user study will also provide insights regarding the possible integration of these visualizations into a mixed-reality environment.

CHAPTER 5

VISUALIZATION OF PREDICTIONS AND USER STUDY

Submitted to IEEE Transactions on Visualization and Computer Graphics

Doga Cagdas DEMIRKAN[8,9], H. Sebnem Duzgun[8]

This chapter addresses Research Question 3: “What are the best ways to visualize prediction data for accurate and fast assessment for users in the field?” by visualizing AI predictions and comparing the visualization platforms with a user study. This dissertation’s overall methodology, step 4: visualization of predictions and user study, is explained in this chapter.

Visual variables in data visualization play a critical role in human cognition, reaction, and understanding of data. Appropriate use of these variables improves the user's interpretation of data. However, there is a knowledge gap in AR and VR regarding the effective use of visual variables. In this study, we perform a user study to investigate the effects of two visual variables, transparency/opacity and complex/simple, to compare in computer screens, AR and VR. First, we developed a simulation to visualize explosive gas emissions in an underground mine. Then we designed simulation visualizations based on four scenarios: i) opaque and complex data, ii) opaque and simple data, iii) transparent and complex data, and iv) transparent and simple data. We tested the four scenarios with 30 human subjects, where we asked subjects to determine the explosive gas volume. Among the 30 subjects, only six of them had previous VR experience and two of them had previous AR experience.

Additionally, we recorded the subjects` time of completion and eye-tracking data. At the end of testing, we asked the subjects 43 questions regarding their experiences with computer screens, AR and VR of which we analyzed the results quantitatively and qualitatively. The quantitative analyses included the accuracy of explosive gas volume detection and completion time. In addition, we compared the saliency maps of the designed simulations with the subject's eye-tracking data to investigate the subjects' attention and reaction in AR, VR and computer screen. In the qualitative analysis, we evaluated subjects` responses to questions about their feelings. The results of the quantitative analysis showed a statistically significant difference between computer screen and VR for the transparent and simple scenario, i.e., subjects spent less time on the computer screen than in VR. However, the results also showed a statistically significant difference in the accuracy of volume determination between VR and computer screen for the transparent and simple scenario. The subjects` accuracy of volume determination was

[8] Corresponding author. Direct correspondence to demirkan@mines.edu
[9] Mining Engineering Department, Colorado School of Mines, 1500 Illinois St., Golden, CO 80401, USA

better in VR. There was no statistically significant difference in terms of time spent and accuracy for the rest of the scenarios.

Moreover, the eye tracker data showed that subjects spent more time in non-salience regions in VR than on the computer screen. Even though the time spent did not make users miss any explosive zones, it affected the volume estimations. In addition, the qualitative analysis revealed that 90% of the subjects preferred to use VR due to the immersive experience, and 67 % felt more confident in VR when investigating the explosive zones and flagging them as dangerous zones. Lastly, 27 % of the subjects indicated eye strain and fatigue after the VR experience.

5.1. Introduction

Data visualization is a crucial part of knowledge extraction and decision making, and effective visualization will affect users' cognition, reaction, and understanding of data [10]. Over several decades, researchers such as Bertin, MacEachren, Morrison, and many others, have proposed effective data visualization guidelines, consisting of visual variables including size, shape, color lightness, and transparency.

Recent technological developments yield novel methods and platforms that provide innovative visualization opportunities for engineers, data scientists, and others [14]. Among the possible platforms, augmented reality (AR) and virtual reality (VR) are increasingly preferred as they are not only capable of representing real-world simulations but also can deliver insight into the phenomena via an immersive experience.

However, current practices and guidelines for data visualization assume data is illustrated either on white paper or on computer screens with normal reading conditions e.g., constant light and reading distance up to one's arm's length. Therefore, there is a knowledge gap in AR and VR platforms regarding visualization guidelines. This knowledge gap needs to be filled to deploy the AR and VR platform's true power.

In this paper, we designed a user study to investigate the effects of two visual variables, transparency/opacity and complex/simple, to compare computer screens, AR and VR. We then identified effective use of these variables in AR and VR.

5.2. Related Work

Visual variables are one of the cornerstones of data visualization. The first categorization of visual parameters was proposed in 1967 by Bertin as size, color, orientation, texture, shape value (brightness), and position (dimensions on the plane) [11][100]. In addition to Bertin's visual variables, MacEachren suggested three more visual parameters: crispness, resolution, and transparency [12]. In 1994, Wolfe discussed the effects of complexity (referred to as cluttering) in visual search and the increase in cognitive load [101].

In 2014, Zhang et al. discussed the 2D visual variables compatibility and limitations in 3D visuals [102][103]. Similar to studies on 2D and 3D compatibility of visual parameters, VR compatibility also needs to be investigated. Inappropriate usage of visual variables might result in users' misinterpreting critical data [104]. Laha et al. studied the effects of visual variables for head tracking, field of regard (FOR) and stereoscopic rendering for volumetric data interpretation. They found that FOR had a positive impact on tasks but that other parameters had mixed effects [105]. Adams et al. studied shadow/shadowless and position (floating/grounded) variables for the depth perception of users in augmented reality. They found that current devices make users underestimate the distance regarding the visual variable but the position of the object and the shadow influence users' decisions [106]. Sun et al. studied color, height and transparency variables for 3D city cadaster visualization in VR. They found that combining all visual variables is more appealing to users, but it has an overwhelming effect [107]. Arjun et al. evaluated the effects of size, orientation, opacity, and shape for chart data understanding. They found that accuracy is affected the most by size and color. Moreover, cognitive load is affected the most by size, opacity and brightness [108]. Covaci et al. tested the perspective view effects on users while throwing a basketball. Although they did not find any statistically significant change in perspective views, basketball release speed in first person perspective view, and release height in first-person, third person and guided third-person view, significantly improved [109].

A saliency map is a computer vision term that highlights visually striking parts of an image for the human eye. It was first proposed by Koch and Ulman [110] and implemented by Itti et al. [111][112]. Although many variations of saliency mapping algorithms exist, from a high-level perspective, these algorithms consider visual features including but not limited to color, orientation, location, and edges [113], and create a 2D image that represents the predictions of human eye movement [114].

Eye trackers can obtain actual eye movements instead of saliency predictions. Eye movement has recently gained grater importance in AR and VR, and developers have been utilizing it for content design and user interactions [115]. For viewpoint selection, visualization, learning, assessment, and monitoring, keeping the correct saliency is essential [116][117]. Failure to develop correct salient regions in visualization might result in increased cognitive load, distraction, and overlooking critical data [118][119][120][121]. Saliency mapping is employed in VR if there is no available eye-tracking hardware [122].

Considering the existing literature, to our knowledge, there are no controlled experiments comparing visual variables in computer screens AR and VR. Moreover, the connection of eye tracker data with saliency mapping for different visual variables has not been investigated yet. Our study aims to fill these gaps by comparing the effects of visual variables in three different platforms, computer screens AR and VR, and by investigating saliency maps against eye tracker data.

5.3. Experimental Design and Evaluation

Visual variables are used to convert non-visual information into visual representations. There are more than 15 visual variables that are proposed in the literature. Some of the parameters are well-defined, including but not limited to size, shape, color and texture. However, some are more abstract and fuzzy yet extensively employed by the researchers, including but not limited to position, resolution and orientation. Moreover, some variables are categorized as preattentive, which are processed subconsciously by the users. A good example of a preattentive variable is color. When humans see the color “red,” they tend to stop or walk away. The well-defined variables are described for looking at a white paper with constant light and reading distance. However, with the utilization of computers, not all well-defined variables are implementable into screens. Therefore more abstract variables have come into play and gained acceptance in the literature.

The rapid development of technology introduced AR and VR into possible data visualization applications with their realism and immersive aspects. The visual variable struggle of implementing white paper from screens has now come forth for screens to AR and VR. Although not all variables can be utilized for all three platforms, transparency and complexity can be well-defined for this task.

Transparency is defined as the permeability of light from the object, which results in the see-through effect, whereas opaque is defined as impenetrable by light. In this user study, a scale is defined from zero to 100, where opaque is represented by 100 and transparent by 30, where 70 percent of light can penetrate through the objects.

Complexity is one of the ambiguous variables and is defined as the scene's understandability. The less complex a scene is, the more insightful it tends to be. In this user study, complexity is defined based on the utilized data. A complex scene is where the entire data is visualized without cleaning the safe zones. On the contrary, a simple scene is where the data is cleared from safe zones, and only critical gas zones are visualized.

We designed a user study to investigate the effects of transparency/opacity and complexity/simplicity, to compare their effectiveness on computer screens, AR, and VR.

5.3.1. Research Questions and Hypotheses

This study asks the following research questions:

1. What are the effects of immersion, and how does the change of visual variables affect users' performance when compared to conventional methods?

For the first question, we investigated the users' accuracy in measuring a quantity on each platform with different visualization methods to propose a guideline for visualization in AR and VR.

2. What are the differences between the saliency of the visuals and the users' focus points in visuals?

For the second question, we studied the consistency of the visual saliency on both computer screens, AR and VR, by evaluating the users` focus on salient regions.

3. What are the users' preferences when interpreting the data, and how do they feel about each platform and visual variable?

For the last question, we explored users' perspectives on each visualization method and why they prefer one over another. A previous study [107] showed that even though users might favor certain specific visualizations, that does not mean they are more likely to be successful or lack side effects like eye strain, headache, or motion sickness.

These research questions yield the following hypotheses:

1A. An immersive environment helps more accurate data interpretation than conventional computer screen visualization.

1B. The visual variables for computer screens do not have the same effects in AR and VR

The first research question is connected to two hypotheses, 1A and 1B. Some studies showed possible advantages for 1A. but did not compare it with any other methods besides VR. For 1B., we expect some difficulties in data interpretation when it comes to opaque and complex data visualizations.

2. Users' focus on computer screens matches the visuals' saliency, but in VR, users spend more time in nonsalient areas.

We expect to observe that users will spend additional time investigating the environment due to the immersive aspect of VR.

3. Users prefer to use VR with simple and transparent data visualizations.

While computer screen visualization is a representation of the model, VR visualization is a real-world scaled model of actual objects. Therefore, we believe users will lean towards VR visualization in general.

5.3.2. Simulation Model and Data

In underground coal mining, methane gas is one of the most dangerous and explosive gasses; however, due to the nature of coal, fluctuating methane gas emissions are expected. When methane concentrations hit critical values, they become explosive. For that reason, it is monitored closely by i) taking continuous readings and ii) simulating and visualizing in computational fluid dynamics software. Mining personnel explore methane data on computer screens which is around 1/200 of the actual size. Good visualization is important for accurate volume analysis to make safety decisions.

For the software side, to mimic the utilized visualization method in industry, we exported methane data [123] with its locations and concentrations from ANSYS Fluent software version 18.2. Then we

created a 1:1 scaled underground mining model using Blender version 2.92.0. Later, we imported the methane data and mining model into Unity version 2020.3.33f1.

Figures 5.1 (a) and 5.1 (b) show industry visualization and our visualizations, respectively. Each visualization is a snapshot of a random time, and the colors represent the methane concentration by percentage volume at the current state.

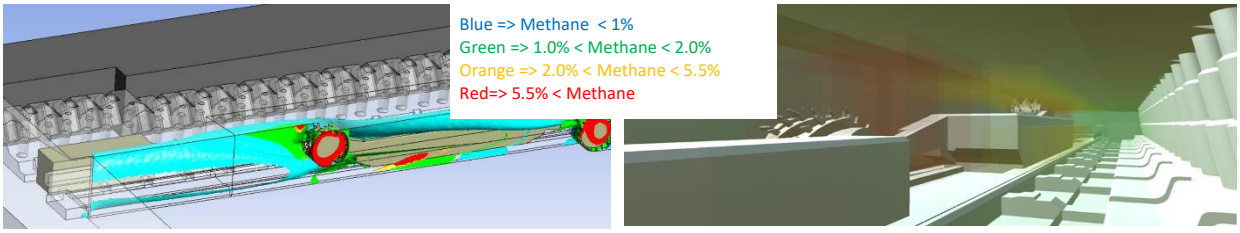

(a) Visualization in Computational Fluid Dynamics (b) Visualization in Unity

Figure 5.1 Visualization of simulation in (a) conventional methods and (b) this study's setup

We used OBS Studio, HP Omnicept, Windows Mixed Reality Portal, and Tobii Ghost to record the screen and eye tracking and smoothly launch the developed visualization of simulations. We utilized an Alienware m17 R3 series gaming laptop with a built-in eye tracker as a computer screen. Lastly, we used HP Reverb G2 Omnicept Edition as the VR headset due to its built-in eye tracker capabilities and Magic Leap as AR headset.

We assumed that the users adopt computers in their daily life and have never used AR and VR joysticks before. So, in regards to the user interface, we kept user interactions minimal to eliminate the potential disadvantages and learning curve of the AR and VR controller.

Finally, with the same data set, we designed simulation visualizations based on four scenarios: i) opaque and complex data visualization (OCV), ii) opaque and simple data visualization (OSV), iii) transparent and complex data visualization (TCV), and iv) transparent and simple data visualization (TSV). We prepared opaque and transparent data visualizations as the material properties of albedo color equals 100 and 30, respectively, in Unity. We developed complex and simple data visualizations for all methane concentrations and only critical methane concentrations (orange and red), respectively.

5.3.3. Participants

We recruited 30 voluntary participants for our study. There were seven females, 22 males, and one undisclosed gender, with ages ranging from 19 to 68.

Only 10 of the participants self-reported having previous VR experience, and two participants reported having previous AR experience. Among the 10 participants that reported experience with VR, only one reported using VR two to three days per week, while others were not regular users. Among all

participants, only seven had been in an underground coal mine before. Only two participants reported having an underground mine experience in VR. In addition, 21 participants reported being familiar with data visualizations, while nine reported the opposite.

5.3.4. Procedure

Participants signed an informed consent form prior to the study. It should be noted this study got exempt status from the Institutional Review Board (IRB). Participants then filled the background questionnaire that captured their experience with computers, AR and VR headsets, data visualizations, and underground mining. The questions were selected from [124], and are provided in Appendix A. The questions were based on ten categories. These categories were engagement, immersion, presence, flow, usability, emotion, skill, judgment, experience, and technology adoption.

After the background questionnaire, we introduced the hardware and explained interactions. We then gave a quick training on underground mining, equipment, and the importance of methane monitoring. Then, we introduced visualizations to the participants. Table 5.1 lists each visualization with its visual variables and platforms.

Table 5.1 Visualization simulations with its visual variables and platform

Platform	Visual Variables
Computer	Opaque + Complex (OCV)
Computer	Transparent + Complex (TCV)
Computer	Opaque + Simple (OSV)
Computer	Transparent + Simple (TSV)
VR	Opaque + Complex (OCV)
VR	Transparent + Complex (TCV)
VR	Opaque + Simple (OSV)
VR	Transparent + Simple (TSV)
AR	Opaque + Complex (OCV)
AR	Transparent + Complex (TCV)
AR	Opaque + Simple (OSV)
AR	Transparent + Simple (TSV)

Participants first conducted the user tests via computer visualizations, followed by AR and VR. We asked participants to estimate the explosive methane volume (red zone) in both visualization

environments. We recorded the time spent by users while they were estimating the volume. During this period, we also collected the eye tracker data for each participant.

After completing the tasks, participants filled out a post questionnaire that captured their opinions and feelings about each visualization. Post questionnaire questions are given in Appendix B.

5.4. Results

We analyzed the results based on both quantitative and qualitative approaches. For the quantitative analysis, we considered participants' total time of volume estimation and the accuracy of the estimated volume. We additionally compared eye tracker data with the saliency maps of the simulations. For the qualitative analysis, we took users' responses to the post questionnaire into account.

We examined the distribution of both the task completion times and volume estimates with a Q-Q plot, as presented in Appendix C. According to the Q-Q plot analysis, collected data was not normally distributed. Therefore, a non-parametric statistical test, namely Kruskal–Wallis, was selected with a p-value of 0.05. It is worth noting that besides Kruskal–Wallis, commonly used non-parametric tests assume equal mean, equal average, or uniform distribution.

Tables 5.2 and 5.3 summarize the quantitative analysis of volume estimation and completion time results. It should be noted that only statistically significant results are presented in these tables. We explain and discuss the tables in more detail in Sections 5.4.1 and 5.4.2.

Table 5.2 Statistically significant results of each platform with visual variables (|ΔV|: mean error in volume estimation, x̄: mean time spent in the tests)

Computer		
		Test Results (P values)
Time (seconds)		
OCV (x̄=69.2)	OSV (x̄=44.7)	0.03
OCV (x̄=69.2)	TCV (x̄=40.7)	0.02
VR		
Error (volume m^3)		
OCV (|ΔV|=6.0)	OSV (|ΔV|=0.10)	1.12e-12
OCV (|ΔV|=6.00)	TCV (|ΔV|=2.28)	1.10e-12
TCV (|ΔV|=2.28)	TSV(|ΔV|=0.15)	0.01
Time (seconds)		
TCV (x̄=74.9)	TSV (x̄=54.5)	0.03
OCV (x̄=6.03)	TCV (x̄=74.9)	3.20e-11
OCV (x̄=6.03)	OSV (x̄=71.2)	4.11e-11
AR		
		Test Results (P values)
Error (volume m^3)		
TCV (|ΔV|=3.63)	TSV (|ΔV|=0.61)	0.02
Time (seconds)		
OCV (x̄=85.6)	OSV (x̄=53.6)	0.03
OCV (x̄=85.6)	TCV (x̄=54.2)	0.03

Table 5.3 Platform comparison(|ΔV|: mean error in volume estimation, $\bar{x}$: mean time spent in the tests)

	Error (volume m^3)		**Test Results (P values)**
TCV	Computer (|ΔV|=1.84)	VR (|ΔV|=2.28)	0.01
TCV	Computer (|ΔV|=1.84)	AR (|ΔV|=3.63)	0.01
OCV	Computer (|ΔV|=1.43)	VR (|ΔV|=6.00)	1.58e-08
OCV	Computer (|ΔV|=1.43)	AR (|ΔV|=2.78)	2.63e-04
OCV	AR (|ΔV|=2.78)	VR (|ΔV|=6.00)	5.40e-11
OSV	Computer (|ΔV|=1.93)	VR (|ΔV|=0.10)	1.52e-04
OSV	Computer (|ΔV|=1.93)	AR (|ΔV|=2.36)	8.52e-04
TSV	Computer (|ΔV|=1.97)	AR(|ΔV|=0.61)	2.99e-06
TSV	AR(|ΔV|=0.61)	VR (|ΔV|=0.15)	0.01
TSV	Computer (|ΔV|=1.97)	VR (|ΔV|=0.15)	3.48e-04
	Time (seconds)		
OCV	Computer ($\bar{x}$=69.2)	VR ($\bar{x}$=6.03)	5.28e-11
OCV	AR ($\bar{x}$=85.6)	VR ($\bar{x}$=6.03)	3.72e-11
TCV	Computer ($\bar{x}$=40.7)	VR ($\bar{x}$=74.9)	7.86e-04
TCV	Computer ($\bar{x}$=40.7)	AR ($\bar{x}$=54.2)	0.03
OSV	Computer ($\bar{x}$= 44.7)	VR ($\bar{x}$= 71.2)	0.01
OSV	Computer ($\bar{x}$=44.7)	AR ($\bar{x}$=53.6)	0.04
TSV	Computer ($\bar{x}$=39.4)	AR ($\bar{x}$= 54.1)	0.02

5.4.1. Volume Estimations

The results for computer visualizations showed that there was not a statistically significant difference in the mean error of volume estimation in any visualization. On the other hand, in VR visualizations, in comparing OCV and OSV, OCV and. TCV, TCV and TSV there was a statistically significant difference in the mean error of volume estimation. Lastly in AR visualizations, in comparing TCV and TSV, there was a statistically significant difference in the mean error of volume estimation.

When comparing platforms for the same visualization variables, computer screens and VR, for TCV, OSV, OCV, and TSV, there was a statistically significant difference in the mean error of volume estimation. Noted are the same results in comparison to computer screens and AR. On the other hand, when comparing AR and VR, only with regards to OCV and TSV, there was a statistically significant difference in the mean error of volume estimation.

5.4.2. Task Completion Times

For the task completion times, in computer visualizations, the comparisons of OCV and OSV, and of OCV and TCV demonstrated a statistically significant difference in the mean time of task completion. In VR visualization,the comparison of TCV and TSV, OCV and TCV, OCV and OSV showed a statistically significant difference in the mean time of task completion. Finally, in AR, the comparisons of OCV and

OSV, and of OCV and TCV showed a statistically significant difference in the mean time of task completion.

When comparing platforms for the same visualization variables, comparing computer screens and VR, the comparison of OCV, TCV and OSV revealed a statistically significant difference in the mean time of task completion. Comparing computer screens and AR, the comparison of TCV OSV TSV revealed a statistically significant difference in the mean time of task completion. When comparing AR and VR only OCV revealed a statistically significant difference in the mean time of task completion.

5.4.3. Comparison of Eye Tracker Data and Saliency Maps

We recorded participants` eye movements while they estimated volume, and we compared eye tracking data with the saliency maps created using the Itti and Koch [111][125] model. The saliency maps are used to examine and find insights about the visualizations. Figure 5.2 and Appendix F compare the saliency of the visualizations with the explosive gas zone and show that they match each other. Also, the saliency maps were compared with the eye-tracking data. This comparison also provided insight into which salient areas were less important and which nonsalient areas were more important for the users.

In computer visualization, the comparison revealed that saliency and eye movements matched 45% to 55 % of the visualization, depending on the visual variables. In VR, the eye tracking data matched 20% to 70 % and in AR 10% to 30% of the salient regions.

Figure 5.2 shows an example of graphical representations of the visualization, heat maps of eye tracker data, saliency maps, and overlay of eye tracker data on saliency maps. All images for each simulation are given in Appendix D.

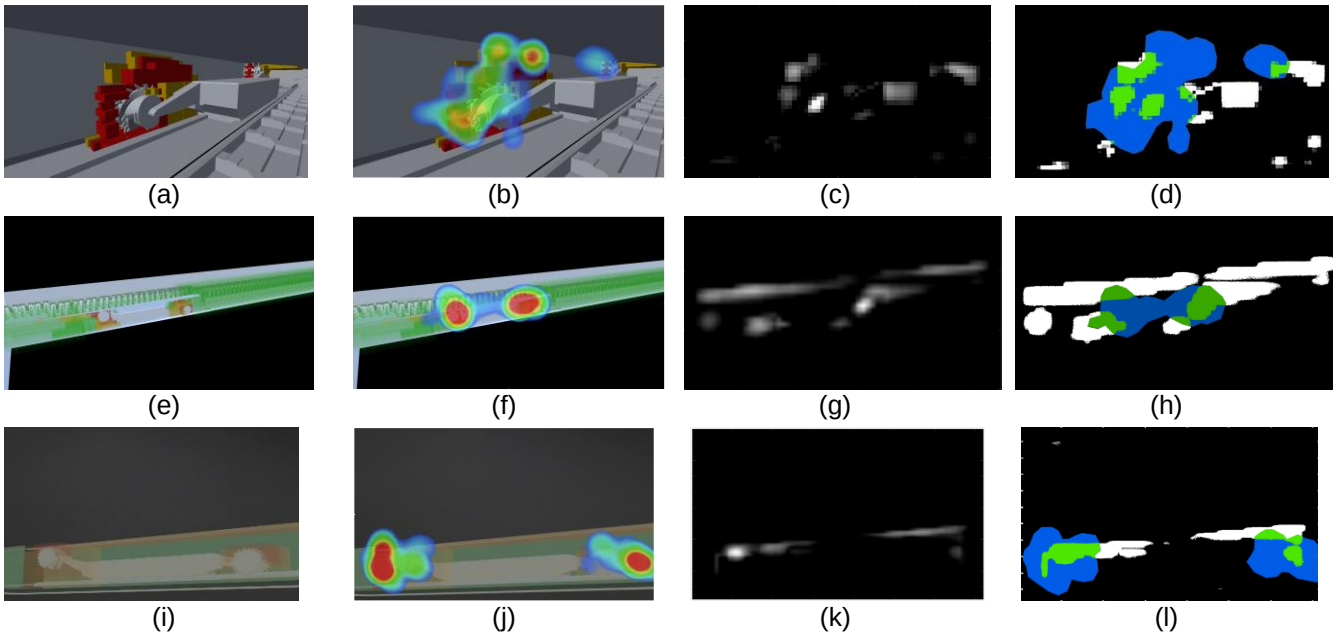

Figure 5.2 Example snapshots of each simulation (a, e and I show the original viewpoints for VR, computer screen and AR, b, f and j show heat maps of the eye tracker, c, g, k show Itti Koch saliency maps, d, h and l show overlay of the eye tracker and saliency map)

5.4.4. Users' Feedback

In the qualitative analysis, responses to the post questionnaires showed that, in computer screen simulations, users favored TCV visualization the most, followed by TSV, then OSV, and finally, OCV. None of the participants reported feeling eye strain, motion sickness, or any negative effects.

In VR simulations, the most preferred visualization was OSV, followed by TSV, then TCV, and then, OCV. On the negative side, 27% of the participants reported feeling eye strain and fatigue after the tests. Also, 10% of participants reported feeling tense, and 6% reported feeling claustrophobic and scared during the test.

In AR simulations, the preferred visualizations were OCV, OSV, and TSV, with nine votes for each, and the least preferred one was TCV. On the negative side, 20% of the participants reported feeling eye strain and 5% fatigue after the test. Only one of the participants reported feeling tense, and none reported feeling claustrophobic or scared.

In comparing computer screens and VR, 27 out of 30 preferred to use VR for such a task. When the reasons for favoring VR were given, the most common answers were realism (67%), the immersive environment (50%), and easy-to-calculate volumes (33%). When the reasons for disfavoring computer screens were given, the most common answers were dimensionless visualization (60%) and difficulty to understand (50%).

In comparing computer screens and AR, 15 out of 30 preferred to use AR. When the reasons for favoring AR were asked, the common answers were investigating 3D from top to bottom (50%). Reasons for disfavoring computer screens were the same as VR, which were dimensionless visualization (33%) and difficulty to understand (33%).

In comparing AR and VR, 17 out of 30 preferred to use VR. The most common reasons for favoring VR were realism (67%), immersive environment (50%), and easy-to-calculate volumes (33%). Reasons for disfavoring AR were lack of realism (67%).

Finally, when participants were asked to rank the three platforms, 17 chose VR, 9 chose AR and three chose computer screens. Figure 5.3 visualizes the most used words are as a word cloud based on the users' feedback.

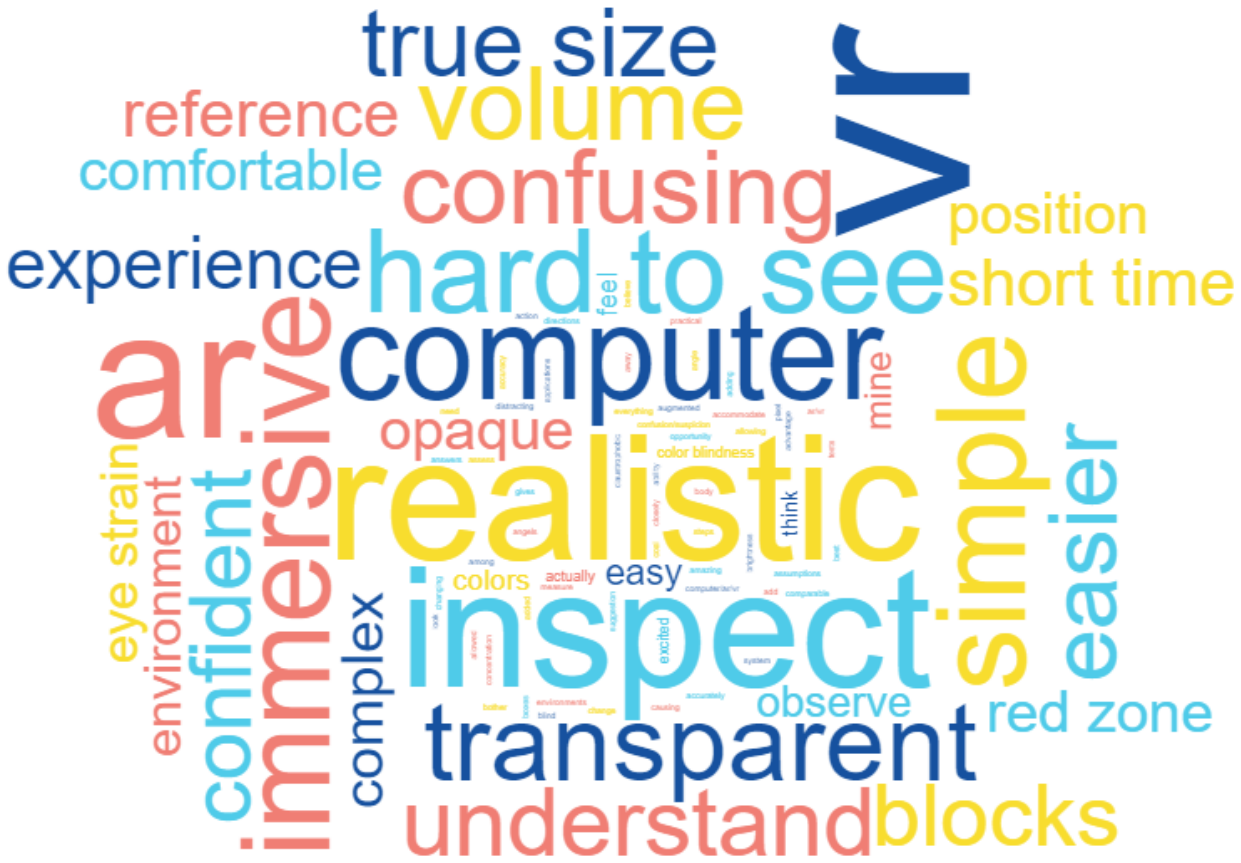

Figure 5.3 Users' Word Cloud

5.5. Discussion

We found that visual variables in computer screens only affects the time spent on assessment in OCV and OSV, and with OCV and TCV. In both cases OCV made users spent more time on their assessment. The comparison between OCV and OSV revealed that complex data made users spend

more time, which is reasonable. While looking at the OCV and TCV, users spent less time since they could see the behind of the visualized data with the help of transparency.

For the VR visualizations, there were three significant results for both accuracy and time spent on the assessment. For accuracy, OCV and OSV, OCV and TCV, TCV and TSV visualizations showed statistically significant differences. In the OCV and OSV comparison, OSV yielded a volume estimation that was 60 times more accurate, which was expected since it is probably harder for users to observe the methane content with the complex data. In the OCV and TCV comparison, transparency helped users with a better view, so the error was less than opaque data by two-fold. Lastly, for TCV and TSV comparison, even though transparency helped users with a better view, data was still blocking some important parts. This is why simple data error outperformed volume estimations with 15 times fewer errors. When it comes to the time spent on assessment, TCV and TSV comparison simple visualization yielded faster results. For the OCV and TCV, OCV and OSV, even if OCV showed faster results, it should be noted that users could not observe the methane cloud due to the opacity of the data. Therefore the response times should not be taken into account as success.

For the AR visualization, in terms of accuracy, only TCV and TSV yielded statistically significant differences. With the simple data, accuracies increased five times compared to complex data. The reason might be that the unnecessary data did not block or distract users while calculating the methane volume. In terms of the time spent in the assessment, OCV and OSV, OCV and TCV, the OCV lagged behind in both comparisons. In the first comparison, simple data yielded faster completion time and with the second one, transparency helped users see whole data without spending much time.

We found that using VR yields higher accuracies in volume estimation when compared to computer screens in OSV and TSV. However, in complex data, regardless of opacity, users had difficulties investigating the data so computer screens are better in TCV and OCV. When comparing computer screens and AR, computer screens yielded better accuracies in all visualization options. When comparing AR and VR, in OCV, AR outperformed VR but it would not be a fair comparison since the VR users were blocked by the opaque data. However, in TSV, when both platform users could see the methane volumes, errors in AR were more than ten times greater when compared to VR.

Even though users knew the scales and measurements of the mining equipment in all platforms, they more easily scaled the model and calculated the volume with less than a 0.15 meter cube error in VR for simple visualizations. Based on the error data, if the task required volume estimation, VR's OSV and TSV was the best option, versus computer screens' TCV and OCV and with AR', any option was the worst. This suggests that if data visualization is opaque or transparent with simple data, VR needs to be utilized for better accuracy. If visualization is done with complex data, regardless of opacity and transparency, computer screens need to be utilized. AR is not a good option for accuracy tasks with the given visual variables.

While VR outperformed the computer screen in terms of accuracy, it yielded an opposite result for the time spent on the task. When it came to the comparison with AR, computer screen task time was always

faster in all visualizations. On the other hand, there were no statistically significant differences in the VR comparison. Participants spent 55 to 75 seconds completing the task in VR and 39 to 70 seconds on computer screens and 54 to 85 seconds in AR. In simple terms, if the task is fast response, computer screens are the best option to visualize data. As it was mentioned before, even if users were familiar with AR and VR technology, they were not used to interacting with or utilizing these devices in their daily life. It might be different when working with experienced users. To better understand this difference, we investigated eye tracking and saliency maps as well.

Eye tracking and salient regions showed consistency in both the computer screens and AR. However, participants spent half of their time in the nonsalient areas in VR. There might be two explanations for VR. First, participants might have scaled the environment with the mining equipment, which is a nonsalient area. Thus looking back and forth between the methane zone and mining equipment might have slowed them down. Even though they lost some time, this might be the reason for close-to-perfect volume estimations. The second reason might be, as stated in the users' VR experiences, that only one of them used a VR device for the last month, and 70% of the participants did not have any experience with VR. Therefore they might have wanted to spend some time in this new and immersive experience.

It was highly likely that both reasons would cause longer times for task completion. The users' volume estimation results supported the first explanation, and their post-experiment surveys supported the second, as they stated that they felt amazed by the realism and the immersive experience.

Finally, regarding the participants' preferences, in computer screens, they preferred the same visual variables as used in the industry, which was transparent and complex data. In VR, they preferred solid and simple data. We hypothesized that they would prefer transparent and simple data since the transparency would let them see visualizations of the back side of the simulated volume in the immersive environment. However, transparency did not affect their preferences. On the other hand, in AR, we hypothesized that transparency might decrease performance of the users since AR’s nature is transparent, which we can partially confirm with the OCV and TSV comparison in terms of completion time.

5.6. Conclusions

The results of this study proved hypothesis 1A, that an immersive environment helps more accurate data interpretation than conventional computer screen visualization, regardless of opacity, provided the visuals are simple.

The results of this study revealed that while OSV and TCV visualization resulted in faster data interpretation in computers, TSV data visualization had significant differences in VR. For volume estimation on computer screens, visualization variables did not affect the accuracy of methane estimation. On the contrary, in VR, simple simulations yielded more accurate results. Moreover, AR lagged behind both in accuracy and time when compared with computer screens. These results prove

hypothesis 1B, stating the same visual variables for computer screens would not have the same effects in AR and VR.

Regarding hypothesis 2,"users' focus on computer screens will match the visuals' saliency, but in AR and VR, users will spend more time in nonsalient areas," saliency maps showed that in computer screens, 50% of eye tracking data matched salient regions, while in AR and VR 33% and 37% of the eye tracking data matched salient regions, respectively. In addition to that, the total time spent in AR and VR was longer than that of computer screens.

For hypothesis 3, "users will prefer to use VR with simple and transparent data," users preferred using VR and felt more confident while making volume estimations. However, they preferred simple opaque data over simple transparent.

There are more visual variables that are utilized by the designers and developers, yet this study tested only two of them. For future work, we plan to add additional variables.

CHAPTER 6

IMPLEMENTATION OF AR ASSISTANCE

An article published in IEEE International Symposium on Mixed and Augmented Reality Adjunct

Doga Cagdas DEMIRKAN[10,11], H. Sebnem Duzgun[10]

This chapter presents proof of concept of real-life implementation of an AR device in an underground mine, which is the implementation section of Step 4 in this dissertation's overall methodology (Figure 2.1).

In this study, we evaluate the performance of AR-assisted navigation in a real underground mine with good and limited illumination conditions as well as without the illumination considering possible search and rescue conditions. For this purpose, we utilized the Lumin SDK's embedded spatial mapping algorithm for mapping and navigating. We used the spatial mapping algorithm to create the mesh model of the escape route and to render it with the user input into the Magic Leap One. Then we compared the spatial mapping algorithm in three different scenarios for the evacuation of an underground mine in an emergency situation. The escape route had two junctions and 30 meters (100 feet). The baseline scenarios were (i) evacuation of the mine in a fully illuminated condition, (ii) evacuation with the headlamp and (iii) without any illumination. In the first scenario (fully illuminated route with the rendered meshes) the evacuation took 40 seconds. In the second scenario (illumination with the headlamp), the evacuation took 44 seconds. For the last scenario (no light source and hence in total darkness) the evacuation took 54 seconds. We found that AR-assisted navigation was effective for supporting search and rescue efforts in high attrition conditions of an underground space.

6.1. Introduction

Indoor navigation is still a challenging task, despite the advancement in global positioning systems (GPS) and related sensor technologies [126]. The highly attenuated and scattered signals of GPS due to the surroundings, such as buildings, trees, and other objects, degrade the position accuracy in indoor environments [127]. Indoor localization and real-time indoor mapping are essential for navigation and situational awareness, especially for emergency management and search and rescue operations [128].

Underground environments, such as tunnels, mines, and caves, are GPS-denied spaces with low visibility and inherent attrition limitations (e.g., dust, confined and rugged navigation paths), which require sophisticated indoor navigation solutions [129]. In this respect, 3D indoor mapping provides first

[10] Corresponding author. Direct correspondence to isleyen@mines.edu
[11] Mining Engineering Department, Colorado School of Mines, 1500 Illinois St., Golden, CO 80401, USA

responders with invaluable support with fast and safe navigation to reach the people who could be injured due to the hazardous conditions of the underground environment (e.g. falling ground, gas leaks, etc.)

Due to the challenging nature of the underground spaces, search and rescue operations need specific assisted technologies for mapping, positioning, and navigation [130]. In this respect, AR-assisted navigation for underground spaces has great potential to leverage search and rescue efforts in emergency evacuation scenarios. However, this has not been explored sufficiently.

In this study, the research question is, how can we improve search and rescue operations in GPS-denied and low to no visibility conditions such as underground mines? The research hypothesis is; AR assisted navigation can decrease the evacuation time and AR assistance can make navigation possible in total darkness.

The main objective of this study was to evaluate one of the newly published embedded mapping solutions by Lumin SDK in a challenging underground space for the search and rescue mission. The contributions of the performed study can be listed as:

- Adopting the newly available embedded spatial mapping algorithm of Lumin SDK for mapping an underground environment.
- Evaluating the performance of the algorithm in different lighting conditions, including limited lighting and total darkness.
- Assessing the effectiveness of the AR-assisted navigation for an emergency evacuation scenario in an underground mine.

6.2. Experimental Design and Evaluation

Lumin is a recently available SDK for Magic Leap One development only. Because of its short past, the number of published works for its performance is limited. There are three possible development platforms for Magic Leap, namely, Unity, Unreal Engine and Native. All of these platforms have their own advantages; however, since Unity is broadly used and accepted, we chose to use Unity for our study.

The followed design steps were i) implementing Lumin SDK to Unity game engine, ii) importing the spatial mapper, iii) adjusting the code with the study needs, iv) optimizing the parameters for scanning and updating the environment, v) coding the necessary interactions, vi) building the application, and vii) running it in Magic Leap One.

In this study, we performed a performance evaluation in the Edgar Experimental Mine, which is an underground mine with several intersecting underground roads. In Figure 6.1, the test area is given with blue and green stars represent the starting and the finishing points of the evacuation route. This route had two intersections, one was at the very beginning of the path and the other is close to the endpoint. It had a total length of 30 meters (100 ft). Since underground mines do not have lighting in all tunnels, we

needed to find a suitable place for a switchable (open/close) illumination source, including at intersections along the way. For this reason, we selected the section of the *experimental mine* in Figure 6.1.

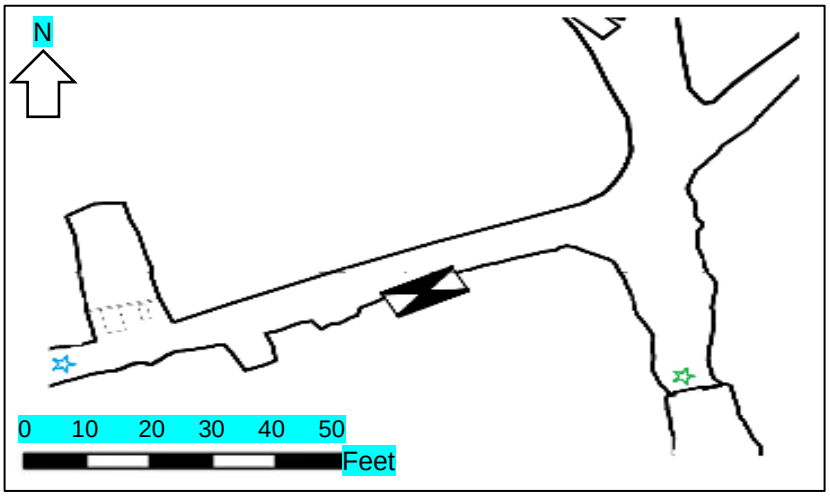

Figure 6.1 Escape route

Independent variables were lighting conditions and AR assistance. For the lighting conditions, variables were *fully* illuminated, *headlamp*, and *total darkness*. For the AR assistance, variables were *assisted* and *no assistance*. We predicted that decreasing illumination was negatively correlated with the completion time of the route, and AR assistance decreased the completion time of the route in any given illumination condition.

Figure 6.2 (a-f) shows three different scenarios that are fully illuminated, illuminated with the headlamp, total darkness, the fully illuminated scene with rendered meshes, illumination with the headlamp with rendered meshes and total darkness without any illumination source with rendered meshes, respectively.

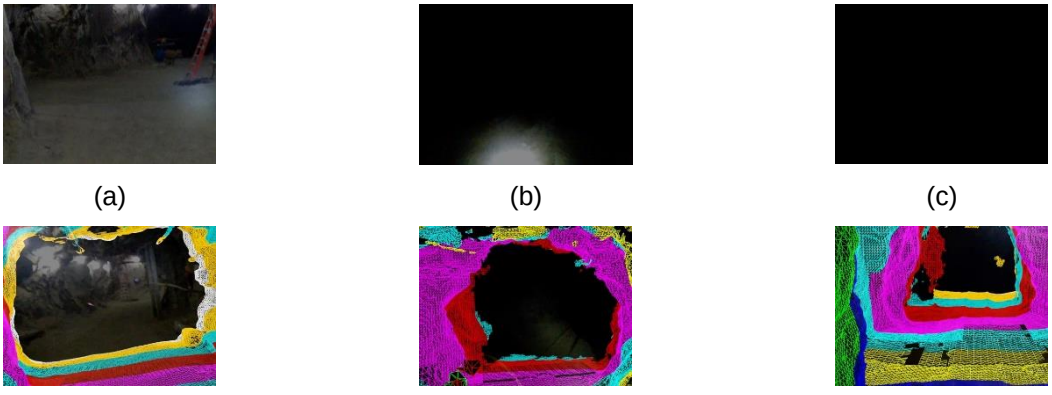

Figure 6.2 Illustration of the tested scenarios (a) fully illuminated scene, (b) illumination with the headlamp, (c) no illumination, (d) fully illuminated scene with rendered meshes, (e) illumination with the headlamp with rendered meshes (f) no illumination with rendered meshes

6.3. Results

Table 6.1 presents evacuation times for a designated path in three different conditions. In addition to being solely fully illuminated, illuminated with the headlamp and no light source route, the rendered meshes were implemented for each evacuation scenario.

Table 6.1 Total time for of completing the route

	Fully illuminated	Illuminated with headlamp	Total darkness
Without meshes	41	46	fail
With meshes	40	44	54

In non-assisted cases, evacuation times for fully illuminated and illumination with the headlamp took 41 and 46 seconds, respectively. In the total darkness case, user could not walk at all, therefore the timing of this scenario is not available. When it comes to the AR assisted cases, it took 40, 44 and 54 seconds for fully illuminated, illuminated with the headlamp and total darkness conditions, respectively.

When we compared the fully illuminated cases, evacuation times were close to one another. That said, implementing meshes decreased the evacuation time. Even if the area was fully illuminated, the AR headset gave the user a more immersive understanding of the environment with situational awareness allowing the user to move faster.

Lastly, in the total darkness, without the AR assistance, users could not move, which was expected. AR assistance in an underground environment was a total triumph. It helped the user to evacuate in a timely manner.

There were a couple of shortfalls while conducting the experiment. First, as Magic Leap is a head-mounted display, walking on a rough path makes it vibrate more than its head pose tracking capabilities. It also tracks the head pose with eye trackers, which caused the tracking failure in a short period of time due to darkness and failed to render meshes. Secondly, it can continue to map the environment and to keep track of the limited lighting conditions, however, head pose could not be located due to the lack of lighting through the eyes. Lastly, we tried to remediate the head pose lost failure problem by implementing a code; however, the current SDK of Lumin does not allow developers to override the failure.

6.4. Conclusions

In this study, we tested the potential of AR assisted navigation for an underground environment in different illumination conditions along with the newly available Lumin SDK's spatial mapper algorithm. Additionally, the evacuation scenario with a designated 30-meter path was compared by using a time of

evaluation metric. We found that in such a challenging underground environment, spatial mapper successfully constructs the twin 3D environment. As a second conclusion, the study indicated that even with the low light conditions, Magic Leap could successfully map the environment and keep track of the position of the user. Last but not least, AR- assisted evacuation improved the unassisted, conventional navigation in the designated path in fully and headlamp illuminated conditions, respectively. Most importantly, unlike the non-assisted case in total darkness, AR made it possible to navigate through the path. Based on these findings it can be concluded that AR is quite effective in assisting navigation in underground spaces in limited or no visibility conditions.

CHAPTER 7

OVERALL CONCLUSIONS AND RECOMMENDATIONS FOR FUTURE WORK

Real-time methane monitoring is still a challenging task. Around the world, methane explosions still cost people's lives. Implementing AI in the mining industry has the potential to reduce accidents, increase safety, decrease lost production time, and hence increase profitability. This dissertation lays the foundations of 3D real-time methane monitoring in longwall coal mining. The methodology included benchmarking the AI algorithms for applicability, modifying an AI algorithm, and representing the results in three platforms for faster and more accurate explosive methane gas monitoring. The proposed prediction methodology was tested with six mining scenarios, and the results were tested with a user study containing 30 people. This dissertation answered three questions with the stated methodology.

The first question was, “What is the best AI method to utilize for 3D methane concentration predictions in real time?” Among the current state of art AI architectures, deep-learning-based time series classification algorithms show promising results. With accuracies between 80% to 93%, the hypothesis that 3D real-time methane prediction can be achievable with AI was proven in Chapter 3.

The second question was, “How can methane monitoring and computational fluid dynamics data be implemented in AI for accurate 3D methane predictions?” The current practices are not sufficient for 3D real-time methane prediction. Moreover, with the first research studies, accuracies were not stable. To improve prediction accuracy, the LSTM algorithm was modified for the needs of underground longwall coal mine measurements by combining the advantages of methane monitors and CFD simulations. The results proved the hypothesis that, with modifications to the long-short term memory algorithm, CFD and methane sensor data could be used to predict methane concentrations in 3D and real-time with robust and higher accuracies (see Chapter 4).

The third and last question was, ”What are the best ways to visualize prediction data for accurate and fast assessment for users in the field?” This question hypothesized that instead of conventional visualization methods, emerging technologies such as VR and AR might help increase accuracy and decrease assessment time hence cognitive load. This hypothesis was partially proven as the VR visualization yielded more accurate methane estimations when compared to computer screens. However, in terms of time spent on the assessment, the computer screen is faster than AR and VR. Chapter 5 showed that while the hypothesis was correct about increasing accuracy, the assessment time increased when using the emerging technologies.

Lastly, Chapter 6 outlined a proof of concept for the future implementation of an AR device for data visualization in an underground mine.

This research had some limitations, which are listed as follows:

i) Current computational power and storage are not sufficient for training an algorithm for long periods of time. With scales of 300m by 9m by 5m mine layout with 180-time steps and 32 million points, the data size is more than 15TB. In this study time, the steps were one second apart. Even if it is chosen one minute apart, three hours of data is not sufficient for constant methane monitoring.

ii) It is not possible to collect real measurement data from a working mine. Although literature proves that CFD simulations can be treated as real data collection, a test needs to be conducted with an actual mine. There are legal and safety issues with that.

iii) There are more than 15 visual variables. However, due to the required number of users for a user study limits the tested, visual variables. For every additional variable, 15 more people are required with three more visualizations which also increases the user's experiment time. In this research, each user spent around one hour. Increasing the study time might affect users' concentration and attention.

iv) The underground tests are conducted in a static environment. The current capacities of AR devices are not agile for dynamic environments. However, rapidly developing technology might catch up with that problem.

Future researchers can go from sensory readings to visualization by taking these steps: i) creating the mine layout with the boundary conditions for CFD simulations, ii) training an AI model with data from the CFD visualizations and predicting future methane concentrations, and iii) implementing these predictions in Unity for visualization purposes for AR and VR. Further recommendations for future work are listed below:

In Chapter 3, we calculated the accuracies for each specific data point over the recording time; however, accuracies over a specific volume (combinations of data points) might also be investigated. Since the EGZs need a certain threshold volume, evaluating over specific volume could increase the robustness of the predictions.

In Chapter 4, the AI predictions were performed for the upcoming 90 seconds. The shutdown of the operation and the estimated evacuation time of the underground personnel were not considered. As a future work, evacuation time might be considered for upcoming predictions.

The methodology presented in this dissertation was developed to address the 3D real-time methane monitoring problems of a single mine design. Expanding the training set with data from multiple mine designs might increase the generalization ability of the system and improve the results.

In Chapter 5, user tests were conducted in a fixed order of PC, AR, and VR. The impact of randomized order was not taken into account. However, each visualization was designed with different methane volumes and locations. Therefore, the participants needed to investigate the EGZs from another level. Moreover, the participants were asked to estimate the specific quantity instead of being asked whether the volume was greater than a certain amount. By taking these steps, the effect of fixed platform order was tried to be minimized. Future studies might consider randomizing the test order.

The visualizations were developed as static images to give each user the exact same snapshot for the volume estimation. It was observed that some users spent more time estimating methane volume and

investigating the surroundings. If the visualizations were dynamically changing, the estimations and errors could not be calculated in an unbiased manner. Future studies might consider comparing static and dynamic visualizations. Lastly, to create visualization guidelines, other visual variables need to be tested with an unbiased user study.

REFERENCES

[1] B. Dudley and others, “BP statistical review of world energy,” *BP Stat. Rev. London, UK, accessed Aug*, vol. 6, no. 2018, p. 116, 2018.

[2] S. S. Peng, *Longwall Mining*. CRC Press, 2019.

[3] M. Qiao, T. Ren, J. Roberts, X. Yang, Z. Li, and J. Wu, “New insight into proactive goaf inertisation for spontaneous combustion management and control,” *Process Saf. Environ. Prot.*, vol. 161, pp. 739–757, May 2022, doi: 10.1016/J.PSEP.2022.03.074.

[4] S. Schatzel, C. Karacan, R. Krog, G. Esterhuizen, and G. Goodman, “Guidelines for the Prediction and Control of Methane Emissions on Longwalls,” *Inf. Circ. 9502*, 2008, [Online]. Available: http://www.cdc.gov/niosh/mining/UserFiles/works/pdfs/2008-114.pdf.

[5] V. Gangrade, S. J. Schatzel, and S. P. Harteis, “A Field Study of Longwall Mine Ventilation Using Tracer Gas in a Trona Mine,” *Mining, Metall. Explor.*, vol. 36, no. 6, pp. 1201–1211, 2019, doi: 10.1007/s42461-019-0096-0.

[6] A. Juganda, “Evaluation of point-based methane monitoring and proximity detection for methane explosive zones in longwall faces of underground coal mines,” Colorado School of Mines, 2020.

[7] A. Juganda, C. Strebinger, J. F. Brune, and G. E. Bogin, “Discrete modeling of a longwall coal mine gob for CFD simulation,” *Int. J. Min. Sci. Technol.*, vol. 30, no. 4, pp. 463–469, 2020, doi: 10.1016/j.ijmst.2020.05.004.

[8] S. G. Davis, D. Engel, and K. van Wingerden, “Complex explosion development in mines: Case study—2010 upper big branch mine explosion,” *Process Saf. Prog.*, vol. 34, no. 3, pp. 286–303, 2015.

[9] D. C. Demirkan, S. Duzgun, A. Juganda, J. Brune, and G. Bogin, “Evaluation of time series artificial intelligence models for real-time/near-real-time methane prediction in coal mines,” *CIM J.*, vol. 0, no. 0, pp. 1–10, 2022, doi: 10.1080/19236026.2022.2072664.

[10] M. Waskom, “Seaborn: Statistical Data Visualization,” *J. Open Source Softw.*, vol. 6, no. 60, p. 3021, 2021, doi: 10.21105/joss.03021.

[11] J. Bertin, *Semiologie graphique*. Paris, 1967.

[12] A. M. MacEachren, *Some Truth With Maps: A Primer on Symbolization and Design*. Association of American Geographers, 1994.

[13] J. L. Morrison, “A theoretical framework for cartographic generalization with the emphasis on the process of symbolization,” *Int. Yearb. Cartogr.*, vol. 14, no. 1974, pp. 115–127, 1974.

[14] A. Yilmaz and S. Duzgun, “A Framework for Visualization of Geospatial Information in 3 D Virtual City Environment for Disaster Risk Management,” 2014.

[15] A. Juganda, “Evaluation of point-based methane monitoring and proximity detection for methane explosive zones in longwall faces of underground coal mines,” p. 255, 2020, [Online]. Available: https://hdl.handle.net/11124/174069.

[16] C. D. Taylor, J. E. Chilton, and T. Mal, “Evaluating performance characteristics of machine-mounted methane monitors by measuring response time.”

[17] C. D. Taylor, J. E. Chilton, and J. A. Zimmer, “Use of a Test Box to Measure Response Times for Machine-Mounted Monitors,” 2002.

[18] C. D. Taylor, E. D. Thimons, and J. A. Zimmer, “FACTORS AFFECTING THE LOCATION OF METHANOMETERS ON MINING EQUIPMENT,” no. Figure 1, pp. 1–5, 1997.

[19] G. V. R. G. Charles D. Taylor, J. Emery Chilton, “Guidelines for the Control and Monitoring of Methane Gas on Continuous Mining Operations,” 2010.

[20] J. A. Marts, R. C. Gilmore, J. F. Brune, G. E. Bogin, J. W. Grubb, and S. Saki, “Dynamic gob response and reservoir properties for active longwall coal mines,” *Min. Eng.*, vol. 66, no. 12, pp. 41–48, 2014.

[21] KRICKOVIC S and FINDLAY C, “Methane emission rate studies in a central Pennsylvania mine,” *U S Bur Mines, Rep Invest 7591*, 1971.

[22] S. S. Peng and H. S. Chiang, “Air velocity distribution measurements on four mechanized longwall coal faces,” *Int. J. Min. Geol. Eng.*, vol. 4, no. 3, pp. 235–246, 1986, doi: 10.1007/BF01560718.

[23] R. B. Krog, S. J. Schatzel, F. Garcia, and J. K. Marshall, “Predicting methane emissions from longer longwall faces by analysis of emission contributors,” *Proc. 11th U.S./North Am. Mine Vent. Symp. - 11th U.S./North Am. Mine Vent. Symp. 2006*, pp. 383–392, 2006, doi: 10.1201/9781439833391.ch54.

[24] V. Gangrade, S. J. Schatzel, S. P. Harteis, and J. D. Addis, “Investigating the Impact of Caving on Longwall Mine Ventilation Using Scaled Physical Modeling,” *Min Met. Explor*, vol. 36, no. 4, pp. 729–740, 2019, doi: 10.1007/s42461-019-0065-7.Investigating.

[25] A. Mellit and S. A. Kalogirou, “Artificial intelligence techniques for photovoltaic applications: A review,” *Prog. Energy Combust. Sci.*, vol. 34, no. 5, pp. 574–632, 2008, doi: https://doi.org/10.1016/j.pecs.2008.01.001.

[26] J. Wang, W. Xu, and Y. Gong, “Real-time driving danger-level prediction,” *Eng. Appl. Artif. Intell.*, vol. 23, no. 8, pp. 1247–1254, 2010, doi: 10.1016/j.engappai.2010.01.001.

[27] J. Kaur and K. S. Mann, “AI based healthcare platform for real time, predictive and prescriptive analytics,” *Commun. Comput. Inf. Sci.*, vol. 805, pp. 138–149, 2018, doi: 10.1007/978-981-13-0755-3_11.

[28] G. Lykou, P. Dedousis, G. Stergiopoulos, and D. Gritzalis, “Assessing Interdependencies and Congestion Delays in the Aviation Network,” *IEEE Access*, vol. 8, pp. 223234–223254, 2020, doi: 10.1109/ACCESS.2020.3045340.

[29] F. Finkeldey, A. Saadallah, P. Wiederkehr, and K. Morik, “Real-time prediction of process forces in milling operations using synchronized data fusion of simulation and sensor data,” *Eng. Appl. Artif. Intell.*, vol. 94, no. October 2019, p. 103753, 2020, doi: 10.1016/j.engappai.2020.103753.

[30] Y. Bengio, “Learning Long-Term Dependencies with Gradient Descent is Difficult,” *IEEE Trans. Neural Networks*, vol. 5, no. 2, pp. 157–167, 1994.

[31] H. Sak, A. Senior, and F. Beaufays, “Long Short-Term Memory Based Recurrent Neural Network Architectures for Large Vocabulary Speech Recognition,” no. Cd, 2014, [Online]. Available:

http://arxiv.org/abs/1402.1128.

[32] M. Phi, “Illustrated Guide to LSTM’s and GRU’s: A step by step explanation,” 2018. https://towardsdatascience.com/illustrated-guide-to-lstms-and-gru-s-a-step-by-step-explanation-44e9eb85bf21 (accessed Dec. 03, 2021).

[33] J. S. Alex Graves, Marcus Liwicki, Santiago Fern´andez Roman Bertolami, Horst Bunke, “A Novel Connectionist System for Unconstrained Handwriting Recognition,” *IEEE Trans. Pattern Anal. Mach. Intell.*, vol. 31, no. 5, pp. 855–68, 2009, doi: 10.1016/j.inoche.2011.04.023.

[34] K. Greff, R. K. Srivastava, J. Koutnik, B. R. Steunebrink, and J. Schmidhuber, “LSTM: A Search Space Odyssey,” *IEEE Trans. Neural Networks Learn. Syst.*, vol. 28, no. 10, pp. 2222–2232, 2017, doi: 10.1109/TNNLS.2016.2582924.

[35] Y. Jansen *et al.*, “Opportunities and Challenges for Data Physicalization To cite this version : HAL Id : hal-01120152 Opportunities and Challenges for Data Physicalization,” 2016.

[36] A. Cairo, *The Functional Art: An introduction to information graphics and visualization*. New Riders, 2012.

[37] C. N. Knaflic, *Storytelling with data: A data visualization guide for business professionals*. John Wiley & Sons, 2015.

[38] C. Ware and J. C. Beatty, “Using color dimensions to display data dimensions,” *Hum. Factors*, vol. 30, no. 2, pp. 127–142, 1988.

[39] R. Tufte Edward, “The visual display of quantitative information.” Cheshire, Connecticut: Graphic Press, 2001.

[40] M. Friendly, “A Brief History of Data Visualization,” in *Handbook of Data Visualization*, Berlin, Heidelberg: Springer Berlin Heidelberg, 2008, pp. 15–56.

[41] S. Garlandini and S. I. Fabrikant, “Evaluating the Effectiveness and Efficiency of Visual Variables for Geographic Information Visualization,” in *Spatial Information Theory*, 2009, pp. 195–211.

[42] Ł. Halik, “The analysis of visual variables for use in the cartographic design of point symbols for mobile Augmented Reality applications,” *Geod. Cartogr.*, vol. 61, no. 1, pp. 19–30, 2018, doi: 10.2478/v10277-012-0019-4.

[43] P. A. Kirschner, “Cognitive load theory: implications of cognitive load theory on the design of learning,” *Learn. Instr.*, vol. 12, no. 1, pp. 1–10, 2002, doi: https://doi.org/10.1016/S0959-4752(01)00014-7.

[44] L. V Monrouxe and C. E. Rees, “Theoretical perspectives on identity: researching identities in healthcare education,” in *Researching Medical Education*, John Wiley & Sons, Ltd, 2015, pp. 129–140.

[45] J. J. G. Merrienboer van and D. H. J. M. Dolmans, “Research on instructional design in the health sciences: from taxonomies of learning to whole-task models,” in *Researching Medical Education*, John Wiley & Sons, Ltd, 2015, pp. 193–206.

[46] J. Leppink, T. Gog van, F. Paas, and J. Sweller, “Cognitive load theory: researching and planning teaching to maximise learning,” in *Researching Medical Education*, John Wiley & Sons, Ltd, 2015, pp. 207–218.

[47] W. C. McGaghie and T. Kristopaitis, “Deliberate practice and mastery learning: origins of expert medical performance,” in *Researching Medical Education*, John Wiley & Sons, Ltd, 2015, pp. 219–230.

[48] K. Marriott *et al.*, *Immersive Analytics*, vol. 11190. Springer, 2018.

[49] T. Dwyer *et al.*, “Immersive Analytics: An Introduction,” in *Immersive Analytics*, K. Marriott, F. Schreiber, T. Dwyer, K. Klein, N. H. Riche, T. Itoh, W. Stuerzlinger, and B. H. Thomas, Eds. Cham: Springer International Publishing, 2018, pp. 1–23.

[50] A. Prouzeau, Y. Wang, B. Ens, W. Willett, and T. Dwyer, “Corsican Twin: Authoring In Situ Augmented Reality Visualisations in Virtual Reality,” 2020, doi: 10.1145/3399715.3399743.

[51] B. Lee, X. Hu, M. Cordeil, A. Prouzeau, B. Jenny, and T. Dwyer, “Shared surfaces and spaces: Collaborative data visualisation in a co-located immersive environment,” *IEEE Trans. Vis. Comput. Graph.*, vol. 27, no. 2, pp. 1171–1181, 2021, doi: 10.1109/TVCG.2020.3030450.

[52] J. Liu, A. Prouzeau, B. Ens, and T. Dwyer, “Design and Evaluation of Interactive Small Multiples Data Visualisation in Immersive Spaces,” *Proc. - 2020 IEEE Conf. Virtual Real. 3D User Interfaces, VR 2020*, no. 1, pp. 588–597, 2020, doi: 10.1109/VR46266.2020.1581122519414.

[53] K. A. Satriadi, B. Ens, M. Cordeil, B. Jenny, T. Czauderna, and W. Willett, “Augmented reality map navigation with freehand gestures,” *26th IEEE Conf. Virtual Real. 3D User Interfaces, VR 2019 - Proc.*, pp. 593–603, 2019, doi: 10.1109/VR.2019.8798340.

[54] A. Ivanov, K. T. Danyluk, and W. Willett, “Exploration & anthropomorphism in immersive unit visualizations,” *Conf. Hum. Factors Comput. Syst. - Proc.*, vol. 2018-April, pp. 0–6, 2018, doi: 10.1145/3170427.3188544.

[55] M. Whitlock, S. Smart, and D. A. Szafir, “Graphical Perception for Immersive Analytics,” *Proc. - 2020 IEEE Conf. Virtual Real. 3D User Interfaces, VR 2020*, pp. 616–625, 2020, doi: 10.1109/VR46266.2020.1582298687237.

[56] Y. Yang, T. Dwyer, K. Marriott, B. Jenny, and S. Goodwin, “Tilt Map: Interactive Transitions Between Choropleth Map, Prism Map and Bar Chart in Immersive Environments,” *IEEE Trans. Vis. Comput. Graph.*, no. June, pp. 1–1, 2020, doi: 10.1109/tvcg.2020.3004137.

[57] M. Cordeil *et al.*, “Embodied Axes: Tangible, Actuated Interaction for 3D Augmented Reality Data Spaces,” *Conf. Hum. Factors Comput. Syst. - Proc.*, 2020, doi: 10.1145/3313831.3376613.

[58] Conferance Ranks, “No Title.” http://www.conferenceranks.com/index.html?searchall=Human+Factors+in+Computing+Systems#data.

[59] B. Ens *et al.*, “Grand Challenges in Immersive Analytics,” vol. 17, pp. 1–17, 2021, [Online]. Available: http://hdl.handle.net/1880/112984.

[60] J. J. Rajan, “Time series classification.” University of Cambridge Cambridge, England, 1994.

[61] K. Li and J. C. Principe, “Transfer Learning in Adaptive Filters: The Nearest Instance Centroid-Estimation Kernel Least-Mean-Square Algorithm,” *IEEE Trans. Signal Process.*, vol. 65, no. 24, pp. 6520–6535, 2017, doi: 10.1109/TSP.2017.2752695.

[62] H. Ismail Fawaz, G. Forestier, J. Weber, L. Idoumghar, and P. A. Muller, “Deep learning for time series classification: a review,” *Data Min. Knowl. Discov.*, vol. 33, no. 4, pp. 917–963, 2019, doi:

10.1007/s10618-019-00619-1.

[63] H. A. Dau *et al.*, “The UCR time series archive,” *IEEE/CAA J. Autom. Sin.*, vol. 6, no. 6, pp. 1293–1305, 2019, doi: 10.1109/JAS.2019.1911747.

[64] A. Bagnall *et al.*, “The UEA multivariate time series classification archive, 2018,” pp. 1–36, 2018, [Online]. Available: http://arxiv.org/abs/1811.00075.

[65] H. I. Fawaz, G. Forestier, J. Weber, L. Idoumghar, and P. A. Muller, “Transfer learning for time series classification,” *Proc. - 2018 IEEE Int. Conf. Big Data, Big Data 2018*, pp. 1367–1376, 2019, doi: 10.1109/BigData.2018.8621990.

[66] R. Ye and Q. Dai, “A novel transfer learning framework for time series forecasting,” *Knowledge-Based Syst.*, vol. 156, no. December 2017, pp. 74–99, 2018, doi: 10.1016/j.knosys.2018.05.021.

[67] P. Gupta, P. Malhotra, J. Narwariya, L. Vig, and G. Shroff, “Transfer Learning for Clinical Time Series Analysis Using Deep Neural Networks,” *J. Healthc. Informatics Res.*, 2019, doi: 10.1007/s41666-019-00062-3.

[68] P. Malhotra, T. V. Vishnu, L. Vig, P. Agarwal, and G. Shroff, “TimeNet: Pre-trained deep recurrent neural network for time series classification,” *ESANN 2017 - Proceedings, 25th Eur. Symp. Artif. Neural Networks, Comput. Intell. Mach. Learn.*, pp. 607–612, 2017.

[69] P. Schäfer and U. Leser, “Fast and Accurate Time Series Classification with WEASEL,” in *Proceedings of the 2017 ACM on Conference on Information and Knowledge Management*, 2017, pp. 637–646, doi: 10.1145/3132847.3132980.

[70] P. Schäfer, “Bag-Of-SFA-Symbols in Vector Space (BOSS VS),” *ZIB Rep.*, vol. 30, no. May, pp. 15–30, 2015, doi: 10.1515/johh-2017-0044.

[71] H. Deng, G. Runger, E. Tuv, and M. Vladimir, “A time series forest for classification and feature extraction,” *Inf. Sci. (Ny).*, vol. 239, pp. 142–153, 2013, doi: 10.1016/j.ins.2013.02.030.

[72] J. Lines, S. Taylor, and A. Bagnall, “Time series classification with HIVE-COTE: The hierarchical vote collective of transformation-based ensembles,” *ACM Trans. Knowl. Discov. Data*, vol. 12, no. 5, 2018, doi: 10.1145/3182382.

[73] P. Marteau, “Time warp edit distance,” *arXiv Prepr. arXiv0802.3522*, 2008, [Online]. Available: http://arxiv.org/abs/0802.3522.

[74] A. Bagnall, J. Lines, A. Bostrom, J. Large, and E. Keogh, “The great time series classification bake off: a review and experimental evaluation of recent algorithmic advances,” *Data Min. Knowl. Discov.*, vol. 31, no. 3, pp. 606–660, 2017, doi: 10.1007/s10618-016-0483-9.

[75] A. Dempster, F. Petitjean, and G. I. Webb, “ROCKET: exceptionally fast and accurate time series classification using random convolutional kernels,” *Data Min. Knowl. Discov.*, vol. 34, no. 5, pp. 1454–1495, 2020, doi: 10.1007/s10618-020-00701-z.

[76] A. Shifaz, C. Pelletier, F. Petitjean, and G. I. Webb, *TS-CHIEF: a scalable and accurate forest algorithm for time series classification*, vol. 34, no. 3. Springer US, 2020.

[77] K. He, X. Zhang, S. Ren, and J. Sun, “Deep residual learning for image recognition,” *Proc. IEEE Comput. Soc. Conf. Comput. Vis. Pattern Recognit.*, vol. 2016-Decem, pp. 770–778, 2016, doi: 10.1109/CVPR.2016.90.

[78] H. Ismail Fawaz *et al.*, “InceptionTime: Finding AlexNet for time series classification,” *Data Min. Knowl. Discov.*, vol. 34, no. 6, pp. 1936–1962, 2020, doi: 10.1007/s10618-020-00710-y.

[79] J. Lines, L. M. Davis, J. Hills, and A. Bagnall, “A shapelet transform for time series classification,” *Proc. ACM SIGKDD Int. Conf. Knowl. Discov. Data Min.*, pp. 289–297, 2012, doi: 10.1145/2339530.2339579.

[80] B. Lucas *et al.*, “Proximity Forest: an effective and scalable distance-based classifier for time series,” *Data Min. Knowl. Discov.*, vol. 33, no. 3, pp. 607–635, 2019, doi: 10.1007/s10618-019-00617-3.

[81] National Institute for Occupational Safety and Health - NIOSH, “Current intelligence bulletin 66: Derivation of Immediately Dangerous to Life or Health (IDLH) Values,” p. 111, 2013.

[82] C. Ö. Karacan, “Modeling and prediction of ventilation methane emissions of U.S. longwall mines using supervised artificial neural networks,” *Int. J. Coal Geol.*, vol. 73, no. 3–4, pp. 371–387, 2008, doi: 10.1016/j.coal.2007.09.003.

[83] H. N. Dougherty and C. Özgen Karacan, “A new methane control and prediction software suite for longwall mines,” *Comput. Geosci.*, vol. 37, no. 9, pp. 1490–1500, 2011, doi: 10.1016/j.cageo.2010.09.003.

[84] A. Duda and A. Krzemień, “Forecast of methane emission from closed underground coal mines exploited by longwall mining – A case study of Anna coal mine,” *J. Sustain. Min.*, vol. 17, no. 4, pp. 184–194, 2018, doi: 10.1016/j.jsm.2018.06.004.

[85] A. A. Sidorenko, P. N. Dmitriev, and Y. G. Sirenko, “Predicting Methane Emissions from Multiple Gas-Bearing Coal Seams to Longwall Goafs at Russian Mines,” *ARPN J. Eng. Appl. Sci.*, vol. 16, no. 8, pp. 851–857, 2021.

[86] P.-H. C. Chen *et al.*, “An augmented reality microscope with real-time artificial intelligence integration for cancer diagnosis,” *Nat. Med.*, vol. 25, no. 9, pp. 1453–1457, 2019, doi: 10.1038/s41591-019-0539-7.

[87] Y. Nyanteh, C. Edrington, S. Srivastava, and D. Cartes, “Application of Artificial Intelligence to Real-Time Fault Detection in Permanent-Magnet Synchronous Machines,” *IEEE Trans. Ind. Appl.*, vol. 49, no. 3, pp. 1205–1214, 2013, doi: 10.1109/TIA.2013.2253081.

[88] A. McGovern *et al.*, “Using artificial intelligence to improve real-time decision-making for high-impact weather,” *Bull. Am. Meteorol. Soc.*, vol. 98, no. 10, pp. 2073–2090, 2017, doi: 10.1175/BAMS-D-16-0123.1.

[89] M. Imran, C. Castillo, J. Lucas, P. Meier, and S. Vieweg, “AIDR: Artificial intelligence for disaster response,” *WWW 2014 Companion - Proc. 23rd Int. Conf. World Wide Web*, pp. 159–162, 2014, doi: 10.1145/2567948.2577034.

[90] M. Dong *et al.*, “Deformation prediction of unstable slopes based on real-time monitoring and deepar model,” *Sensors (Switzerland)*, vol. 21, no. 1, pp. 1–18, 2021, doi: 10.3390/s21010014.

[91] H. Rodríguez-Rangel, L. A. Morales-Rosales, R. Imperial-Rojo, M. A. Roman-Garay, G. E. Peralta-Peñuñuri, and M. Lobato-Báez, “Analysis of Statistical and Artificial Intelligence Algorithms for Real-Time Speed Estimation Based on Vehicle Detection with YOLO,” *Appl. Sci.*, vol. 12, no. 6, pp. 1–20, 2022, doi: 10.3390/app12062907.

[92] Wahyono, A. Harjoko, A. Dharmawan, F. D. Adhinata, G. Kosala, and K. H. Jo, “Real-Time Forest

Fire Detection Framework Based on Artificial Intelligence Using Color Probability Model and Motion Feature Analysis," *Fire*, vol. 5, no. 1, 2022, doi: 10.3390/fire5010023.

[93] A. Alléon, G. Jauvion, B. Quennehen, and D. Lissmyr, "PlumeNet: Large-Scale Air Quality Forecasting Using A Convolutional LSTM Network," 2020, [Online]. Available: http://arxiv.org/abs/2006.09204.

[94] R. J. Hyndman and G. Athanasopoulos, *Forecasting: principles and practice*. OTexts, 2018.

[95] O. Calin, "Recurrent Neural Networks BT - Deep Learning Architectures: A Mathematical Approach," O. Calin, Ed. Cham: Springer International Publishing, 2020, pp. 543–559.

[96] S. Hochreiter and J. Schmidhuber, "Long Short-Term Memory," *Neural Comput.*, vol. 9, no. 8, pp. 1735–1780, 1997, doi: 10.1162/neco.1997.9.8.1735.

[97] C. Olah, "Understanding LSTM Networks," *Colah's Blog*, 2015. https://colah.github.io/posts/2015-08-Understanding-LSTMs/#fn1 (accessed Sep. 06, 2022).

[98] A. Gholamy, V. Kreinovich, and O. Kosheleva, "Why 70/30 or 80/20 Relation Between Training and Testing Sets : A Pedagogical Explanation," *Dep. Tech. Reports*, pp. 1–6, 2018.

[99] I. Guyon, "A scaling law for the validation-set training-set size ratio," *AT&T Bell Lab.*, pp. 1–11, 1997, [Online]. Available: http://citeseerx.ist.psu.edu/viewdoc/download?doi=10.1.1.33.1337&rep=rep1&type=pdf.

[100] J. Bertin, *Semiology of Graphics: Diagrams, Networks, Maps*. UMI Research Press, 1983.

[101] J. M. Wolfe, "Guided Search 2.0 A revised model of visual search," *Psychon. Bull. Rev.*, vol. 1, no. 2, pp. 202–238, 1994, doi: 10.3758/BF03200774.

[102] Z. P. Zhang and J. Liu, "Research on the symbol vision variable of the three-dimension virtual battle environment," *Geomatics Spat. Inf. Technol.*, vol. 37, no. 9, pp. 7–9, 2014.

[103] S. Hong, B. Mao, and B. Li, "Preliminary Exploration of Three-Dimensional Visual Variables in Virtual Reality," in *2018 International Conference on Virtual Reality and Visualization (ICVRV)*, 2018, pp. 28–34.

[104] A. Dasgupta, J. Poco, Y. Wei, R. Cook, E. Bertini, and C. T. Silva, "Bridging Theory with Practice: An Exploratory Study of Visualization Use and Design for Climate Model Comparison," *IEEE Trans. Vis. Comput. Graph.*, vol. 21, no. 9, pp. 996–1014, 2015, doi: 10.1109/TVCG.2015.2413774.

[105] B. Laha, K. Sensharma, J. D. Schiffbauer, and D. A. Bowman, "Effects of immersion on visual analysis of volume data," *IEEE Trans. Vis. Comput. Graph.*, vol. 18, no. 4, pp. 597–606, 2012, doi: 10.1109/TVCG.2012.42.

[106] H. Adams, J. Stefanucci, S. Creem-Regehr, and B. Bodenheimer, "Depth Perception in Augmented Reality: The Effects of Display, Shadow, and Position," *Proc. - 2022 IEEE Conf. Virtual Real. 3D User Interfaces, VR 2022*, pp. 792–801, 2022, doi: 10.1109/VR51125.2022.00101.

[107] T. Sun, Y. Cao, and B. Mao, "3D city cadaster data visualization and viewer behavior analysis in virtual reality environment," *Proc. - 2020 IEEE/WIC/ACM Int. Jt. Conf. Web Intell. Intell. Agent Technol. WI-IAT 2020*, pp. 936–939, 2020, doi: 10.1109/WIIAT50758.2020.00143.

[108] S. Arjun, G. S. R. Reddy, A. Mukhopadhyay, S. Vinod, and P. Biswas, “Evaluating Visual Variables in a Virtual Reality Environment,” *34th Br. Hum. Comput. Interact. Conf. Interact. Conf. BCS HCI 2021*, pp. 133–138, 2021, doi: 10.14236/ewic/HCI2021.1.

[109] A. Covaci, A. H. Olivier, and F. Multon, “Visual Perspective and Feedback Guidance for VR Free-Throw Training,” *IEEE Comput. Graph. Appl.*, vol. 35, no. 5, pp. 55–65, 2015, doi: 10.1109/MCG.2015.95.

[110] C. Koch and S. Ullman, “Shifts in selctive visual attention: twords the underlying neural circuitry,” *Hum. Neurobiol*, vol. 4, no. 10, pp. 219–227, 1985.

[111] L. Itti, C. Koch, and E. Niebur, “A Model of Saliency-Based Visual Attention for Rapid Scene Analysis,” *IEEE Trans. Pattern Anal. Mach. Intell.*, vol. 20, no. 11, pp. 1254–1259, 1998.

[112] E. Niebur and C. Koch, “Control of selective visual attention: modeling the {``}where{''} pathway,” *Adv. Neural Inf. Process. Syst.*, vol. 8, 1996.

[113] R. Veale, Z. M. Hafed, and M. Yoshida, “How is visual salience computed in the brain? Insights from behaviour, neurobiology and modeling,” *Philos. Trans. R. Soc. B Biol. Sci.*, vol. 372, no. 1714, 2017, doi: 10.1098/rstb.2016.0113.

[114] L. Itti and C. Koch, “Computational Modelling of,” *Neuroscience*, vol. 2, no. February, pp. 1–11, 2001, [Online]. Available: http://www.psypress.com/computational-modelling-9781841698557.

[115] Z. Hu, “Gaze Analysis and Prediction in Virtual Reality,” *Proc. - 2020 IEEE Conf. Virtual Real. 3D User Interfaces, VRW 2020*, pp. 543–544, 2020, doi: 10.1109/VRW50115.2020.00123.

[116] T. H. N. Huy, M. K. J. Carlon, and J. S. Cross, “Simulated Gaze Tracking using Computer Vision for Virtual Reality,” *Proc. 2022 8th Int. Conf. Immersive Learn. Res. Network, iLRN 2022*, pp. 1–5, 2022, doi: 10.23919/iLRN55037.2022.9815891.

[117] G. Arvanitis, A. S. Lalos, and K. Moustakas, “Saliency mapping for processing 3D Meshes in industrial modeling applications,” *IEEE Int. Conf. Ind. Informatics*, vol. 2019-July, pp. 683–686, 2019, doi: 10.1109/INDIN41052.2019.8972024.

[118] J. Hosseinkhani and C. Joslin, “Significance of Bottom-Up Attributes in Video Saliency Detection without Cognitive Bias,” in *2018 IEEE 17th International Conference on Cognitive Informatics & Cognitive Computing (ICCI*CC)*, 2018, pp. 606–613, doi: 10.1109/ICCI-CC.2018.8482037.

[119] Y. Wang, H. Su, B. Zhang, and X. Hu, “Learning Reliable Visual Saliency For Model Explanations,” *IEEE Trans. Multimed.*, vol. 22, no. 7, pp. 1796–1807, 2020, doi: 10.1109/TMM.2019.2949872.

[120] N. D. B. Bruce and J. K. Tsotsos, “Saliency based on information maximization,” *Adv. Neural Inf. Process. Syst.*, pp. 155–162, 2005.

[121] S. Duzgun, E. Isleyen, D. ~C. Demirkan, R. Orsvuran, E. Bozdag, and D. Pugmire, “Virtual and Augmented Reality for Visualization of Big Data: Examples from Deep Earth to Subsurface,” in *AGU Fall Meeting Abstracts*, Dec. 2019, vol. 2019, pp. IN21B-05.

[122] A. De Abreu, C. Ozcinar, and A. Smolic, “Look around you: Saliency maps for omnidirectional images in VR applications,” *2017 9th Int. Conf. Qual. Multimed. Exp. QoMEX 2017*, pp. 1–6, 2017, doi: 10.1109/QoMEX.2017.7965634.

[123] D. C. Demirkan, H. S. Duzgun, A. Juganda, J. Brune, and G. Bogin, “Real-Time Methane

Prediction in Underground Longwall Coal Mining Using AI," *Energies*, vol. 15, no. 17, pp. 1–12, 2022, doi: 10.3390/en15176486.

[124] K. Tcha-Tokey, O. Christmann, E. Loup-Escande, and S. Richir, "Proposition and Validation of a Questionnaire to Measure the User Experience in Immersive Virtual Environments," *Int. J. Virtual Real.*, vol. 16, no. 1, pp. 33–48, 2016, doi: 10.20870/ijvr.2016.16.1.2880.

[125] D. Walther and C. Koch, "Modeling attention to salient proto-objects.," *Neural networks Off. J. Int. Neural Netw. Soc.*, vol. 19, no. 9, pp. 1395–1407, Nov. 2006, doi: 10.1016/j.neunet.2006.10.001.

[126] M. A. Al-ammar, S. Alhadhrami, and A. Al-salman, "Comparative Survey of Indoor Positioning Technologies , Techniques , and Algorithms," *2014 Int. Conf. Cyberworlds*, pp. 245–252, 2014, doi: 10.1109/CW.2014.41.

[127] G. Dedes and A. G. Dempster, "Indoor GPS Positioning Challenges and Opportunities," in *EEE 62nd Vehicular Technology Conference*, 2005, pp. 412–415.

[128] A. Sochenkova, N. Podzharaya, and K. Samouylov, "Augmented Reality Application to Emergency Systems with Usage of SLAM," in *2019 8th Mediterranean Conference on Embedded Computing (MECO)*, 2019, no. June, pp. 1–4, doi: 10.1109/meco.2019.8760019.

[129] R. Zlot and M. Bosse, "Efficient Large-Scale 3D Mobile Mapping and Surface Reconstruction of an Underground Mine," in *Field and Service Robotics: Results of the 8th International Conference*, K. Yoshida and S. Tadokoro, Eds. Berlin, Heidelberg: Springer Berlin Heidelberg, 2014, pp. 479–493.

[130] W. Wang, W. Dong, Y. Su, D. Wu, and Z. Du, "Development of Search-and-rescue Robots for Underground Coal Mine Applications," *J. F. Robot.*, vol. 31, no. 3, pp. 386–407, 2014, doi: 10.1002/rob.

APPENDIX A

COMMITTEE EXEMPTION NOTICE

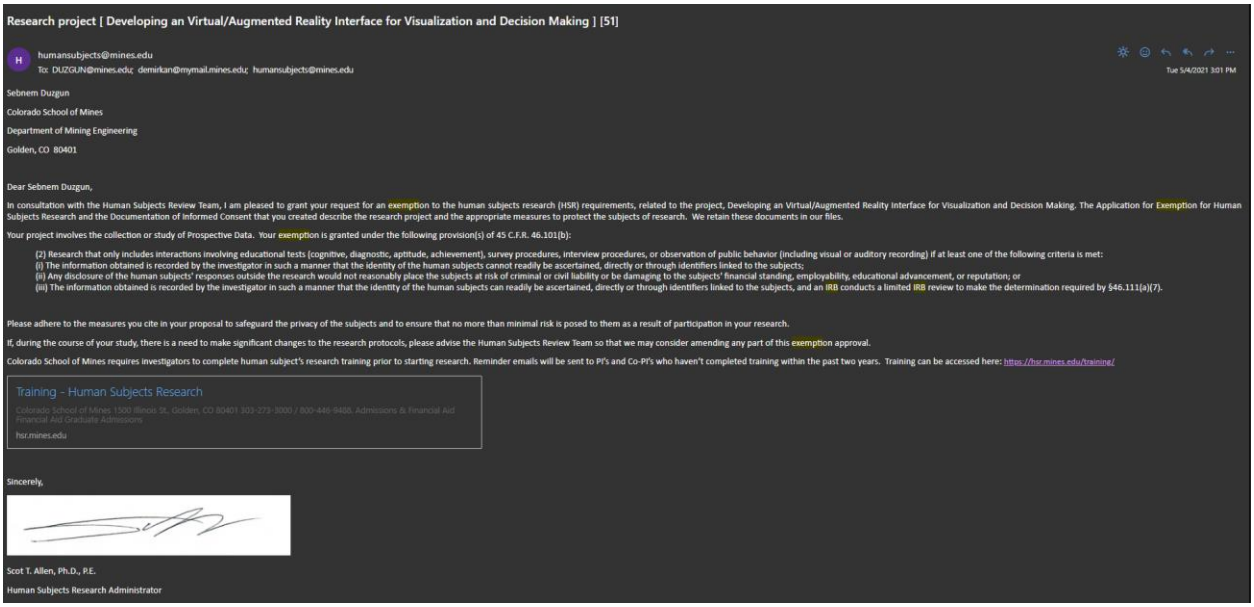

Research project [Developing an Virtual/Augmented Reality Interface for Visualization and Decision Making] [51]

humansubjects@mines.edu
To: DUZGUN@mines.edu; demirkan@mymail.mines.edu; humansubjects@mines.edu
Tue 5/4/2021 3:01 PM

Sebnem Duzgun
Colorado School of Mines
Department of Mining Engineering
Golden, CO 80401

Dear Sebnem Duzgun,

In consultation with the Human Subjects Review Team, I am pleased to grant your request for an exemption to the human subjects research (HSR) requirements, related to the project, Developing an Virtual/Augmented Reality Interface for Visualization and Decision Making. The Application for Exemption for Human Subjects Research and the Documentation of Informed Consent that you created describe the research project and the appropriate measures to protect the subjects of research. We retain these documents in our files.

Your project involves the collection or study of Prospective Data. Your exemption is granted under the following provision(s) of 45 C.F.R. 46.101(b):

(2) Research that only includes interactions involving educational tests (cognitive, diagnostic, aptitude, achievement), survey procedures, interview procedures, or observation of public behavior (including visual or auditory recording) if at least one of the following criteria is met:
(i) The information obtained is recorded by the investigator in such a manner that the identity of the human subjects cannot readily be ascertained, directly or through identifiers linked to the subjects;
(ii) Any disclosure of the human subjects' responses outside the research would not reasonably place the subjects at risk of criminal or civil liability or be damaging to the subjects' financial standing, employability, educational advancement, or reputation; or
(iii) The information obtained is recorded by the investigator in such a manner that the identity of the human subjects can readily be ascertained, directly or through identifiers linked to the subjects, and an IRB conducts a limited IRB review to make the determination required by §46.111(a)(7).

Please adhere to the measures you cite in your proposal to safeguard the privacy of the subjects and to ensure that no more than minimal risk is posed to them as a result of participation in your research.

If, during the course of your study, there is a need to make significant changes to the research protocols, please advise the Human Subjects Review Team so that we may consider amending any part of this exemption approval.

Colorado School of Mines requires investigators to complete human subject's research training prior to starting research. Reminder emails will be sent to PI's and Co-PI's who haven't completed training within the past two years. Training can be accessed here: https://hsr.mines.edu/training/

Training - Human Subjects Research
Colorado School of Mines 1500 Illinois St., Golden, CO 80401 303-273-3000 / 800-446-9488. Admissions & Financial Aid Financial Aid Graduate Admissions
hsr.mines.edu

Sincerely,

Scot T. Allen, Ph.D., P.E.
Human Subjects Research Administrator

Figure A.1 IRB Committee Exemption Notice

APPENDIX B

PRETEST SURVEY

Name

Email

Age

To which gender identity do you most identify?

Educational background.

Have you ever worked in the mining industry?

Have you ever been in an underground mine?

Have you ever been in an underground longwall coal mine?

Are you familiar with Augmented Reality and Virtual Reality?

Do you have any gaming experience with Augmented Reality and Virtual Reality?

Do you have any gaming experience with Augmented Reality and Virtual Reality? if yes, how often do you play?

Are you familiar with data visualization and/or technical drawings?

APPENDIX C

USER STUDY TRAINING SLIDES AND QUESTIONNAIRE

Table C.1 User Study Training Slides and Questions

<table>
<tr>
<td>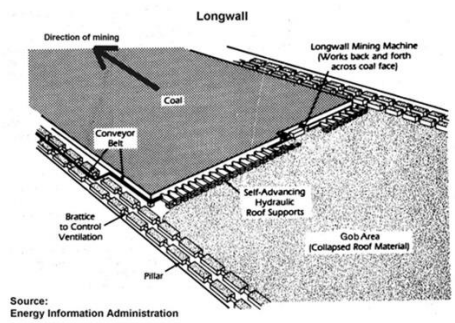
</td>
<td>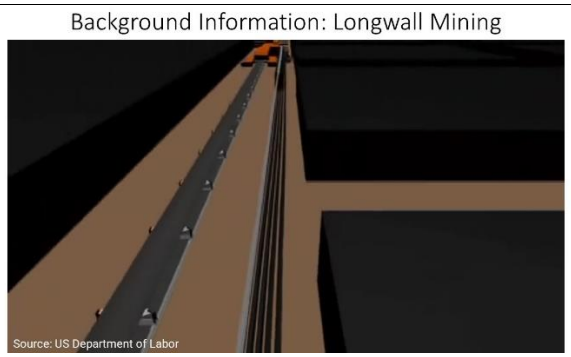
</td>
</tr>
<tr>
<td>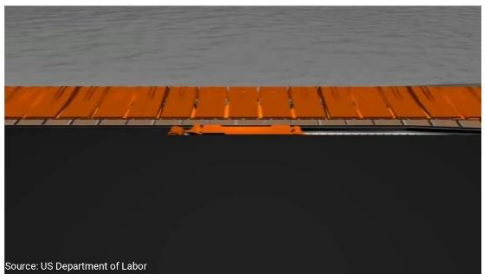
</td>
<td>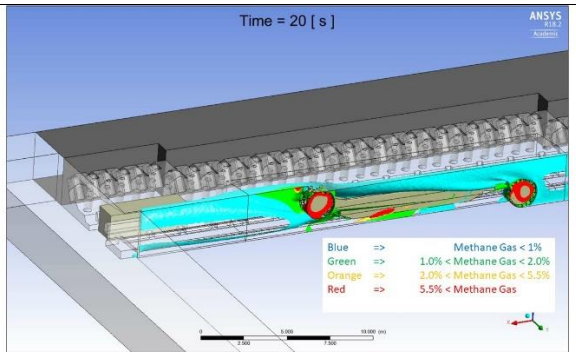
</td>
</tr>
<tr>
<td>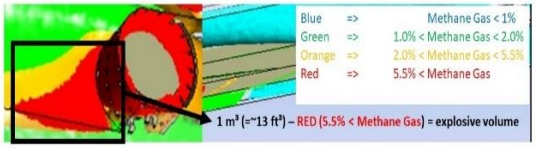
</td>
<td>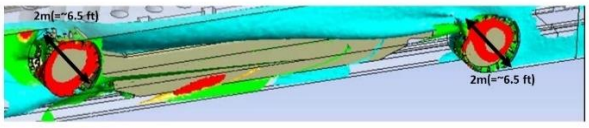
</td>
</tr>
<tr>
<td colspan="2">What is the diameter of the shearer?
What does the blue color represent?
What does the green color represent?
What does the orange color represent?
What does the red color represent?
Which one is the explosive range?
What is the lowest explosive volume?</td>
</tr>
</table>

APPENDIX D
POSTTEST SURVEY

Do you think the visuals were easy to understand?

Which visual do you prefer most? [1 - Prefer the most]

Which visual do you prefer most? [2]

Which visual do you prefer most? [3]

Which visual do you prefer most? [4 - Prefer the least]

Which device do you prefer most? [1 - Prefer the most]

Which device do you prefer most? [2]

Which device do you prefer most? [3 - Prefer the least]

What is the reason for #1 preference?

What is the reason for #3 preference?

[Visuals are in good size]

[Colors are distinguishable]

[I was able to actively survey the virtual environment using vision]

[I was able to examine objects closely]

[I was involved in the virtual environment experience]

[The visual display quality distracted me from performing assigned tasks]

[I could concentrate on the assigned tasks rather than on the devices]

[I felt stimulated by the virtual environment]

[I felt physically fit in the virtual environment]

[I got scared by something happening in the virtual environment]

[I felt I could perfectly control my actions]

[Time seemed to flow differently than usual]

[I thought there was too much inconsistency in the virtual environment]

[I enjoyed being in this virtual environment]

[I got tense in the virtual environment]

[I worried whether I was able to cope with all the instructions that was]

[The virtual environment scared me since I do not fully understand it]

[Personally, I would say the virtual environment is practical]

[Personally, I would say the virtual environment is confusing]

[I found that this virtual environment is likable]

[I suffered from fatigue during my interaction with the virtual environment]

[I suffered from headache during my interaction with the test]

[I suffered from eyestrain during my interaction with the virtual test]

In your opinion, what were the positive points about your experience?

In your opinion, what were the negative points about your experience?

Do you have suggestions to improve this virtual reality environment?

APPENDIX E

Q-Q PLOTS

Normal Q-Q Plot – C1 (Complex – Solid – Computer Screen Data)

Volume

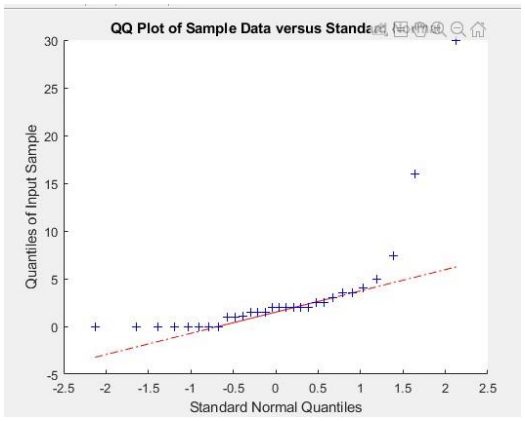

Not a normal dist. – non-parametric test

Time

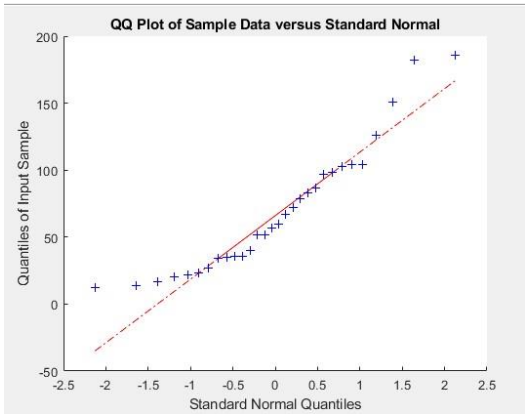

Not a normal dist. – non-parametric test

Normal Q-Q Plot – C2 (Complex – Solid – Computer Screen Data)

Volume

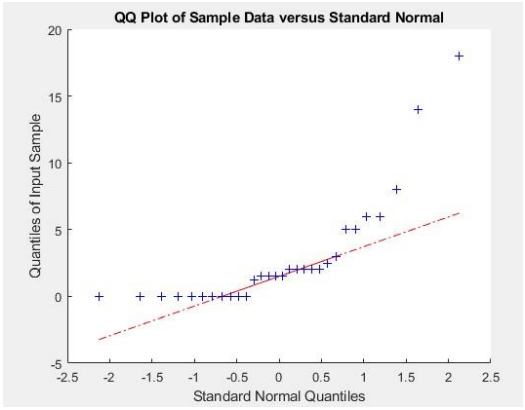

Not a normal dist. – non-parametric test

Time

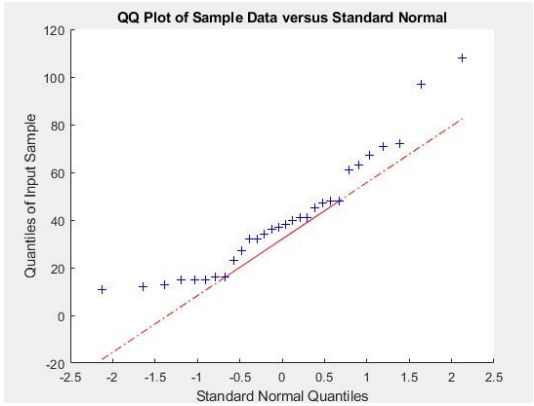

Not a normal dist. – non-parametric test

Figure E.1 Q-Q Plots of Accuracy and Time Data from User Study

Normal Q-Q Plot – C3 (Complex – Solid – Computer Screen Data)

Volume

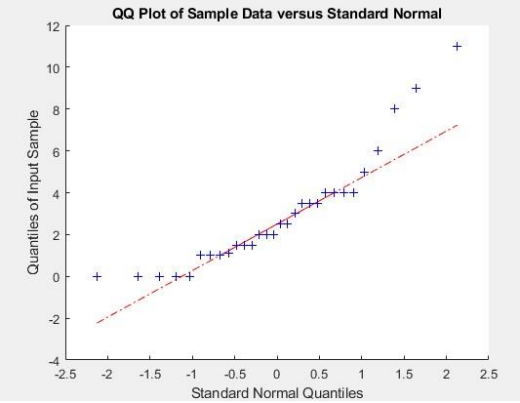

Not a normal dist. – non-parametric test

Time

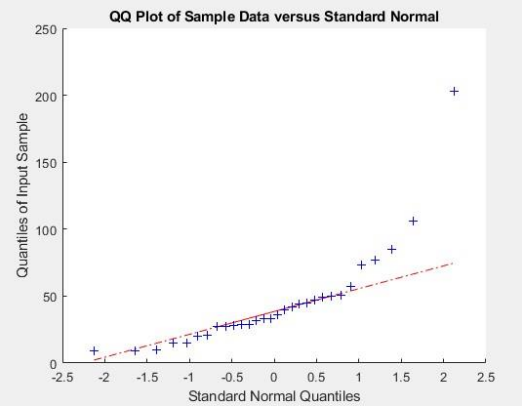

Not a normal dist. – non-parametric test

Normal Q-Q Plot – C4 (Complex – Solid – Computer Screen Data)

Volume

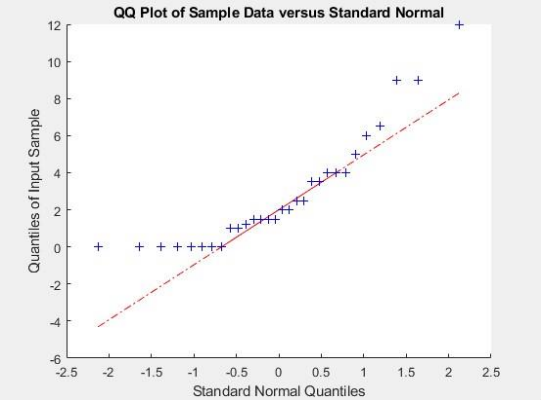

Not a normal dist. – non-parametric test

Time

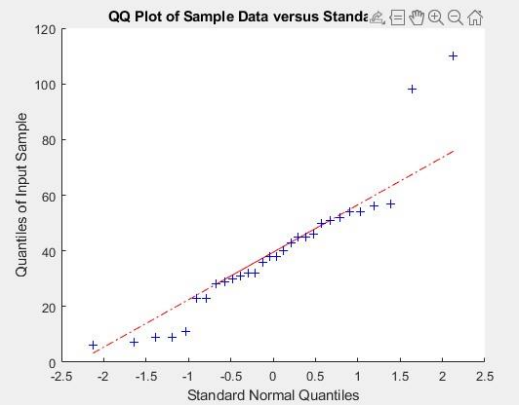

Not a normal dist. – non-parametric test

Figure E.1 Continued

Normal Q-Q Plot – AR1 (Complex – Solid – Computer Screen Data)

Volume

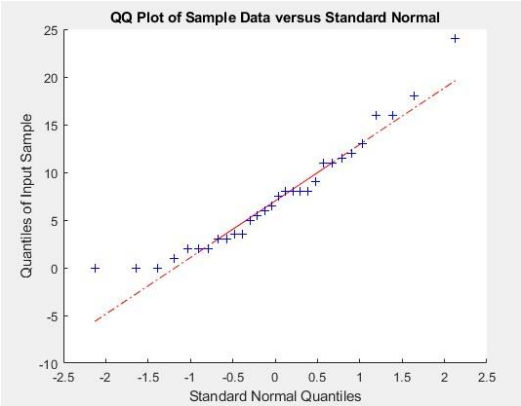

Not a normal dist. – non-parametric test

Time

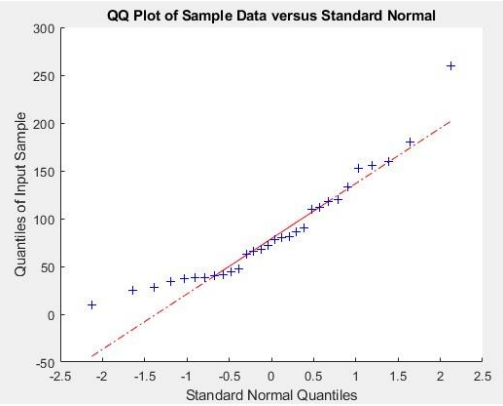

Not a normal dist. – non-parametric test

Normal Q-Q Plot – AR2 (Complex – Solid – Computer Screen Data)

Volume

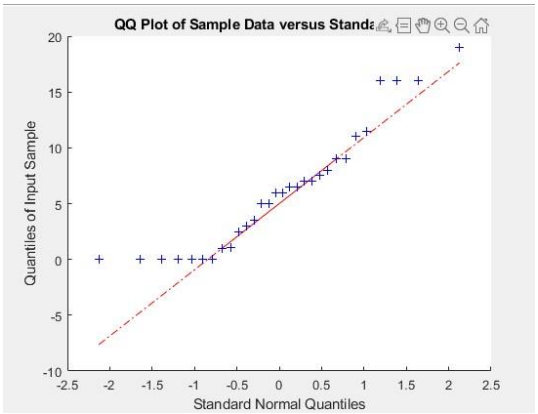

Not a normal dist. – non-parametric test

Time

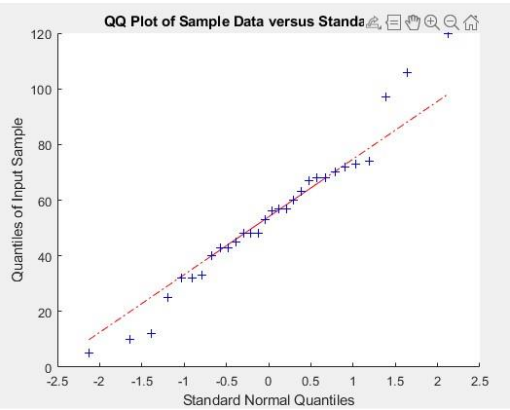

Not a normal dist. – non-parametric test

Figure E.1 Continued

Normal Q-Q Plot – AR3 (Complex – Solid – Computer Screen Data)

Volume

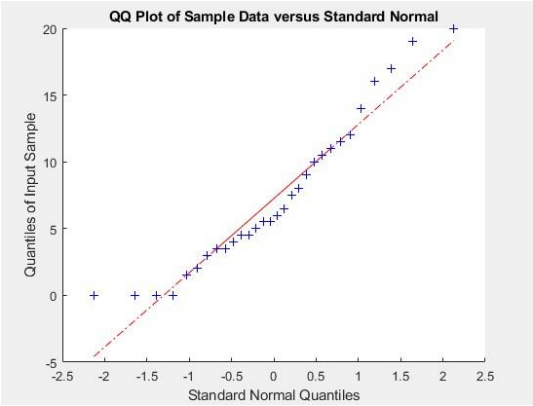

Not a normal dist. – non-parametric test

Time

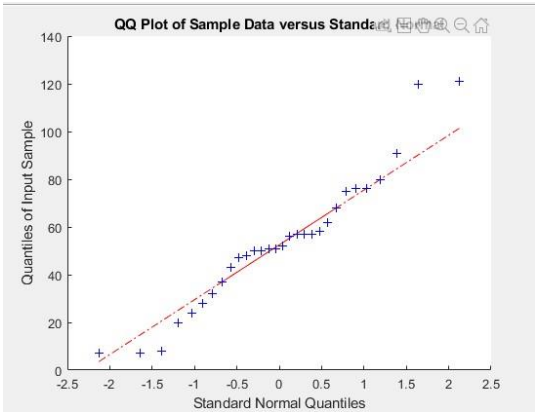

Not a normal dist. – non-parametric test

Normal Q-Q Plot – AR4 (Complex – Solid – Computer Screen Data)

Volume

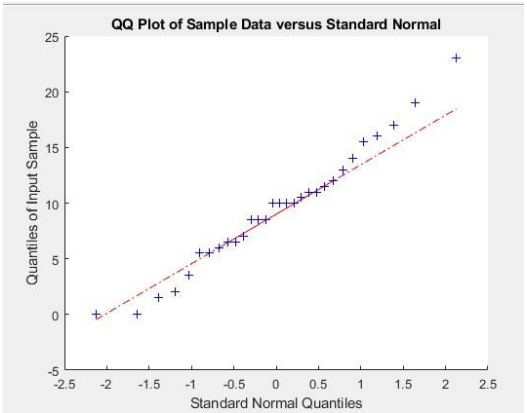

Not a normal dist. – non-parametric test

Time

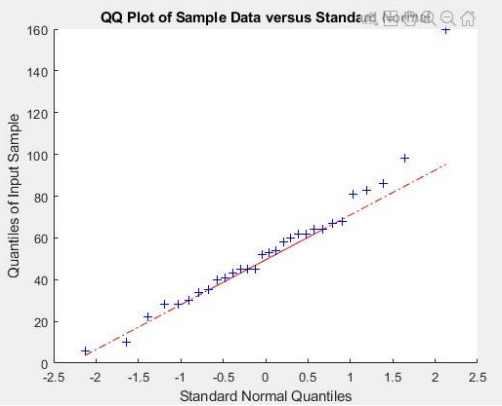

Not a normal dist. – non-parametric test

Figure E.1 Continued

Normal Q-Q Plot – VR1 (Complex – Solid – Computer Screen Data)

Volume

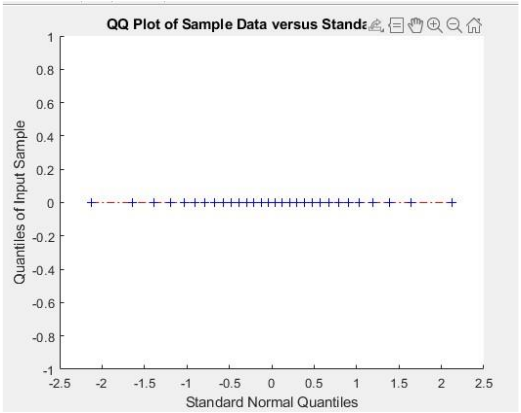

Not a normal dist. – non-parametric test

*in this setting, no one can see any zone
(all answers = 0)
Expected graph

Time

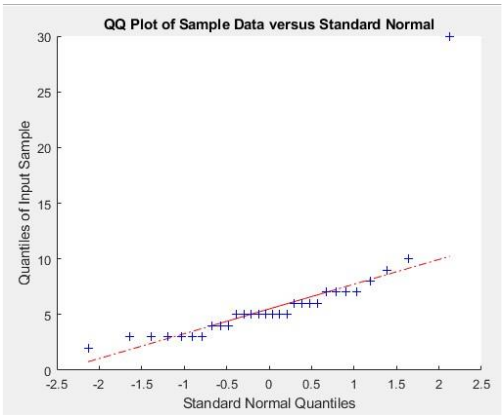

Not a normal dist. – non-parametric test

Normal Q-Q Plot – VR2 (Complex – Solid – Computer Screen Data)

Volume

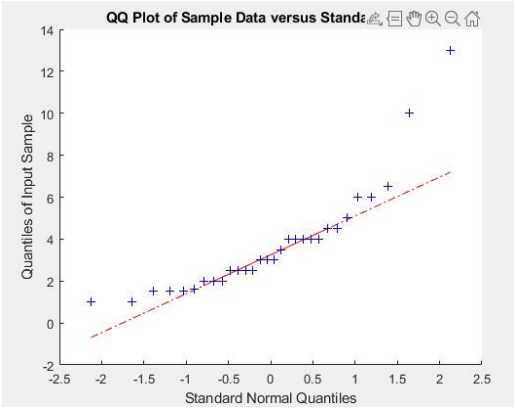

Not a normal dist. – non-parametric test

Time

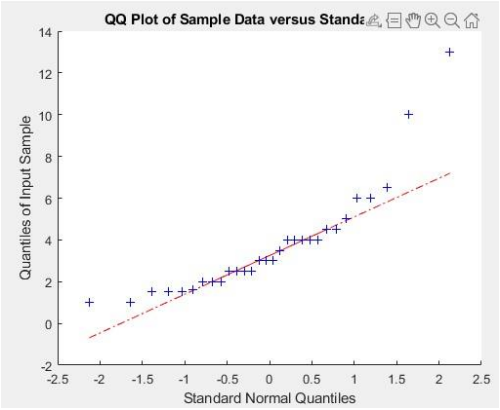

Not a normal dist. – non-parametric test

Figure E.1 Continued

Normal Q-Q Plot – VR3 (Complex – Solid – Computer Screen Data)

Volume

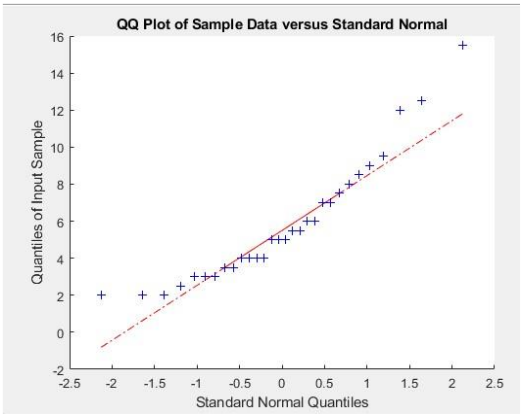

Not a normal dist. – non-parametric test

Time

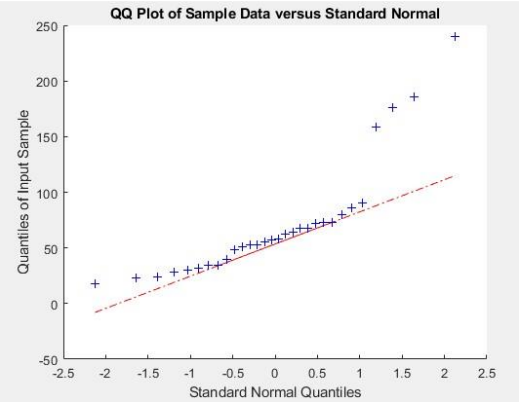

Not a normal dist. – non-parametric test

Normal Q-Q Plot – VR4 (Complex – Solid – Computer Screen Data)

Volume

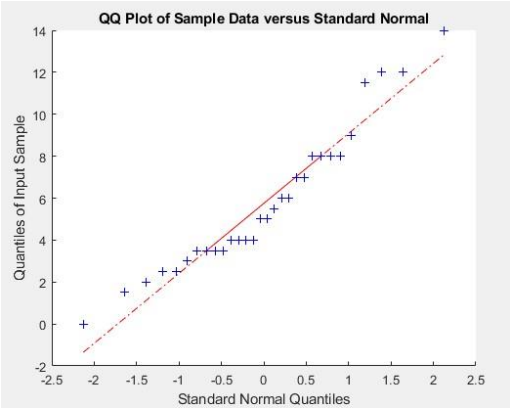

Not a normal dist. – non-parametric test

Time

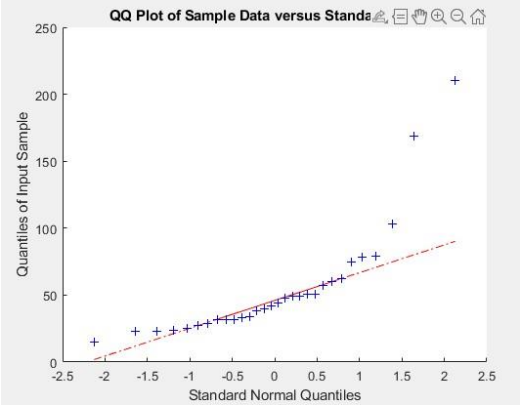

Not a normal dist. – non-parametric test

Figure E.1 Continued

APPENDIX F

SIMULATION VISUALIZATIONS, EYE TRACKER HEAT MAPS AND SALIENCY MAPS

Table F.1 Original image, heatmap, saliency and overlay

Original Image	Heatmap Overlay	Saliency Map	Overlay of Saliency and HeatMap
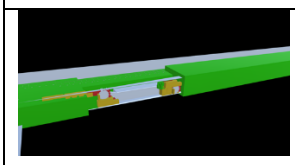	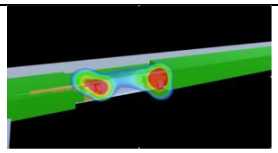	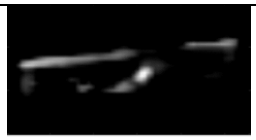	
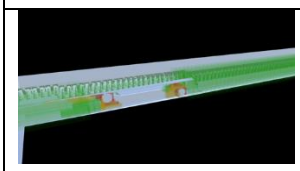	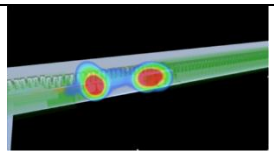	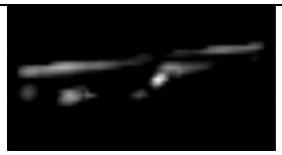	
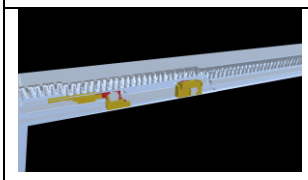	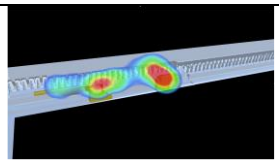		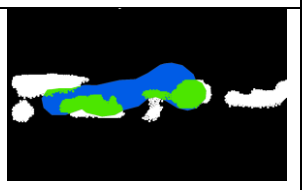
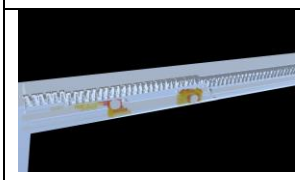	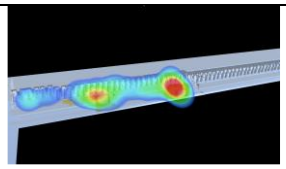	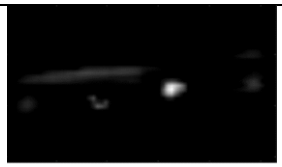	
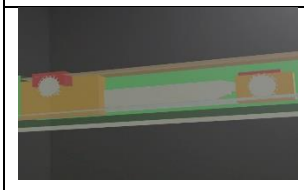	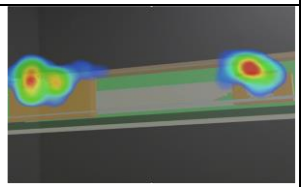	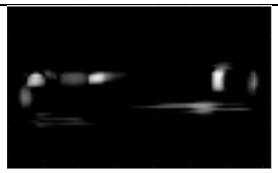	
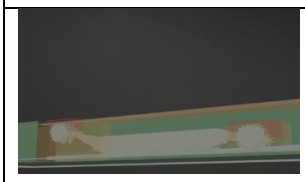	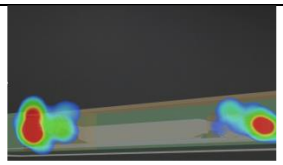	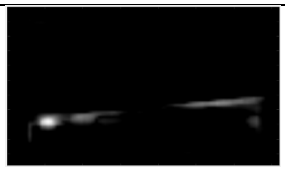	
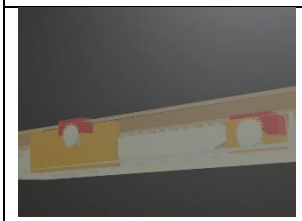	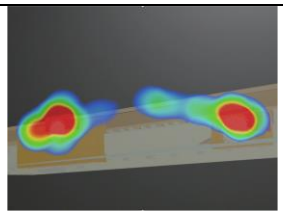		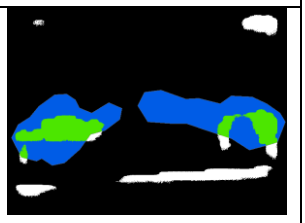

Table F.1 Continued

Original Image	Heatmap Overlay	Saliency Map	Overlay of Saliency and HeatMap
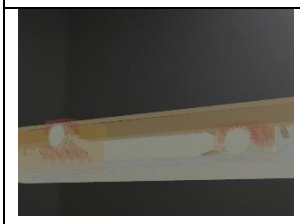	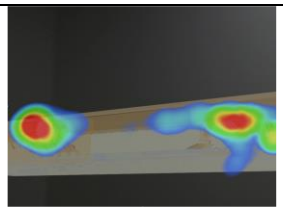	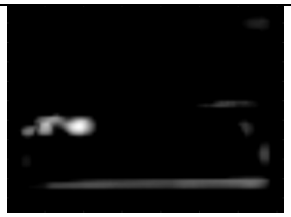	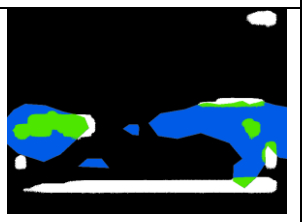
	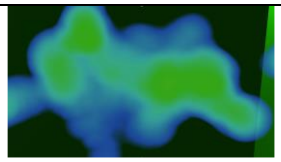		
	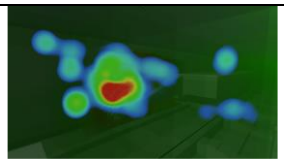	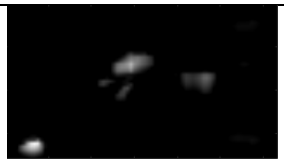	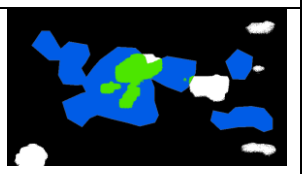
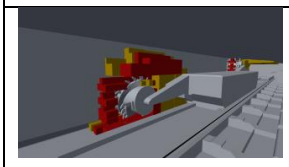	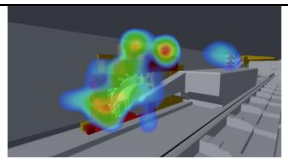	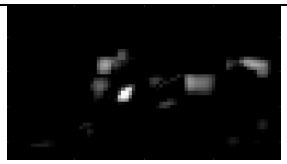	
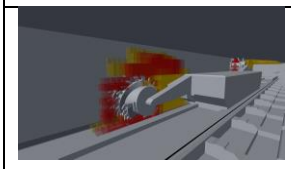	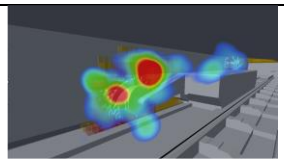	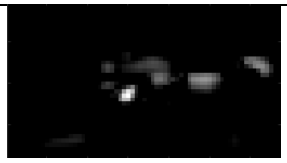	

APPENDIX G

PERMISSION TO USE COPYRIGHTED MATERIALS

Permission to include previously published materials in this dissertation are listed below.

1) Copyright permission from Informa UK Limited, trading as Taylor & Taylor & Francis Group. The content in Chapter 3 is reprinted from the article cited below:

D. C. Demirkan, S. Duzgun, A. Juganda, J. Brune & G. Bogin (2022) Evaluation of time series artificial intelligence models for real-time/near-real-time methane prediction in coal mines, CIM Journal, 13:3, 97-106, DOI: 10.1080/19236026.2022.2072664

[External] ucim20:Evaluation of time series artificial intelligence models for real-time/near-real-time methane prediction in coal mines

Taylor & Francis Journal Permissions Support <taylorandfrancissupport@tandf.co.uk>
Wed 12/7/2022 7:56 AM
To: Doga Cagdas Demirkan <demirkan@mines.edu>

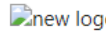

Our Ref: ucim/02813329

12/7/2022

Dear Requester,

Thank you for your correspondence requesting permission to reproduce content from a Taylor & Francis Group journal content in your thesis to be posted on your university's repository.

We will be pleased to grant free permission on the condition that your acknowledgement must be included showing article title, author, full Journal title, and **© copyright # [year]**, reprinted by permission of Informa UK Limited, trading as Taylor & Taylor & Francis Group, http://www.tandfonline.com

This permission does not cover any third party copyrighted work which may appear in the article by permission. Please ensure you have checked all original source details for the rights holder and if need apply for permission from the original rightsholder.

Please note that this license **does not allow you to post our content on any other third-party websites.**

Please note permission does not provide access to our article, if you are affiliated to an institution and your institution holds a subscription to the content you are requesting you will be able to view the article free of charge, if your institution does not hold a subscription or you are not affiliated to an institution that has a subscription then you will need to purchase this for your own personal use as we do not provide our articles free of charge for research.

Thank you for your interest in our Journal.

With best wishes,

Taylor & Francis Journal Permissions
journalpermissions@tandf.co.uk
Web: www.tandfonline.com
+ 4 Park Square, Milton Park, Abingdon, OX14 4RN
(+44 (0)20 8052 0600

2) Copyright permission from MDPI, the publisher of *Energies,* is not required for the inclusion of Chapter 4 from *Energies*. MDPI's policy states that "No special permission is required to reuse all or part of article published by MDPI, including figures and tables.", and "Everyone is free to re-use the published material if proper accreditation/citation of the original publication is given." (https://www.mdpi.com/openaccess). The content in Chapter 4 is reprinted from the article cited below:

D. C. Demirkan, H. S. Duzgun, A. Juganda, J. Brune, and G. Bogin, "Real-Time Methane Prediction in Underground Longwall Coal Mining Using AI," Energies, vol. 15, no. 17, p. 6486, Sep. 2022, doi: 10.3390/en15176486.

3) Permission to use Chapters 3 and 4, from co-author Aditya Juganda is provided below.

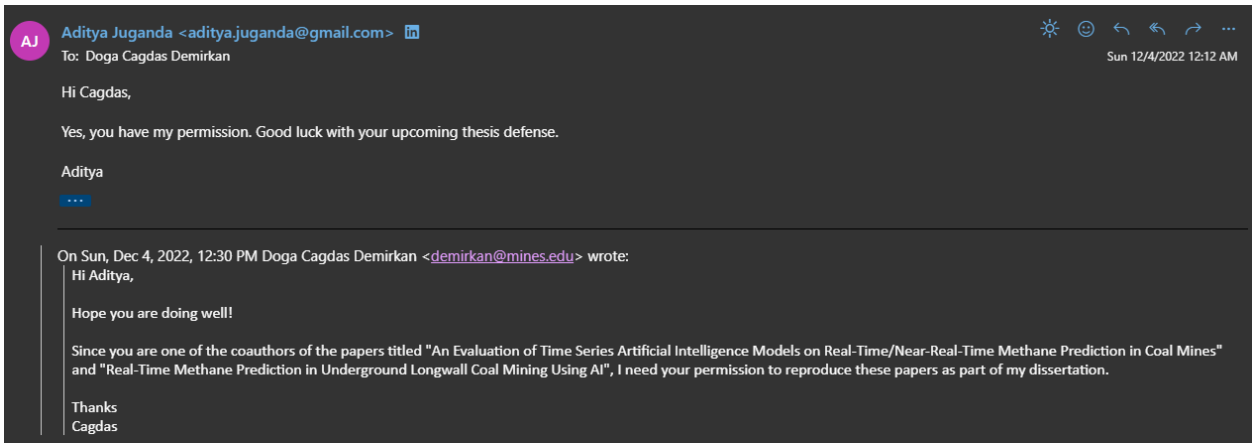

4) Copyright permission from IEEE. The content in Chapter 6 is reprinted from the article cited below:

D. C. DEMIRKAN and S. Duzgun, "An Evaluation of AR-Assisted Navigation for Search and Rescue in Underground Spaces," 2020 IEEE International Symposium on Mixed and Augmented Reality Adjunct (ISMAR-Adjunct), 2020, pp. 1-2, doi: 10.1109/ISMAR-Adjunct51615.2020.00017.

IEEE
Requesting permission to reuse content from an IEEE publication

An Evaluation of AR-Assisted Navigation for Search and Rescue in Underground Spaces

Conference Proceedings: 2020 IEEE International Symposium on Mixed and Augmented Reality Adjunct (ISMAR-Adjunct)
Author: Doga Cagdas DEMIRKAN
Publisher: IEEE
Date: November 2020

Copyright © 2020, IEEE

Thesis / Dissertation Reuse

The IEEE does not require individuals working on a thesis to obtain a formal reuse license, however, you may print out this statement to be used as a permission grant:

Requirements to be followed when using any portion (e.g., figure, graph, table, or textual material) of an IEEE copyrighted paper in a thesis:

1) In the case of textual material (e.g., using short quotes or referring to the work within these papers) users must give full credit to the original source (author, paper, publication) followed by the IEEE copyright line © 2011 IEEE.
2) In the case of illustrations or tabular material, we require that the copyright line © [Year of original publication] IEEE appear prominently with each reprinted figure and/or table.
3) If a substantial portion of the original paper is to be used, and if you are not the senior author, also obtain the senior author's approval.

Requirements to be followed when using an entire IEEE copyrighted paper in a thesis:

1) The following IEEE copyright/ credit notice should be placed prominently in the references: © [year of original publication] IEEE. Reprinted, with permission, from [author names, paper title, IEEE publication title, and month/year of publication]
2) Only the accepted version of an IEEE copyrighted paper can be used when posting the paper or your thesis on-line.
3) In placing the thesis on the author's university website, please display the following message in a prominent place on the website: In reference to IEEE copyrighted material which is used with permission in this thesis, the IEEE does not endorse any of [university/educational entity's name goes here]'s products or services. Internal or personal use of this material is permitted. If interested in reprinting/republishing IEEE copyrighted material for advertising or promotional purposes or for creating new collective works for resale or redistribution, please go to http://www.ieee.org/publications_standards/publications/rights/rights_link.html to learn how to obtain a License from RightsLink.

If applicable, University Microfilms and/or ProQuest Library, or the Archives of Canada may supply single copies of the dissertation.